Cyclophane-based Supramolecular Mechanophores Using Charge-Transfer Complexes

（電荷移動錯体を利用したシクロファン型超分子メカノフォア）

A Thesis

Submitted for the Degree of

Doctor of Life Science

By

Thazhathethil Shakkeeb

Laboratory of Smart Molecules

Transdisciplinary Life Science Course

Graduate School of Life science

Hokkaido University, Japan

December 2022

DECLARATION

I hereby declare that the matter embodied in this thesis entitled **"Cyclophane-based supramolecular mechanophores using charge-transfer complexes"** is the result of investigations carried out by me under the supervision of **Prof. Nobuyuki Tamaoki** at the laboratory of Smart Molecules, Transdisciplinary Life Science Course, Graduate School of Life Science, Hokkaido University, Japan, and it has not been submitted elsewhere for the award of any degree of diploma.

In keeping with the general procedure of reporting scientific observations, proper acknowledgement has been made whenever the work described based on the findings of the other investigators.

Thazhathethil Shakkeeb

CERTIFICATE

I hereby certify that the work described in this thesis entitled **"Cyclophane-based Supramolecular mechanophores using charge-transfer complexes"** has been carried out by **Thazhathethil Shakkeeb,** under the supervision of **Prof. Nobuyuki Tamaoki** at the laboratory of Smart Molecules, Transdisciplinary Life Science Course, Graduate School of Life Science, Hokkaido University, Japan.

Prof. Nobuyuki Tamaoki

(Research Supervisor)

Table of Contents

Chapter 1

General Introduction

1.1 Forces

In our daily life, we often use or experience various types of forces during our activities. Force is an external factor that moves or retards the motion of objects. Force is required to push or pull an object. Force inflicts changes in the shape, size, and direction of objects. The forces can be classified into non-contact and contact forces. The naturally occurring forces such as gravitational force, electromagnetic force, and nuclear forces are non-contact forces. The nuclear force is responsible for binding two nucleons in a nucleus. While, the electromagnetic forces, the attractive or repulsive interactions between two charged particles, are fundamental for several chemical reactions, binding of atoms, and structure of different solids. A contact force is the result of physical contact between two objects, where one of the objects exerts a force on the other. Cutting vegetables, pulling trolleys, crushing ice cubes, kicking football, and pushing doors are examples of contact forces that we use in our day-to-day life.

Generally, light, electricity, and mostly heat is used to proceed chemical reactions. Recently, mechanical force is also intentionally used to break and create chemical bonds to drive photophysical changes in compounds.[1–7] The required mechanical force to cleave a covalent bond or to induce structural rearrangements in molecular units can be transduced through ball milling, grinding, shearing, stretching, or compression.[8] Other methods to induce the mechanochemical activation are using atomic force microscopy (AFM)[9] or ultrasonication.[10,11]

In the body of living organisms, cells and tissues are always subjected to mechanical forces. The cells generate mechanical forces to contract, migrate, remodel, and to sense the extracellular microenvironment.[12] It is possible to quantify the force generated or transmitted across proteins by incorporating fluorescence resonance energy transfer (FRET)-based donor acceptor pairs inside the proteins.[13–19] In 2010, Grashoff et al. demonstrated that the force

across vinculin proteins in stable focal adhesions is approximately 2.5 pN. Vinculin is an intracellular focal adhesion protein that contains a head domain (Vh) and tail domain (Vt) separated by a flexible linker. [13] The research group used fluorescence resonance energy transfer between two fluorophores named mTFP1 and venus(A260K) to study the force across vinculin. The donor and acceptor fluorophores were linked by a flexible spider silk protein flagelliform. The FRET efficiency decreased owing to an increase in the distance between fluorophores at high tension.

In the current day and age, polymers are widely used in a wide range of everyday applications, including laboratory apparatus, medical equipment, automobile parts, electronic devices, machines, as well as engineering materials. Accurate evaluation and visualization of the forces generating inside the polymers are significant owing to the elucidation of the failure mechanism of polymer materials, the extension of the service life of materials, and the development of more sophisticated polymer materials. Application of sufficient mechanical force on polymer materials can cause covalent bond scission. The required force for covalent bond scission ranges between 200 pN to several nN.[2] The force calculated for scission of carbon–carbon bond is around 7 nN.[20] In 1930s, Staudinger group reported the reduction of molecular weight of polystyrene under mastication.[21,22] In 1950s, Melville and Murray reported the ultrasonication induced degradation of poly(methacrylate) polymer in solution.[23] Later in 2005, Moore and coworkers reported ultrasonication induced dinitrogen molecule liberation from a polymer that contains mechanically weak azo group near the chain mid-point.[24] In 2006, Dr. Ken Caster introduced the term “mechanophores” for the force-sensitive molecular units that possesses mechanically labile bonds.[5]

1.2 Mechanophores

Mechanophores are the molecular structures that exhibit physical or chemical response upon application of external mechanical forces.[5] The mechanical forces applied on the mechanophores inflicts covalent bond scission or conformational changes. The mechanical activation of the mechanophores often leads to changes in absorption and photoluminescence spectra or chemical responses such as small molecule release[25] and catalytic reactions.[26] Mechanophores that releases photoluminescent small molecules upon application of mechanical forces inflict changes in absorption or photoluminescence spectra of the polymer that contains covalently incorporated mechanophore.[27]

1.2.1 Mechanochromic mechanophores and Mechanochromic luminescent Mechanophores Using Covalent Bond Scission

The mechanophores that exhibit color changes (mechanochromic mechanophores) or luminescence changes (mechanochromic luminescent mechanophores) are useful to easily detect mechanical deformation.[4–7] Covalent introduction of mechanochromic mechanophores into polymers are appropriate to study the deformation events easily and unambiguously. Many mechanophores have been reported to exhibit covalent bond scission during the activation process. In 2009, the first color changing mechanophore, spiropyran, was reported by Moore and co-workers (Figure 1-1a).[28] Spiropyran is a colorless photochromic molecule that forms colored π-conjugated merocyanine through 6-π electrocyclic ring opening reaction under UV irradiation. They covalently introduced a spiropyran mechanophore into poly(methylacrylate) (PMA) polymer. Upon uniaxial deformation of the colorless polymer that contains spiropyran, a reddish colored merocyanine was formed due to the force induced C–O bond cleavage followed by 6-π electrocyclic ring opening reaction. Moreover, the properties of spiropyran mechanophores have been well investigated by changing polymers introduced to the

mechanophore.[29–31] Changing the attachment position was found to change the activation behavior.[30,31]

Various mechanophores which follows the same activation mechanism of spiropyran were developed by the modification of pyran moiety in the spiropyran such as spirothiopyran (STP),[32] 3H-naphthopyran,[33] bisnaphthopyran (BNP),[34] and 2H-naphthopyran (Figure 1-1).[35] The spirothiopyran exhibits yellow color when covalently incorporated into polyester or polyethylene polymers. When an external mechanical force is applied, the polymers show green color due to the formation of thiomerocyanine through 6-π electrocyclic ring opening reaction (Figure 1-1b).[32] The DMF solution of polyester containing STP exhibited yellow color and the color changed to green by sonication of the solution for 3 minutes. The color change is ascribed to the formation of thiomerocyanine.

Naphthopyran is a pyran derivative which shows reversible mechanochromic color change to form colored merocyanine under UV light through 6-π electrocyclic ring opening reaction. Robb and Moore first reported naphthopyran as a mechanochromic mechanophore (Figure 1-1c).[33] They synthesized three regioisomers of naphthopyran by varying the attachment positions of polymer. Three polydimethylsiloxane polymers in which the mechanophores are incorporated distinctly were prepared to study the mechanochemical activation of naphthopyran regioisomers. Only the polymer containing NP5 regioisomer in which the polymer is attached at the fifth position on the naphthalene ring exhibited mechanochromic color change to orange yellow upon stretching due to force induced electrocyclic ring opening reaction. In contrast, the polymers containing the covalently incorporated other regioisomers NP8 and NP9 did not exhibit any color change upon mechanical stretching.

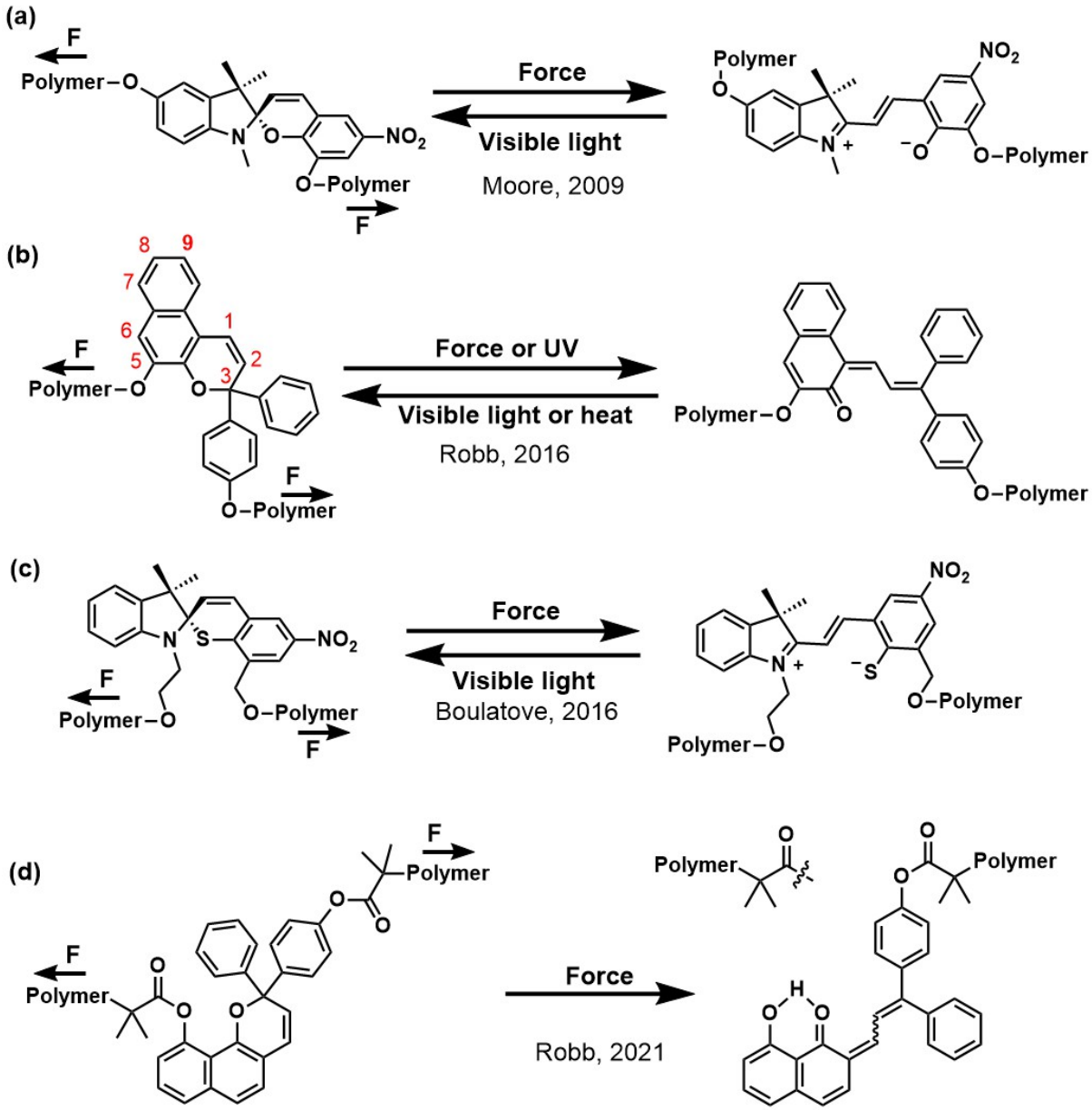

Figure 1-1. Activation of various mechanophores. (a) Spiropyran; (b) 3H-naphthopyran; (c) spirothiopyran; and (d) 2H-naphthopyran.

In 2019, Robb and group reported a bisnaphthopyran (BNP) mechanophore combines two naphthopyran units and forms two merocyanines through consecutive 6-π electrocyclic ring opening reactions upon illumination with UV light.[34] The two naphthopyran rings in the BNP can be effectively activated in a single step upon ultrasonication of BNP incorporated PMA polymer. The application of mechanical force causes C-O bond rupture *via* 6-π

electrocyclic ring opening of both naphthopyran rings and the color of PMA turns to purple. Furthermore, the same research group also reported a 2H-naphthopyran mechanophore that forms permanent merocyanine and irreversible color change, which are ascribed to the formation intramolecular hydrogen bonding in the merocyanine product formed through the ring opening reaction (Figure 1-1d).[35]

The colorless, tetrasubstituted, neutral triarylmethane (Tr) derivatives undergo heterolytic bond scission and form resonance stabilized colored triarylmethyl cations when irradiated with UV light. Recently, Weder group reported a Tr mechanophore that follows heterolytic covalent bond scission mechanism under the application of mechanical force (Figure 1-2).[36] The mechanical stretching of poly(*N,N*-dimethylacrylamide) or compression of poly(methyl acrylate-*co*-2-hydroxyethyl acrylate) polymers containing Tr motifs as cross-linkers leads to the formation of Tr cations and the polymers become colored. Moreover, the polymer exhibited the characteristic absorption spectrum of Tr cations.

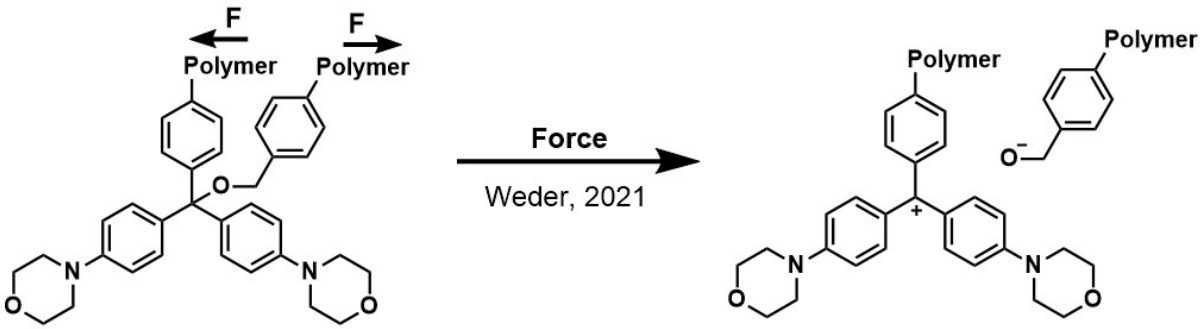

Figure 1-2. Activation of triarylmethane-based mechanophore.

Several photoluminescent mechanophores have been reported to exhibit photoluminescence spectral changes owing to covalent bond scission, which includes 1,2-dioxetane,[37,38] ladderanes,[39–42] Diels-alder adducts,[43–51] rhodamine derivatives,[52,53] coumarin dimer,[54] dithiomaleimide,[55] and benzoxazole.[56] All those mechanophores show either force-induced fluorescence turn-on or fluorescence turn-off. In 2012, Sijbesma and coworkers reported a bis(adamantyl)-1,2-dioxetane based mechanophore (Figure 1-3).[37]

Bis(adamantyl)-1,2-dioxetane forms two adamantanone units, one of that is in excited state, upon force induced activation. 1,2-Dioxetane was covalently integrated into PMA polymer backbone to study the mechanoresponsive luminescence. Sonication of polymer solution or stretching of polymer film caused activation of mechanophore accompanied by blue chemiluminescence due to relaxation of excited adamantanone unit. The mechanophore acted as energy donor and exhibited fluorescence resonance energy transfer during stretching in the presence of appropriate energy acceptors, and the emission color was tuned by varying the acceptors.

Figure 1-3. Activation of 1,2-dioxetane based mechanophore.

Recently, Xia and coworkers reported a ladderane and benzo ladderane mechanophores that form π-conjugated polymer under mechanical force due to ring opening reactions.[39–41] Followed by this work, the same group reported a bicyclo[2.2.0]hex-5-ene-2,3-peri-naphthalene mechanophore that forms conjugated polymers and exhibits turn-on luminescence (Figure 1-4).[42] Ultrasonication of polymer containing mechanophore solution or grinding of bulk polymer containing mechanophore caused force induced ring opening and formation of yellow luminescent conjugated polymer.

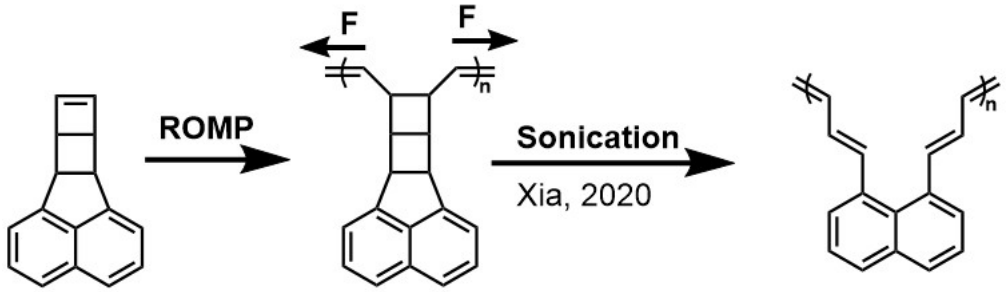

Figure 1-4. Activation of ladderane-based mechanophore.

In 2012, Chung group reported an anthracene dimer mechanophore. When a colorless polymer containing anthracene dimer was cracked, strong luminescence was observed from anthracene, and the polymer's photophysical properties were altered (Figure 1-5a).[43] Similar to the anthracene dimer mechanophore, Diels-Alder adducts of anthracene can also act as effective photoluminescent mechanophores owing to the high quantum efficiency of anthracene moieties that form activation of mechanophores. Polymers containing anthracene-maleimide adduct[44–50] or π-extended anthracene-maleimide adduct[51] also exhibited photophysical changes due to generation of anthracene or π-extended anthracene as the retro-DA product (Figure 1-5b,c).

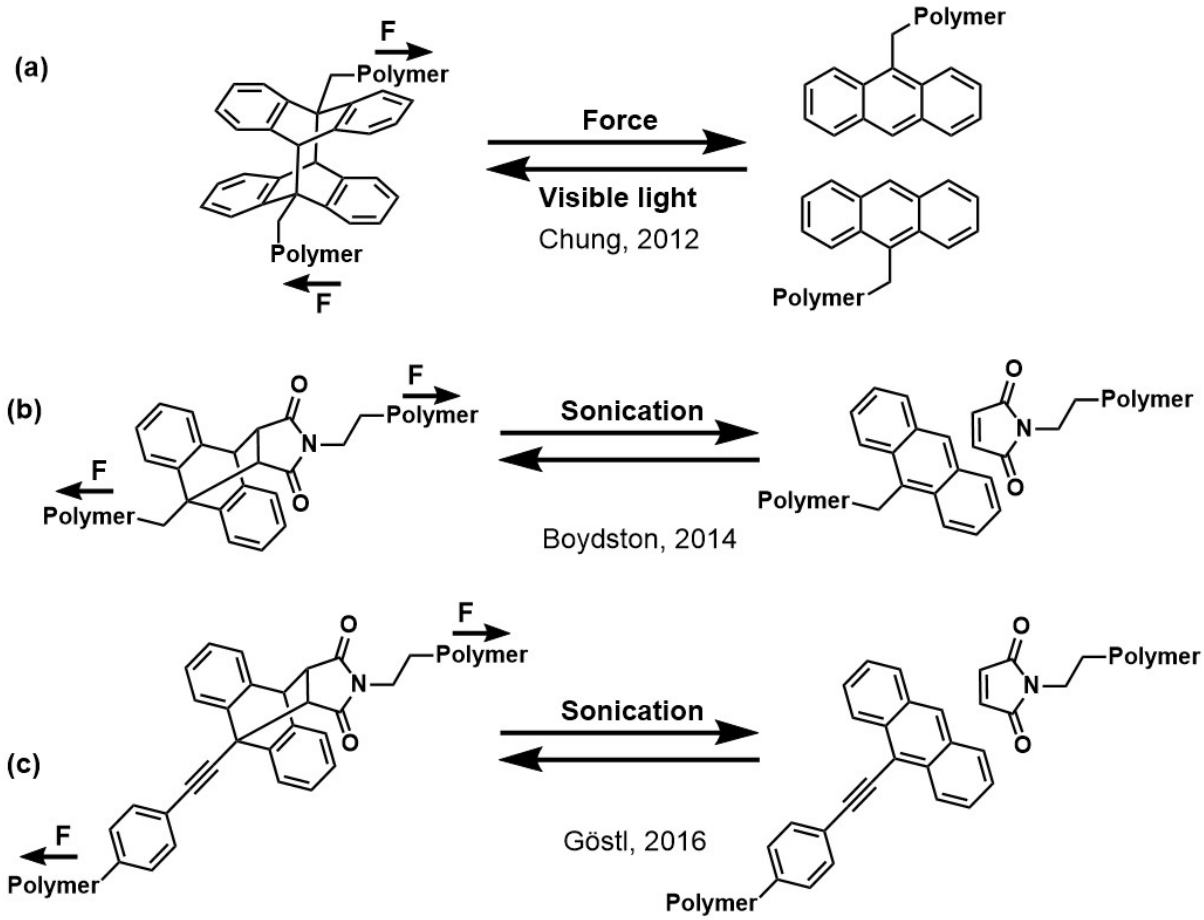

Figure 1-5. Activation of various mechanophores. (a) Anthracene dimer; (b) anthracene-maleimide adduct; (c) π-extended anthracene-maleimide adduct.

Similar to the spiropyran, the rhodamine derivatives undergo electrocyclic ring opening reaction of spirolactam cycle to form planarized zwitterion under UV irradiation. In 2015, Jia and coworkers reported a rhodamine-based mechanophore.[52] The colorless polystyrene that containing rhodamine mechanophore exhibited color change and fluorescence color change under mechanical force. Following the pioneering works by Jia group, Bai and coworkers reported a new rhodamine based mechanophore that was covalently incorporated to polyethyl acrylate polymer backbone.[53] The polymer films exhibited dark red color and red luminescence upon stretching due to the formation of planar zwitterion (Figure 1-6).

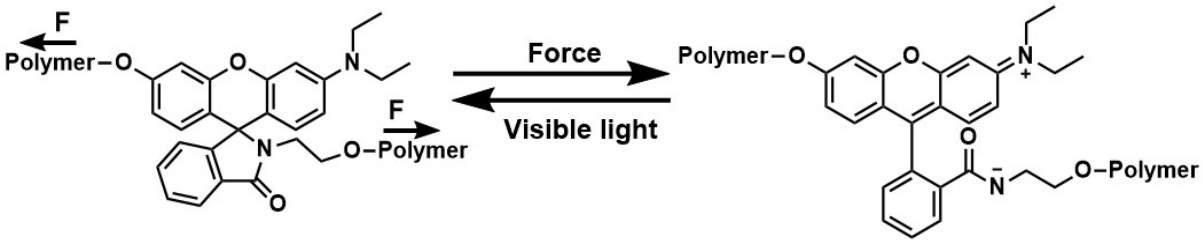

Figure 1-6. Activation of rhodamine-based mechanophore.

The mechanoradicals are generated through the homolytic cleavage of bonds in response to an applied mechanical force. Generally, the radicals formed from the mechanophores are colored and stable under ambient conditions. The generation of radicals causes changes in the absorption spectra and in some cases exhibits photoluminescence color changes.[57–61] Diarylbibenzofuranone (DABBF) is a homodimer of arylbenzofuranone and can generate highly stable carbon centered radical by heating or light irradiation. In 2015, Otsuka and coworkers reported a DABBF mechanophore (Figure 1-7a).[57] The pale-yellow colored polyurethane elastomer containing covalently integrated DABBF mechanophore exhibited blue color upon uniaxial tensile deformation due to the generation of highly stable blue colored carbon centered radicals in air at room temperature. The generated radicals recombined after relaxation of the polymer films or at constant strain.

.

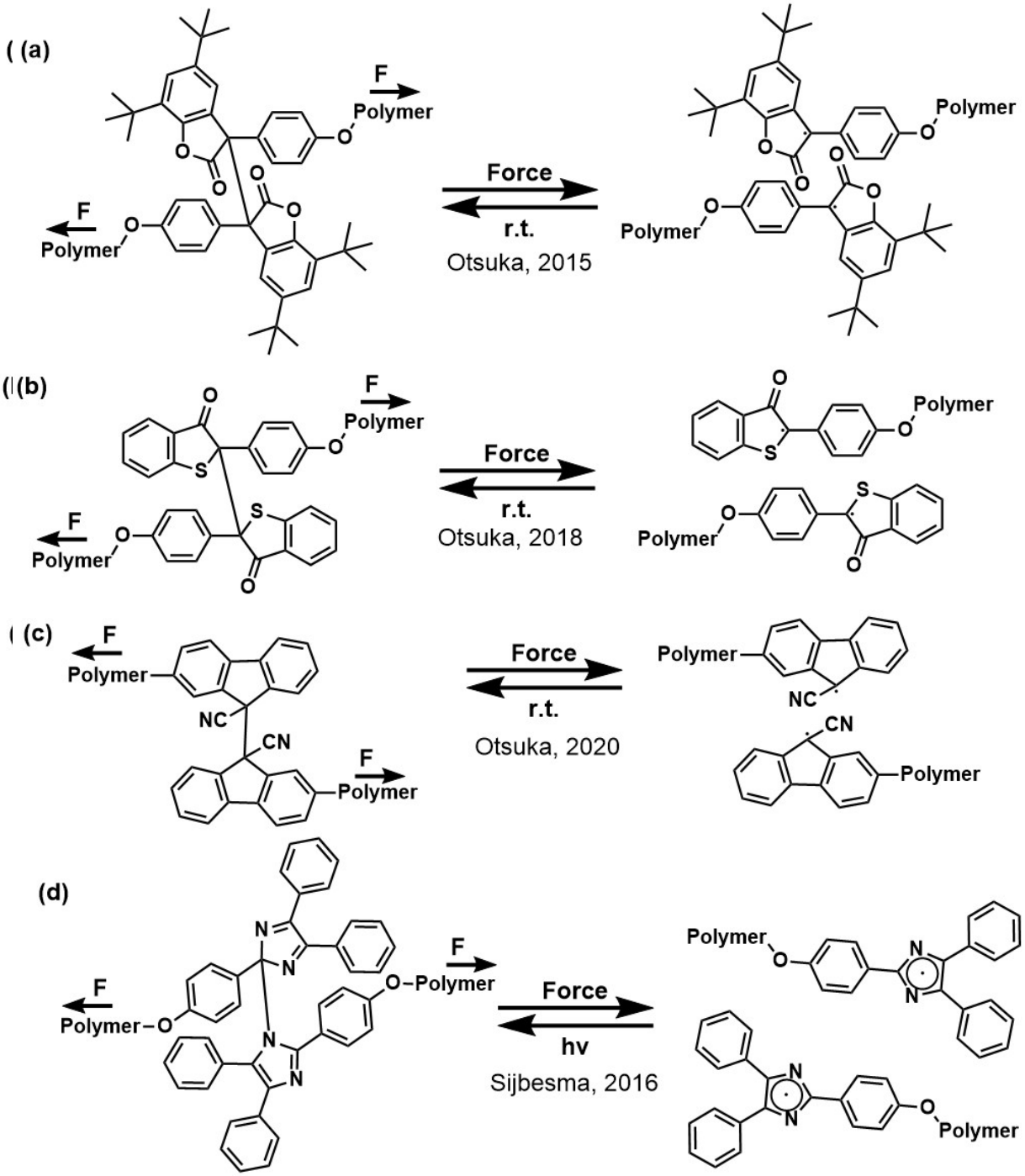

Figure 1-7. Activation of various mechanophores that form radicals. (a) Diarylbibenzofuranone; (b) diarylbibenzothiophenonyl; (c) difluorenylsuccinonitrile; and (d) hexaarylbiimidazole.

In 2017, Otsuka group reported a tetraarylsuccuinonitrile (TASN) based mechanophore.[62] Upon milling of colorless polystyrene in which mechanophore is covalently integrated exhibits pink color and yellow luminescence color under UV irradiation at room

temperature due to formation of stable carbon centred radicle through homolytic C–C bond cleavage. Furthermore, TASN was covalently integrated into the backbone of poly(hexyl methacrylate) and the colorless polymer films exhibited pink color upon stretching. Following the same strategy, Otsuka and co-workers demonstrated green color exhibited by a diarylbibenzothiophenonyl mechanophore that was covalently incorporated into polystyrene polymer backbone (Figure 1-7b).[63] Subsequent works by the same group lead to the development of a difluorenylsuccinonitrile based mechanophore in 2020 (Figure 1-7c).[64] The mechanophore which was cross-linked to polymers exhibited force induced generation of pink cyanofluorenyl radicals upon stretching, and color of the film changed to pink. In 2016, Göstl and Sijbesma reported a hexaarylbiimidazole (HABI) based mechanophore that form colored triphenylimidazolyl radicals under external mechanical force (Figure 1-7d).[65] DMF swollen organogel of HABI incorporated polyurethane turns highly colored when cooling with liquid nitrogen due to the force-induced generation of triphenylimidazolyl radicals.

1.2.2 Mechanophores Working Without Covalent Bond Scission

The mechanophores in which the activation process does not require covalent bond scissions are another category of candidates to study the polymer deformation. Here, application of mechanical force to the mechanophores inflicts changes in the inter- and intramolecular interactions,[66–72] changes in coordination states of metal complexes,[73–85] changes in the fluorescence resonance energy transfer (FRET),[76–80] and change in the excited-state intramolecular proton transfer (ESIPT).[81] Instant reversibility and low activation energy are the advantages of the mechanophores working without covalent bond scission over the mechanophores that relies on covalent bond scission.

The efficiency of FRET can be varied by applying force on the donor acceptor pair embedded in polymer,[76,77] DNA strands,[78,79] or universal-joint type skeleton.[80] In 2011, Takeuchi's group reported a universal-joint like mechanophore that comprised of two

bithiophene energy donors and a porphyrin energy acceptor (Figure 1-8).[80] The mechanophore was used as a cross-linker and covalently incorporated to PDMS polymer. In the relaxed state of the polymer films, the orientation of bithiophene donor and porphyrin acceptor caused effective FRET. The tensile stretching of films inflicted re-orientation of donor and acceptor, hence the relative orientation of the transition dipole moments perpendicularly aligned to decrease in the efficiency of FRET.

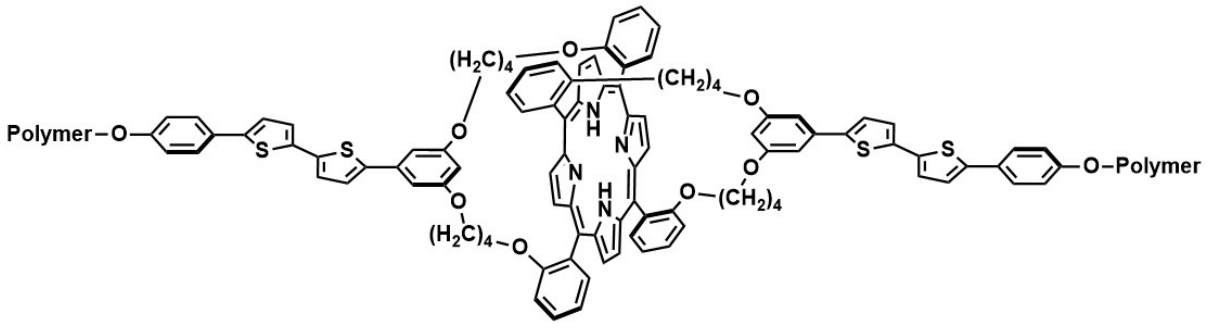

Takeuchi, 2011

Figure 1-8. Molecular structure of the universal-joint type mechanophore.

Filonenko and co-workers reported a different strategy for the activation of mechanophore. They developed an organocopper-based mechanophore that exhibits phosphorescence emission.[73] Here, the ligand exchange in the mechanophore causes increase in the non-radiative decay and hence the phosphorescence emission intensity decreases. The mechanophore was covalently introduced into polyurethane elastomer and the stretching of polyurethane films caused increase in the phosphorescence emission intensity due to suppression of ligand exchange. Moreover, a derivative of the mechanophore in which more sterically hindered co-ligand was developed and stretching of polyurethane film causes changes in the emission color owing to the changes in the distance between Cu^+ cation center and non-coordinating PF_6^- or BF_4^- counterions (Figure 1-9).[75]

Very recently, Raisch and Sommer et al. reported a new donor-acceptor torsional spring-like mechanophore based on *ortho*-substituted diketopyrrolopyrole.[72] The

mechanophore shows a red shift in absorption and emission bands upon deformation of the polymer due to planarization of diketopyrrolopyrole (Figure 1-10).

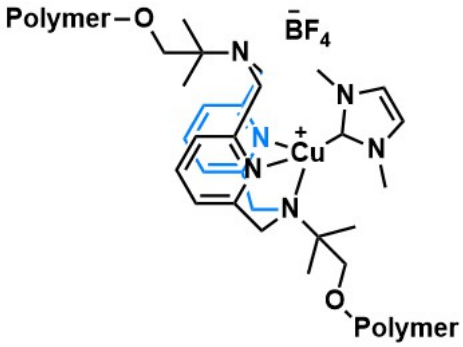

Filonenko, 2018

Figure 1-9. Molecular structure of the organocopper-based mechanophore.

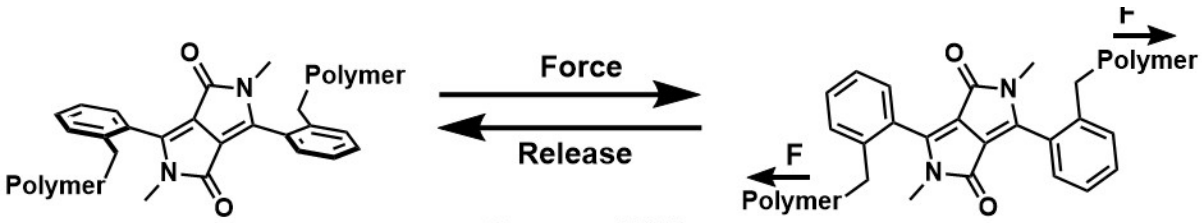

Sommer, 2021

Figure 1-10. Activation of torsional spring based mechanophore.

Recently, Saito group reported a FLAP mechanophore which exhibits dual fluorescence between interchangeable bent and planar conformations (Figure 1-11a).[70] The FLAP mechanophore consists of a central cyclooctatetraene (COT) ring bearing anthraceneimide wings. The polyurethane elastomer in which FLAP molecule is chemically doped exhibits blue emission from the bent conformation in the force-free state. The mechanical stretching induces compulsory planarization and causes increase of green emission Following the work, Saito and coworkers modified the FLAP molecule, the anthraceneimide wings were replaced with pyreneimide wings (Figure 1-11b).[71] The new FLAP mechanophore exhibited mechanical stretching induced emission color change from green to blue due to planarization of FLAP molecule.

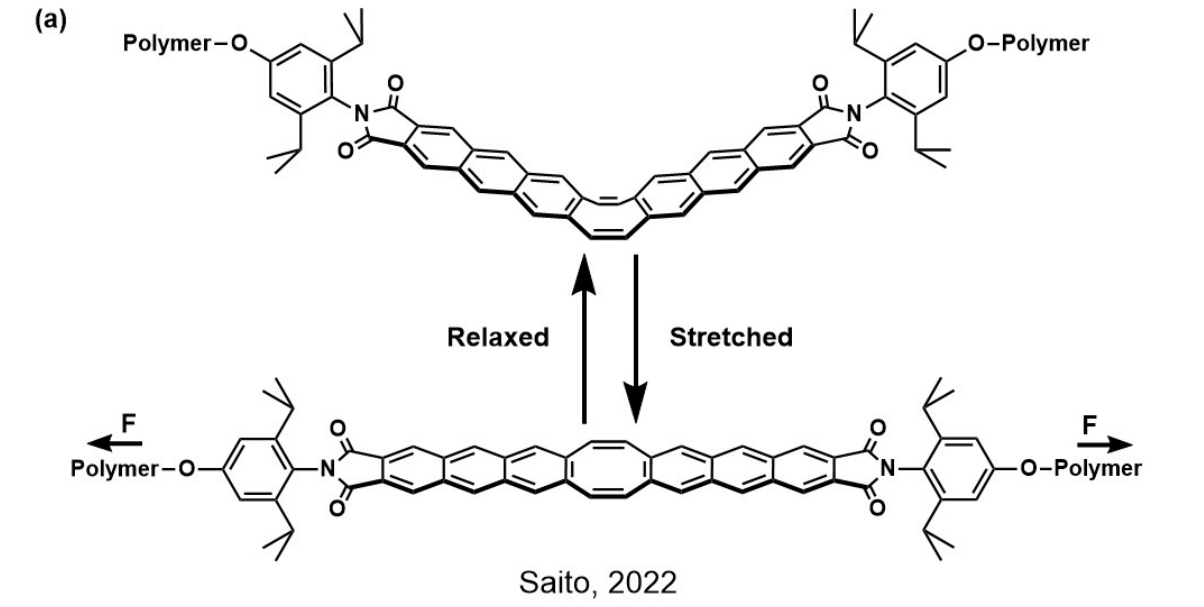

Saito, 2022

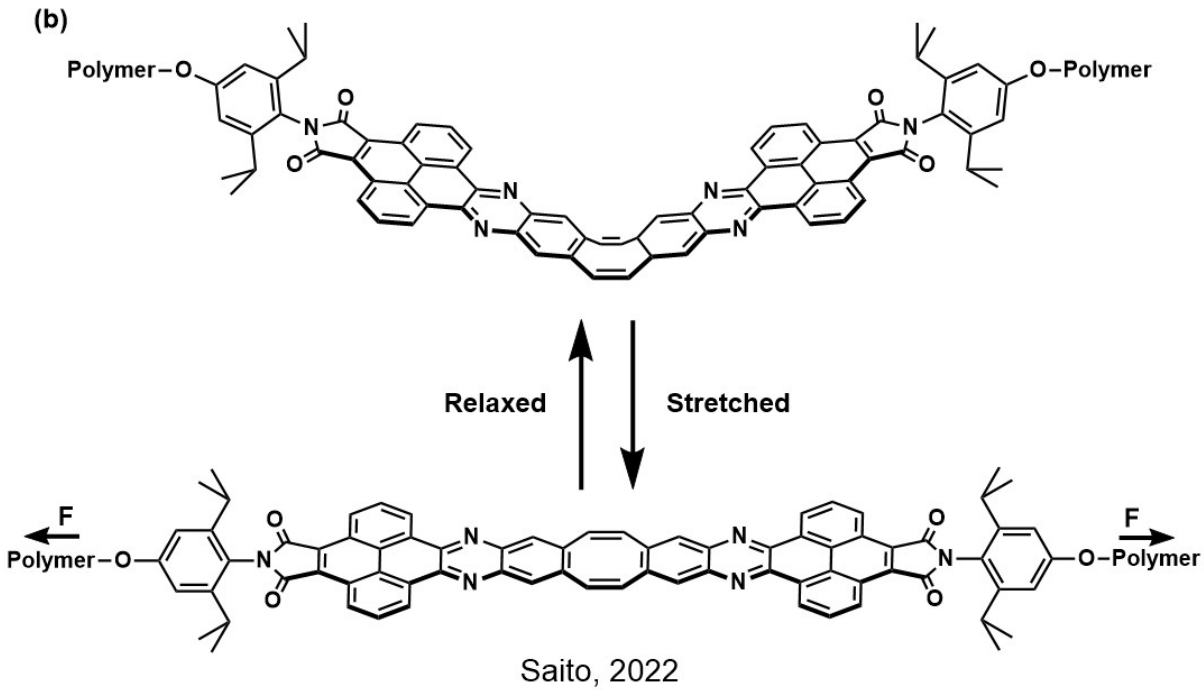

Saito, 2022

Mechanophores exhibiting shift in the absorption and emission spectra by controlling the ESIPT efficiency was recently reported by Ma and coworkers (Figure 1-12).[81] The group developed [(2-hydroxyphenyl)benzimidazole] mechanophore. The mechanophore that exhibits characteristic dual emission between enol and keto forms was covalently incorporated to

polyurethane elastomer. Stretching of polyurethane films caused increase in enol emission due to force-induced change in the dihedral angle between donor and acceptor.

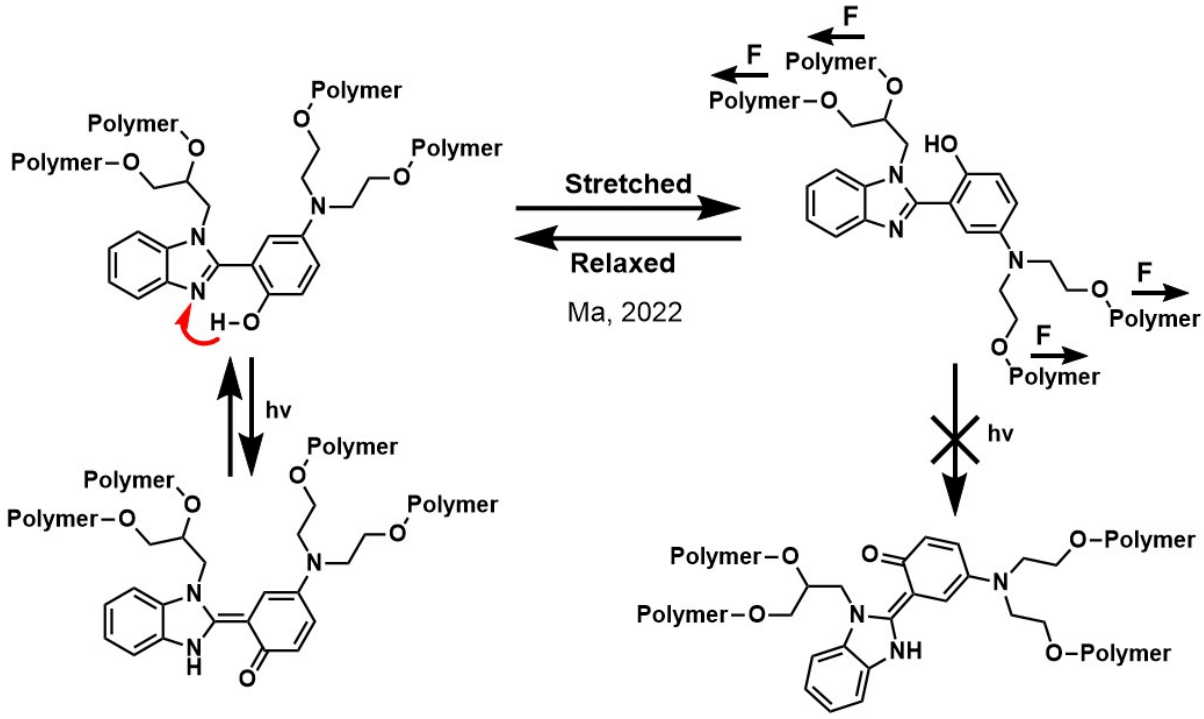

Figure 1-12. Activation of ESIPT based mechanophore.

1.2.3 Supramolecular Mechanophores

The supramolecular mechanophores are a special category of mechanophores working without covalent bond scission. In the supramolecular mechanophores, the π-π interactions or charge-transfer interactions are strategically developed to prepare materials that can show clear and visually discernible emission color changes to the applied mechanical force.

Sagara group exploited the shuttling function of rotaxane to develop rotaxane-based supramolecular mechanophores exhibiting on-off switching of luminescence.[82–85] In 2018, their group reported the first example of rotaxane-based supramolecular mechanophore (Figure 1-13,14).[82] The mechanophore consists of a ring featuring a π-extended benzothiadiazole luminophore and a dumbbell shaped molecule having naphthalene diimide quencher which are

interlocked together. In the force-free state, the luminophore emission is completely quenched due to the charge-transfer interaction between the luminophore and quencher. The force induced spatial separation of luminophore and quencher caused luminescence turn on. The mechanophore was covalently integrated into polyurethane elastomer to study the mechanoresponsive luminescence behavior. The polyurethane films in which the rotaxane is covalently integrated did not exhibit luminophore emission in the force-free state. A strong green emission from the benzothiadiazole luminophore was generated upon uniaxial tensile deformation of the polyurethane films. The instantly reversible on-off switching of the luminophore emission was observed for several stretching and relaxation cycles. Furthermore, Sagara group developed a series of rotaxane-based supramolecular mechanophores by using the luminophores π-extended anthracene (green emission), pyrene (blue emission), or 4-(dicyanomethylene)-2-methyl-6-(4-dimethylaminostyryl)-4*H*-pyran (DCM) (orange emission) and NDI quencher.(Figure 1-15). [83] All the three rotaxanes exhibited reversible on-off switching of their respective luminophore emission upon deformation. Moreover, the group developed a polyurethane elastomer by physically blending the three different polyurethanes in appropriate ratio. The polyurethane film exhibited white luminescence upon stretching (Figure 1-16).

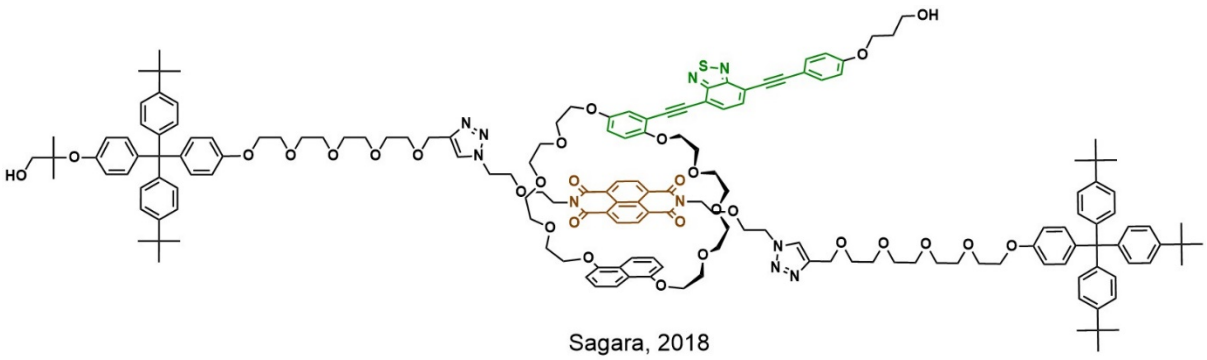

Figure 1-13. Molecular structure of the first rotaxane-based mechanophore having benzothiadiazole luminophore and naphthalene diimide quencher.

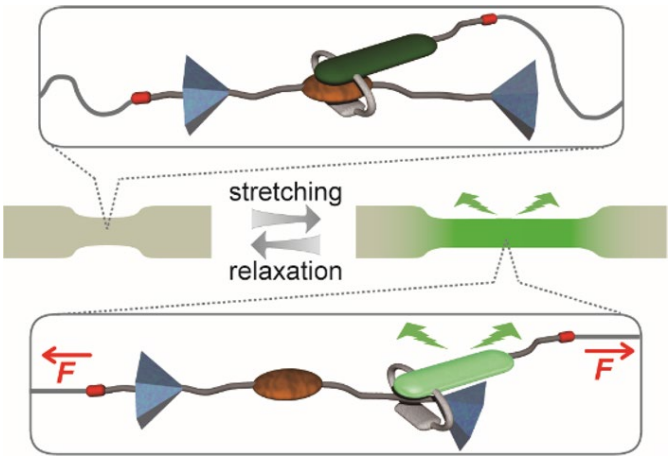

Figure 1-14. Operating principle of rotaxane-based mechanophore having benzothiadiazole luminophore and naphthalene diimide quencher.

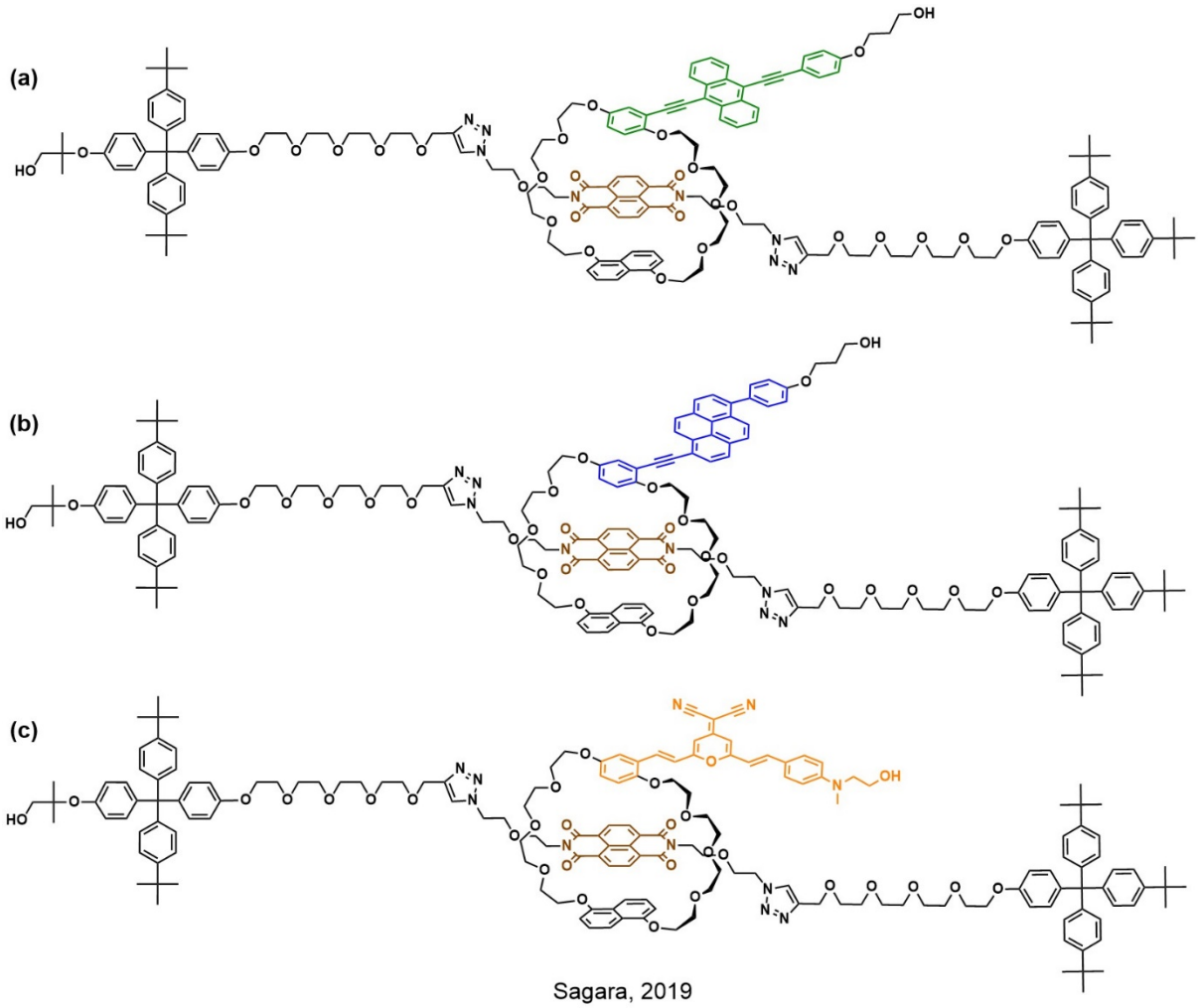

Figure 1-15. Molecular structures of rotaxane-based mechanophores with naphthalene diimide quencher and different luminophores (a) π-extended anthracene; (b) π-extended pyrene; and (c) 4-(dicyanomethylene)-2-methyl-6-(4-dimethylaminostyryl)-4*H*-pyran.

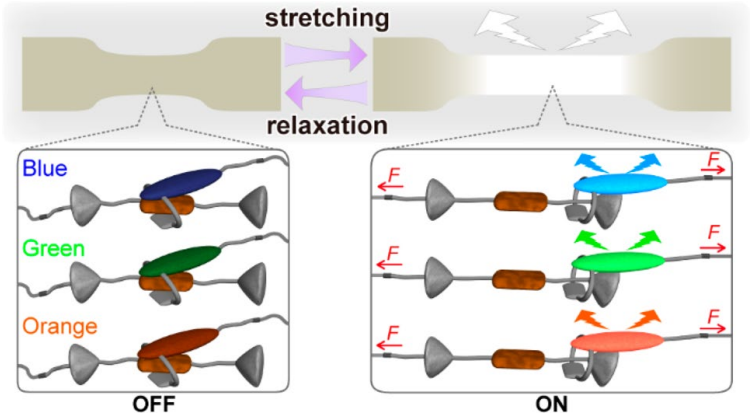

Figure 1-16. Schematic illustration of deformation of polyurethane film that exhibits white emission in the stretched state.

Imato and co-workers reported a new fluorescence turn-on, irreversible loop-like mechanophore exploiting the charge-transfer complexes (Figure 1-17).[86] The mechanophore contains a luminescent pyrene derivative and two naphthalene diimide (NDI) groups. The luminophore and quenchers are connected by short flexible linkers. The mechanophore was covalently integrated into the backbone of polycaprolactone chain. The charge-transfer interactions between electron rich pyrene and electron deficient NDI groups caused the complete quenching of luminophore emission and hence no emission was observed from the polymer film in the force-free state. The stretching of polymer films lead to irreversible turn on of monomer emission due to the disruption of charge transfer complex and spatial separation of luminophore and quenchers.

Recently, Weder's group reported a loop-forming mechanophore having the excimer-forming perylene diimide dye (PDI) (Figure 1-18).[87,88] The mechanophore consists of two PDI moieties which are covalently connected by a short linker, and the motif was covalently incorporated to PDI using atom transfer radical polymerization reaction.[87] The PDIs form folded loops due to the strong π-π interactions. The loops exhibited orange excimer-dominated emission in the force-free state of the polymer and the intensity of green monomer emission increased owing the unfolding of PDI luminophores. The mechanophore exhibited reversible

mechanoresponsive luminescence behavior. The detailed study and characterization show that the mechanochromic response purely depends on the applied strain.

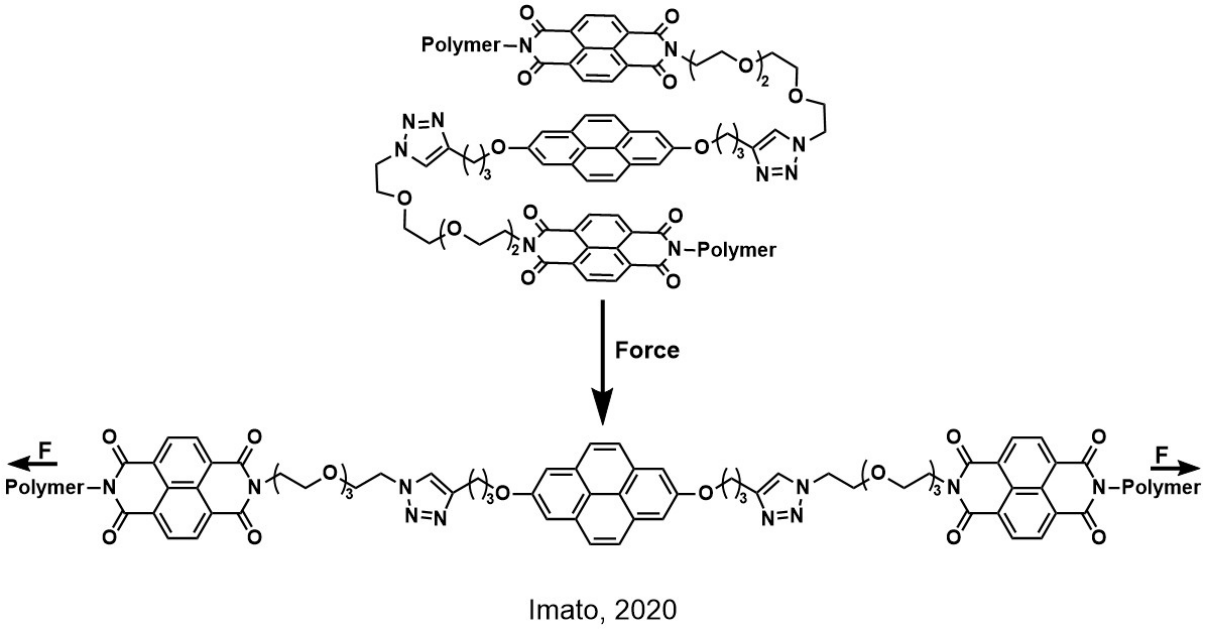

Imato, 2020

Figure 1-17. Activation of charge-transfer complex-based mechanophore.

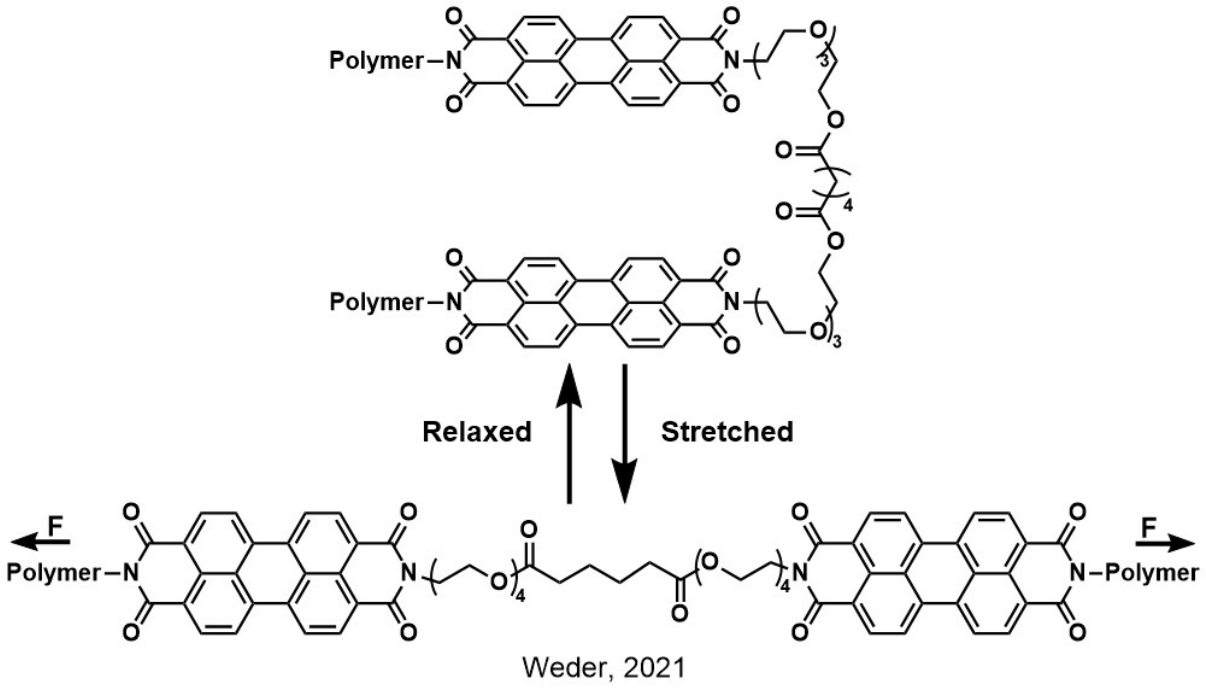

Weder, 2021

Figure 1-18. Activation of loop-based mechanophore.

1.3 Cyclophanes

Charles Pederson discovered the first polyether macrocyclic compound dibenzo[18]crown-6.[89] After the development of crown ethers by Pederson, Donald Cram and Jean-Marie Lehn utilized the macrocyclic compounds for establishing the research fields, host-guest chemistry and supramolecular chemistry. Three scientists shared the Nobel prize in chemistry in 1987 for their pioneer contributions. Cyclophanes are organic compounds in which two or more atoms of an aromatic ring are incorporated into a cyclic structure. Cram and coworkers reported paracyclophanes and metacylophanes as the initial developments in the cyclophane chemistry.[90–92] So far, several cyclophane derivatives have been reported, such as cycobis(paraquat-*p*-phenylene),[93] cycloparapenylenes,[94] calixarenes (Figure 1-19a),[95] oxacalixarenes,[96] resorcinarenes (Figure 1-19b),[97] calixpyrolles,[98] and pillarenes.[99] Fluorescence cyclophanes possess several applications including sensors, bioimaging, optoelectronics, catalysis, and drug delivery.[100] Sagara and coworkers have reported mechanoresponsive luminescent cyclophanes that exhibit mechanically induced emission color changes in the bulk states (Figure 1-20).[101–104] Several cyclophanes have been reported to exhibit charge-transfer interactions between electron donating and electron accepting aromatic rings (Figure 1-21).[105–106]

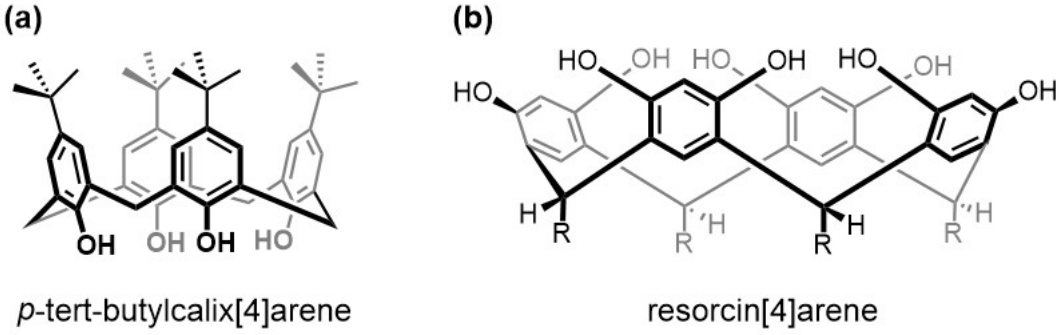

Figure 1-19. Molecular structures of (a) *p*-tert-butylcalix[4]arene and (b) resorcin[4]arene.

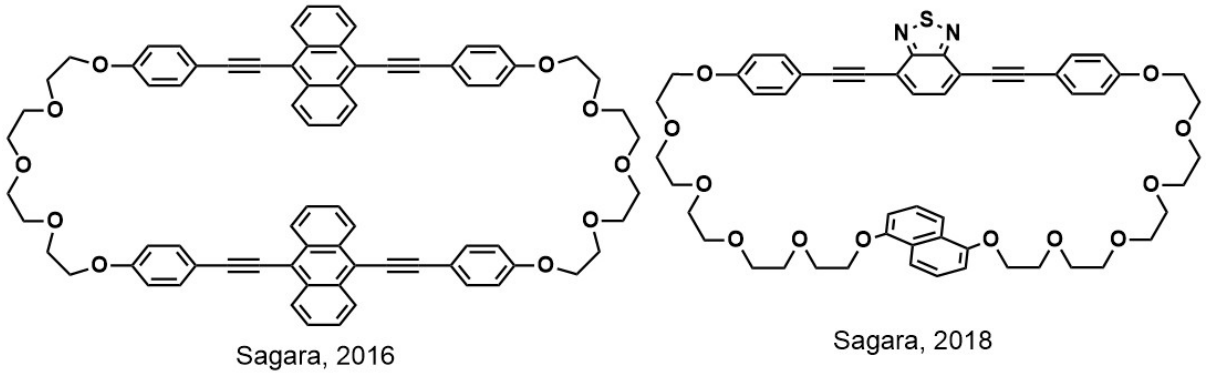

Figure 1-20. Molecular structures of cyclophane-based mechanochromic mechanophores.

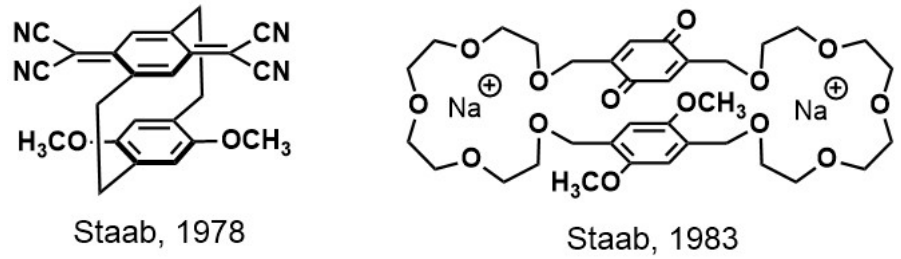

Figure 1-21. Molecular structures of cyclophanes forming charge-transfer complexes.

1.3.1 Cyclophane-based Supramolecular Mechanophores

Recently, Sagara and coworkers reported a cyclophane-based supramolecular mechanophore which contains two 1,6-bis(phenylethynyl)pyrene luminophores (Figure 1-22,23).[107] Even though several mechanochromic luminescent cyclophanes have been reported to show emission color changes in bulk crystalline or liquid crystalline state.[101–104] The cyclophane exhibits intramolecular green excimer emission in the force-free state. The application of mechanical forces caused spatial separation of monomers in the cyclophane, and emission became blue monomer emission. The stretching of polyurethane elastomer that contains covalently incorporated cyclophane exhibited instantly reversible change in emission color between excimer-dominated cyan and monomer-dominated blue. However, emission color change is not so clear for the polyurethane films because the cyclophane is kinetically trapped into arrangement where the luminophore cannot form excimer.

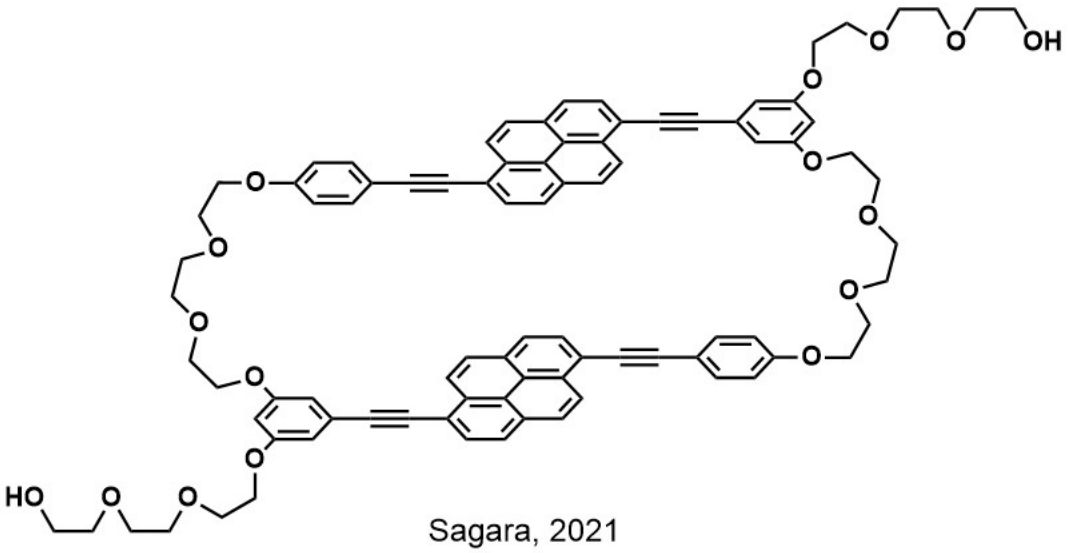

Figure 1-22. Molecular structure of the first cyclophanes-based supramolecular mechanophore.

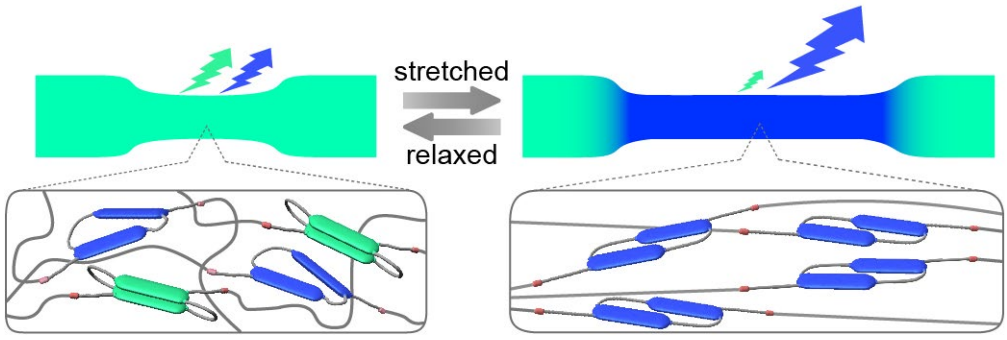

Figure 1-23. Operating principle of cyclophane-based mechanophore having two 1,6-bis(phenylethynyl)pyrene luminophores that is covalently introduced into polyurethane elastomer.

1.4 Objectives and Outline of This Thesis

The aim of this thesis is to develop cyclophane-based supramolecular mechanophores utilizing charge-transfer interactions. As I already discussed in the previous sections, the mechanochromic mechanophores are reliable molecular probes for the easy and discernible detection of polymer failures owing to the changes in the absorption and/or photoluminescence properties. Activation of mechanophores can be done by applying mechanical forces through grinding, stretching, compression, and sonication methods. Many mechanophores have been reported to require covalent bond scission for the activation. Such mechanophores have the drawbacks of high activation energy and most of the such mechanophores are irreversible in nature.

Supramolecular mechanophores can be activated without covalent bond scission and are based on altering π-π interactions or charge-transfer (CT) interactions in the molecules, which leads to changes in the photophysical properties. Additionally, the supramolecular mechanophores possess the advantages of instant reversibility and low activation energy. However, the number of supramolecular mechanophores is still limited.

I developed a cyclophane-based supramolecular mechanophore that contains a 1,6-bis(phenylethynyl)pyrene luminophore and a pyromellitic diimide quencher. A polyurethane elastomer containing the mechanophore displays orange emission in the absence of force, which is dominated by the CT-emission. Uniaxial tensile stretching causes ratiometric changes in emission color, due to the spatial separation between the luminophore and quencher. The response is rapid and reversible in nature.

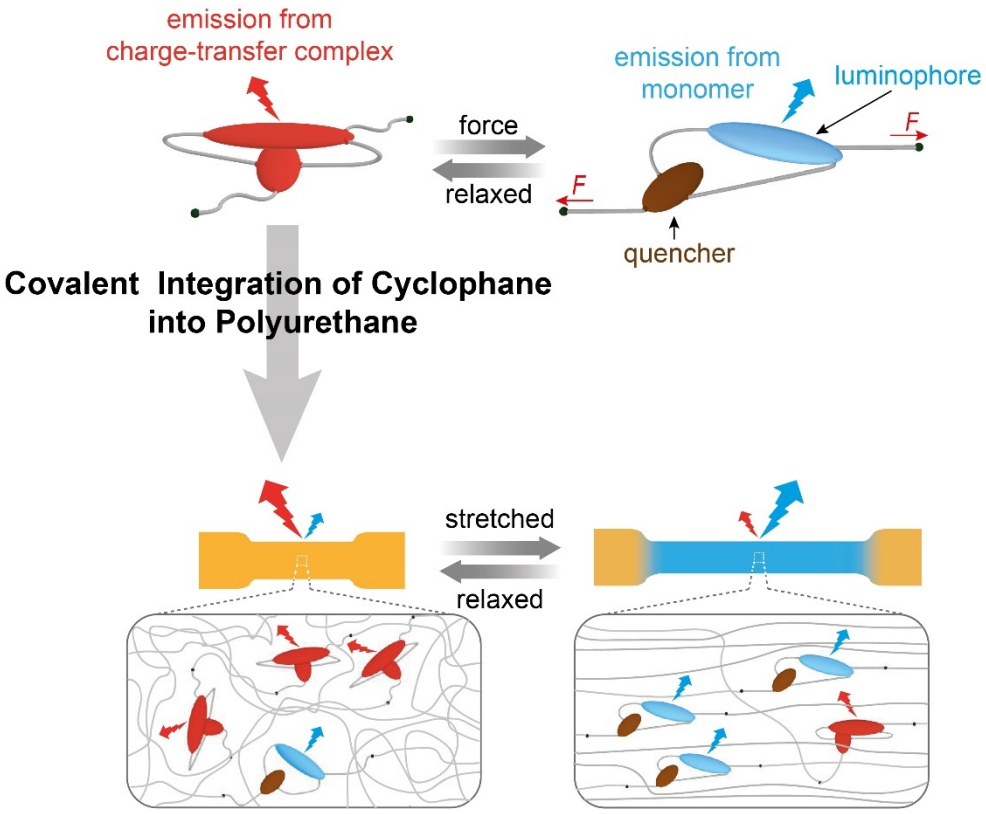

The thesis contains three chapters including general introduction and conclusions. In the first chapter, I discuss a general introduction and background studies of mechanophores.

In the second chapter, I discuss the synthesis, characterization and the mechanoresponsive luminescence behavior of cyclophane-based supramolecular mechanophores. The photophysical properties of cyclophane and a linear reference compound having one luminophore and quencher is also discussed. Furthermore, I explain the procedure for the covalent integration of both cyclophane and linear reference compounds into different polyurethane elastomers and preparation of polymer films using solvent casting method. Subsequently, I discuss the photophysical properties, thermal properties, mechanical properties, and deformation studies of the polyurethane films.

In the third chapter of the thesis, I discuss the general summary of the thesis and prospects of cyclophane-based supramolecular mechanophores.

1.5 References

[1] M. M. Caruso, D. A. Davis, Q. Shen, S. A. Odom, N. R. Sottos, S. R. White, J. S. Moore, *Chem. Rev.* **2009**, *109*, 5755–5798.

[2] J. Li, C. Nagamani, J. S. Moore, *Acc. Chem. Res.* **2015**, *48*, 2181–2190.

[3] G. De Bo, *Macromolecules* **2020**, *53*, 7615–7617.

[4] H. Traeger, D. J. Kiebala, C. Weder, S. Schrettl, *Macromol. Rapid Commun.* **2021**, *42*, 2000573.

[5] Y. Chen, G. Mellot, D. van Luijk, C. Creton, R. P. Sijbesma, *Chem. Soc. Rev*. **2021**, *50*, 4100–4140.

[6] S. He, M. Stratigaki, S. P. Centeno, A. Dreuw, R. Göstl, *Chem. Eur. J.* **2021**, *27*, 15889−15897.

[7] M. Xuan, C. Schumacher, C. Bolm, R. Göstl, A. Herrmann, *Adv. Sci.* **2022**, *9*, 2105497.

[8] G. Kaupp, CrystEngComm **2009**, *11*, 388–403.

[9] P. A. May and J. S. Moore, *Chem. Soc. Rev.* **2013**, *42*, 7497–7506.

[10] J. Liang and J. M. Fernandez, ACS Nano **2009**, *3*, 1628–1645.

[11] Y. Liu and G. J. Vancso, *Prog. Polym. Sci.* **2020**, *104*, 101232.

[12] C. Matellan, A. E. del Río Hernández, *ACS Biomater. Sci. Eng.* **2019**, *5*, 3703–3719.

[13] C. Grashoff, B. D. Hoffman, M. D. Brenner, R. Zhou, M. Parsons, M. T. Yang, M. A. McLean, S. G. Sligar, C. S. Chen, T. Ha, M. A. Schwartz, *Nature* **2010**, *466*, 263−266.

[14] M. Morimatsu, A. H. Mekhdjian, A. S. Adhikari, A. R. Dunn, *Nano Lett.* **2013**, *13*, 3985−3989.

[15] T. Iskratsch, H. Wolfenson, M. P. Sheetz, *Nat. Rev. Mol. Cell Biol.* **2014**, *14*, 825–833.

[16] Y. Zhang, C. Ge, C. Zhu, K. Salaita, *Nat. Commun.* **2014**, *5*, 5167.

[17] A. Freikamp, A.-L. Cost, C. Grashoff, *Trends Cell Biol.* **2016**, *26*, 838–847.

[18] Y. Liu, K. Galior, V. P.-Y. Ma, K. Salaita, *Acc. Chem. Res.* **2017**, *50*, 2915–2924.

[19] J. M. Brockman, A. T. Blanchard, V. P.-Y. Ma, W. D. Derricotte, Y. Zhang, M. E. Fay, W. A. Lam, F. A. Evangelista, A. L. Mattheyses, K. Salaita, *Nat. Methods* **2017**, *15*, 115.

[20] M. K. Beyer, *J. Chem. Phys.* **2000**, *112*, 7307–7312.

[21] H. Staudinger, H. F. Bondy, *Ber. Dtsch. Chem. Ges. B* **1930**, *63*, 734−736.

[22] H. Staudinger, E. O. Leupold, *Ber. Dtsch. Chem. Ges. B* **1930**, *63*, 730−733.

[23] H. W. Melville, A. J. R. Murray, *Trans. Faraday Soc.* **1950**, *46*, 996−1009.

[24] K. L. Berkowski, S. L. Potisek, C. R. Hickenboth, J. S. Moore, *Macromolecules* **2005**, *38*, 8975−8978.

[25] A. B. Versaw, T. Zeng, X. Hu, M. J. Robb, *J. Am. Chem. Soc.* **2021**, *143*, 21461−21473.

[26] A. Piermattei, S. Karthikeyan and R. P. Sijbesma, *Nat. Chem.* **2009**, *1*, 133–137.

[27] X. Hu, T. Zeng, C. C. Husic and M. J. Robb, *J. Am. Chem. Soc.* **2019**, *141*, 15018–15023.

[28] D. A. Davis, A. Hamilton, J. Yang, L. D. Cremar, D. Van Gough, S. L. Potisek, M. T. Ong, P. V. Braun, T. J. Martinez, S. R. White, J. S. Moore, N. R. Sottos, *Nature* **2009**, *459*, 68−72.

[29] C. K. Lee, D. A. Davis, S. R. White, J. S. Moore, N. R. Sottos, P. V. Braun, *J. Am. Chem. Soc.* **2010**, *132*, 16107−16111.

[30] T. A. Kim, M. J. Robb, J. S. Moore, S. R. White, N. R. Sottos, *Macromolecules* **2018**, *51*, 9177−9183.

[31] Y. Lin, M. H. Barbee, C.-C. Chang, S. L. Craig, *J. Am. Chem. Soc.* **2018**, *140*, 15969−15975.

[32] H. Zhang, F. Gao, X. Cao, Y. Li, Y. Xu, W. Weng, R. Boulatov, *Angew. Chem. Int. Ed.* **2016**, *55*, 3040–3044.

[33] M. J. Robb, T. A. Kim, A. J. Halmes, S. R. White, N. R. Sottos, J. S. Moore, *J. Am. Chem. Soc.* **2016**, *138*, 12328–12331.

[34] M. E. McFadden, M. J. Robb, *J. Am. Chem. Soc.* **2019**, *141*, 11388–11392.

[35] M. E. McFadden, M. J. Robb, *J. Am. Chem. Soc*. **2021**, *143*, 7925−7929.

[36] J. R. Hemmer, C. Rader, B. D. Wilts, C. Weder, J. A. Berrocal, *J. Am. Chem. Soc.* **2021**, *143*, 18859−18863.

[37] Y. Chen, A. J. H. Spiering, S. Karthikeyan, G. W. M. Peters, E. W. Meijer, R. P. Sijbesma, *Nat. Chem.* **2012**, *4*, 559−562.

[38] E. Ducrot, Y. Chen, M. Bulters, R. P. Sijbesma, C. Creton, *Science* **2014**, *344*, 186−189.

[39] Z. Chen, J. A. M. Mercer, X. Zhu, J. A. H. Romaniuk, R. Pfattner, L. Cegelski, T. J. Martinez, N. Z. Burns, Y. Xia, *Science* **2017**, *357*, 475−479.

[40] J. K. Su, J. D. Feist, J. Yang, J. A. M. Mercer, J. A.H. Romaniuk, Z. Chen, L. Cegelski, N. Z. Burns, Y. Xia, *J. Am. Chem. Soc.* **2018**, *140*, 12388−12391.

[41] J. Yang, M. Horst, J. A. H. Romaniuk, Z. Jin, L. Cegelski, Y. Xia, *J. Am. Chem. Soc.* **2019**, *141*, 6479−6483.

[42] M. Horst, J. Yang, J. Meisner, T. B. Kouznetsova, T. J. Martínez, S. L. Craig, Y. Xia, *J. Am. Chem. Soc.* **2021**, *143*, 12328−12334.

[43] Y.-K. Song, K.-H. Lee, W.-S. Hong, S.-Y. Cho, H.-C. Yu, C.-M. Chung, *J. Mater. Chem.* **2012**, 22, 1380–1386.

[44] D. C. Church, G. I. Peterson, A. J. Boydston, *ACS Macro Lett.* **2014**, *3*, 648–651.

[45] C. P. Kabb, C. S. O'Bryan, C. D. Morley, T. E. Angelini, B. S. Sumerlin, *Chem. Sci.* **2019**, *10*, 7702–7708.

[46] H. Li, R. Göstl, M. Delgove, J. Sweeck, Q. Zhang, R. P. Sijbesma, J. P. A. Heuts, *ACS Macro Lett.* **2016**, *5*, 995–998.

[47] J. Li, T. Shiraki, B. Hu, R. A. Wright, B. Zhao, J. S. Moore, *J. Am. Chem. Soc.* **2014**, *136*, 15925–15928.

[48] G. I. Peterson, J. Lee, T.-L. Choi, *Macromolecules* **2019**, *52*, 9561–9568.

[49] A. R. Sulkanen, J. Sung, M. J. Robb, J. S. Moore, N. R. Sottos, G. Y. Liu, *J. Am. Chem. Soc.* **2019**, *141*, 4080–4085.

[50] S. S. M. Konda, J. N. Brantley, B. T. Varghese, K. M. Wiggins, C. W. Bielawski, D. E. Makarov, *J. Am. Chem. Soc.* **2013**, *135*, 12722–12729.

[51] R. Göstl, R. P. Sijbesma, *Chem. Sci.*, **2016**, *7*, 370–375.

[52] Z. Wang, Z. Ma, Y. Wang, Z. Xu, Y. Luo, Y. Wei, X. Jia, *Adv. Mater.* **2015**, *27*, 6469–6474.

[53] T. Wang, N. Zhang, J. Dai, Z. Li, W. Bai, R. Bai, *ACS Appl. Mater. Interfaces* **2017**, *9*, 11874–11881.

[54] Z. S. Kean, G. R. Gossweiler, T. B. Kouznetsova, G. B. Hewage, S. L. Craig, *Chem. Commun.* **2015**, *51*, 9157–9160.

[55] M. Karman, E. Verde-Sesto, C. Weder, Y. C. Simon, *ACS Macro Lett.* **2018**, *7*, 1099–1104.

[56] M. Karman, E. Verde-Sesto, C. Weder, *ACS Macro Lett.* **2018**, *7*, 1028–1033.

[57] K. Imato, A. Irie, T. Kosuge, T. Ohishi, M. Nishihara, A. Takahara, H. Otsuka, *Angew. Chem. Int. Ed.* **2015**, *54*, 6168−6172.

[58] T. Kosuge, X. Zhu, V. M. Lau, D. Aoki, T. J. Martinez, J. S. Moore, H. Otsuka, *J. Am. Chem. Soc.* **2019**, *141*, 1898−1902.

[59] S. Kato, S. Furukawa, D. Aoki, R. Goseki, K. Oikawa, K. Tsuchiya, N. Shimada, A. Maruyama, K. Numata, H. Otsuka, *Nat. Commun.* **2021**, *12*, 126.

[60] K. Seshimo, S. Hio, W. Takuma, A. Daisuke, S. Hajime, M. Koichiro, M. Yuchen, I. Akira, N. Shotaro, K. Takashi, I. Hiroshi, O. Hideyuki, *Angew. Chem. Int. Ed.* **2021**, *60*, 8406−8409.

[61] Y. Lu, H. Sugita, K. Mikami, D. Aoki, H. Otsuka, *J. Am. Chem. Soc.* **2021**, *143*, 17744−17750.

[62] T. Sumi, R. Goseki, H. Otsuka, *Chem. Commun.* **2017**, *53*, 11885.

[63] K. Ishizuki, D. Aoki, R. Goseki, H. Otsuka, *ACS Macro Lett.* **2018**, *7*, 556–560.

[64] H. Sakai, D. Aoki, K. Seshimo, K. Mayumi, S. Nishitsuji, T. Kurose, H. Ito, H. Otsuka, *ACS Macro Lett.* **2020**, *9*, 1108–1113.

[65] F. Verstraeten, R. Göstl, R. P. Sijbesma, *Chem. Commun.* **2016**, *52*, 8608–8611.

[66] Q. Verolet, A. Rosspeintner, S. Soleimanpour, N. Sakai, E. Vauthey, S. Matile, *J. Am. Chem. Soc.* **2015**, *137*, 15644−15647.

[67] A. Colom, E. Derivery, S. Soleimanpour, C. Tomba, M. Dal Molin, N. Sakai, M. González-Gaitán, S. Matile, A. Roux, *Nat. Chem.* **2018**, *10*, 1118−1125.

[68] J. García-Calvo, J. Maillard, I. Fureraj, K. Strakova, A. Colom, V. Mercier, A. Roux, E. Vauthey, N. Sakai, *J. Am. Chem. Soc.*, **2020**, *142*, 12034–12038.

[69] T. Yamakado, K. Otsubo, A. Osuka, S. Saito, *J. Am. Chem. Soc.* **2018**, *140*, 6245–6248.

[70] R. Kotani, S. Yokoyama, S. Nobusue, S. Yamaguchi, A. Osuka, H. Yabu, S. Saito, *Nat. Commun.* **2022**, *13*, 303.

[71] T. Yamakado, S. Saito, *J. Am. Chem. Soc.* **2022**, *144*, 2804−2815.

[72] M. Raisch, W. Maftuhin, M. Walter, M. A. Sommer, *Nat. Commun.* **2021**, *12*, 4243.

[73] G. A. Filonenko, J. R. Khusnutdinova, *Adv. Mater.* **2017**, *22*, 1700563.

[74] G. A. Filonenko, J. A. M. Lugger, C. Liu, E. P. A. van Heeswijk, M. M. R. M. Hendrix, M. Weber, C. Müller, E. J. M. Hensen, R. P. Sijbesma, E. A. Pidko, *Angew. Chem. Int. Ed.* **2018**, *57*, 16385.

[75] G. A. Filonenko, D. Sun, M. Weber, C. Müller, E. A. Pidko, *J. Am. Chem. Soc.* **2019**, *141*, 9687−9692.

[76] N. Bruns, K. Pustelny, L. M. Bergeron, T. A. Whitehead, D. S. Clark, *Angew. Chem. Int. Ed.* **2009**, *48*, 5666−5669.

[77] M. Taki, T. Yamashita, K. Yatabe, V. Vogel, *Soft Matter* **2019**, *15*, 9388−9393.

[78] R. Merindol, G. Delechiave, L. Heinen, L. H. Catalani, A. Walther, *Nat. Commun.* **2019**, *10*, 528.

[79] R. Glazier, J. M. Brockman, E. Bartle, A. L. Mattheyses, O. Destaing, K. Salaita, *Nat. Commun.* **2019**, *10*, 4507.

[80] S. Ogi, K. Sugiyasu, M. Takeuchi, *Bull. Chem. Soc. Jpn.* **2011**, *84*, 40−48.

[81] H. Hu, X. Cheng, Z. Ma, R. P. Sijbesma, Z. Ma, *J. Am. Chem. Soc.* **2022**, *144*, 9971−9979.

[82] Y. Sagara, M. Karman, E. Verde-Sesto, K. Matsuo, Y. Kim, N. Tamaoki, C. Weder, *J. Am. Chem. Soc.* **2018**, *140*, 1584−1587.

[83] Y. Sagara, M. Karman, A. Seki, M. Pannipara, N. Tamaoki, C. Weder, *ACS Cent. Sci.* **2019**, *5*, 874−881.

[84] T. Muramatsu, Y. Sagara, H. Traeger, N. Tamaoki, C. Weder, *ACS Appl. Mater. Interfaces* **2019**, *11*, 24571−24576.

[85] T. Muramatsu, Y. Okado, H. Traeger, S. Schrettl, N. Tamaoki, W. Weder, Y. Sagara, *J. Am. Chem. Soc.* **2021**, *143*, 9884−9892.

[86] K. Imato, R. Yamanaka, H. Nakajima, N. Takeda, *Chem. Commun.* **2020**, *56*, 7937−7940.

[87] H. Traeger, Y. Sagara, D. J. Kiebala, S. Schrettl, C. Weder, *Angew. Chem. Int. Ed.* **2021**, *60*, 16191−16199.

[88] H. Traeger, Y. Sagara, J. A. Berrocal, S. Schrettl, C. Weder, *Polym. Chem.* **2022**, *13*, 2860−2869.

[89] C. J. Pedersen, *J. Am. Chem. Soc.* **1967**, *89*, 2495–2496.

[90] D. J. Cram, H. Steinberg, *J. Am. Chem. Soc.* **1951**, *71*, 5692–5704.

[91] R. W. Griffin Jr., *Chem. Rev.* **1963**, *63*, 45–54.

[92] D. J. Cram, J. M. Cram, *Acc. Chem. Res.* **1971**, *4*, 204–213.

[93] E. J. Dale, N. A. Vermeulen, M. Jurı´cˇek, J. C. Barnes, R. M. Young, M. R. Wasielewski, J. F. Stoddart, *Acc. Chem. Res.* **2016**, *49*, 262–273.

[94] D. Wu, W. Cheng, X. Ban, J. Xia, *Asian J. Org. Chem.* **2018**, *7*, 2161–2181.

[95] A. von Baeyer, *Ber. Dtsch. Chem. Ges.* 1872, *5*, 280–282.

[96] K. Cottet, P. M. Marcos, P. J. Cragg, *Beilstein J. Org. Chem.* **2012**, *8*, 201–226.

[97] P. Timmerman, W. Verboom, D. N. Reinhoudt, *Tetrahedron*, **1996**, *52*, 2663–2704.

[98] S. K. Kim and J. L. Sessler, *Acc. Chem. Res.* **2014**, *47*, 2525–2536.

[99] M. Xue, Y. Yang, X. Chi, Z. Zhang, F. Huang, *Acc. Chem. Res.* **2012**, *45*, 1294–1308.

[100] I. Roy, A. H. G. David, P. J. Das, D. J. Pe, J. F. Stoddart, *Chem. Soc. Rev.* **2022**, 10.1039/d0cs00352b.

[101] Y. Sagara, Y. C. Simon, N. Tamaoki, C. Weder, *Chem. Commun.* **2016**, *52*, 5694–5697.

[102] Y. Sagara, C. Weder, N. Tamaoki, *Chem. Mater.* **2017**, *29*, 6145−6152.

[103] Y. Sagara, A. Seki, Y. Kim, N. Tamaoki, *J. Mater. Chem. C* **2018**, *6*, 8453.

[104] S. Shimizu, S. Thazhathethil, K. Takahashi, T. Nakamura, Y. Sagara, *Mol. Syst. Des. Eng.* **2021**, *6*, 1039–1046.

[105] H. A. Staab, H. -E. Menke, *Tetrahedron Lett.* **1978**, 1955.

[106] H. A. Staab, G. H. Knaus, H. -E. Menke, C. Krieger, *Chem. Ber.* **1983**, *116*, 2785.

[107] Y. Sagara, H. Traeger, J. Li, Y. Okado, S. Schrettl, N. Tamaoki, C. Weder, *J. Am. Chem. Soc.* **2021**, *143*, 5519−5525.

Chapter 2

Excited State Charge-Transfer Complexes Enable Fluorescence Color Changes in a Supramolecular Cyclophane Mechanophore

2.1 Introduction

Mechanochromic mechanophores, i.e., molecular entities whose optical properties change in response to mechanical force, allow detecting mechanical events in polymers, and are useful for mechanistic studies, sensing applications, and failure detection.[1–6] Numerous mechanophores that undergo mechanically activated bond scission have been reported.[7–32] There is also an increasing number of mechanophores that rely on changes in inter- and intramolecular interactions,[4] such as altering coordination states of metal complexes,[33,34] conformational changes of π-conjugated structures,[35–41] changing efficiency of fluorescence resonance energy transfer,[42–46] or controlling excited-state intramolecular proton transfer.[47] The activation of such mechanophores occurs generally at low force and is reversible. Besides, several motifs have been developed, whose mechanochromic response results from changing arrangements of π-conjugated moieties.[48–55] Most of them combine an emitter/quencher pair and the fluorescence is turned on upon mechanically triggered separation.[48–51] Examples of mechanophores which change their emission color are more limited.[52–54] This operating mode is attractive because the *ratiometric* signals produced are independent of the acquisition parameters. We demonstrated this operating mode with a cyclophane containing two identical, excimer-forming luminophores.[54] However, since the extent of excimer formation was limited in polymer, the mechanochromic luminescence was difficult to assess by the unassisted eye. We show here that this problem is overcome in a cyclophane-based mechanophore in which the intramolecular assembly of a blue-light emitting 1,6-bis(phenylethynyl)pyrene luminophore and a pyromellitic diimide (PMDI) quencher leads to the formation of a charge-transfer (CT) complex with reddish-orange emission (Figure 1a). An instantly reversible and easily detectable emission color change is observed when polyurethane elastomers containing the new mechanophore are deformed and the CT-complexes are separated (Figure 1b). This is

the first supramolecular mechanophore in which CT-complex emission is strategically exploited.

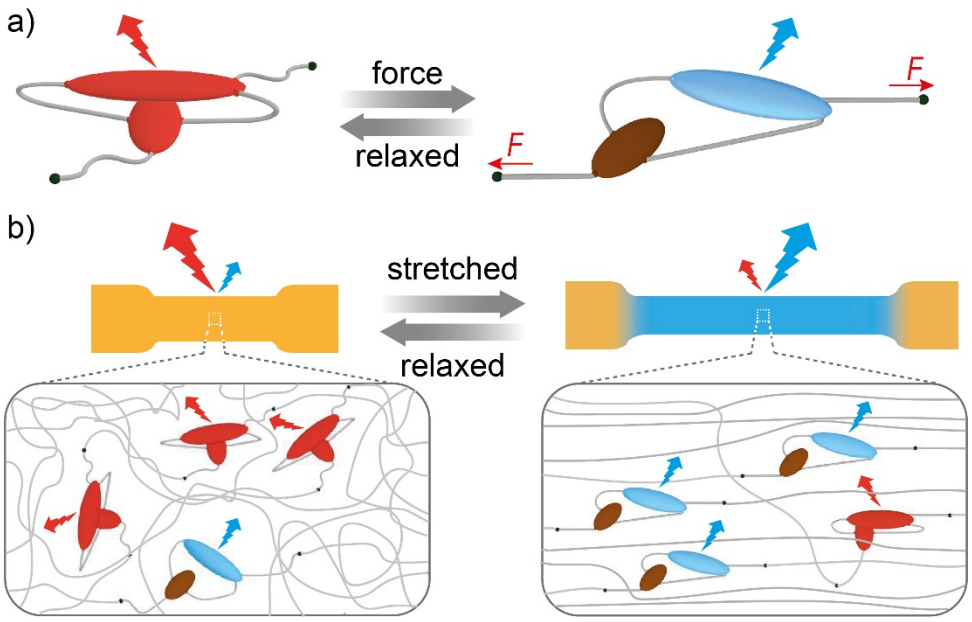

Figure 2-1. Depiction of a) the cyclophane-based mechanophore and b) its function in polymer. In the idle state, the luminophore (blue) and quencher (brown) form a CT-complex (red), which disassemble upon deformation.

2.2 Results and Discussion

2.2.1 Molecular Design

The cyclophane-based mechanophore **1** (Figure 2-2) contains the electron-rich 1,6-bis(phenylethynyl)pyrene motif, a widely used emitter with high quantum efficiency,[56–58] and the electron-deficient PMDI quencher, which forms CT-complexes with pyrene.[59,60] Triethylene glycol and ethylene glycol chains were attached to the luminophore and quencher, respectively, to allow the covalent incorporation of mechanophore **1** into polymers (Figure 2-2, Schemes 2-1,2-2). The key step in the synthesis of **1** is a Cu(I)-catalyzed Huisgen reaction[61] between a luminophore derivative carrying two alkynes and a PMDI featuring two 5-azidopentyls (Scheme 2-2). The high yield of this reaction (71%) is attributed to intramolecular CT-interactions between the luminophore and the PMDI. The linear reference compound **2** featuring the same luminophore and quencher and reference luminophore **3** were also prepared (Scheme 2-3). Compounds **1**–**3** were characterized by ^{1}H and ^{13}C NMR spectroscopy and high-resolution electrospray ionization mass spectrometry (see Experimental). The ^{1}H NMR signals corresponding to the pyrene protons of **1** are shifted upfield compared to those of **3**, due to pyrene-PDMI interactions (Figure 2-3).

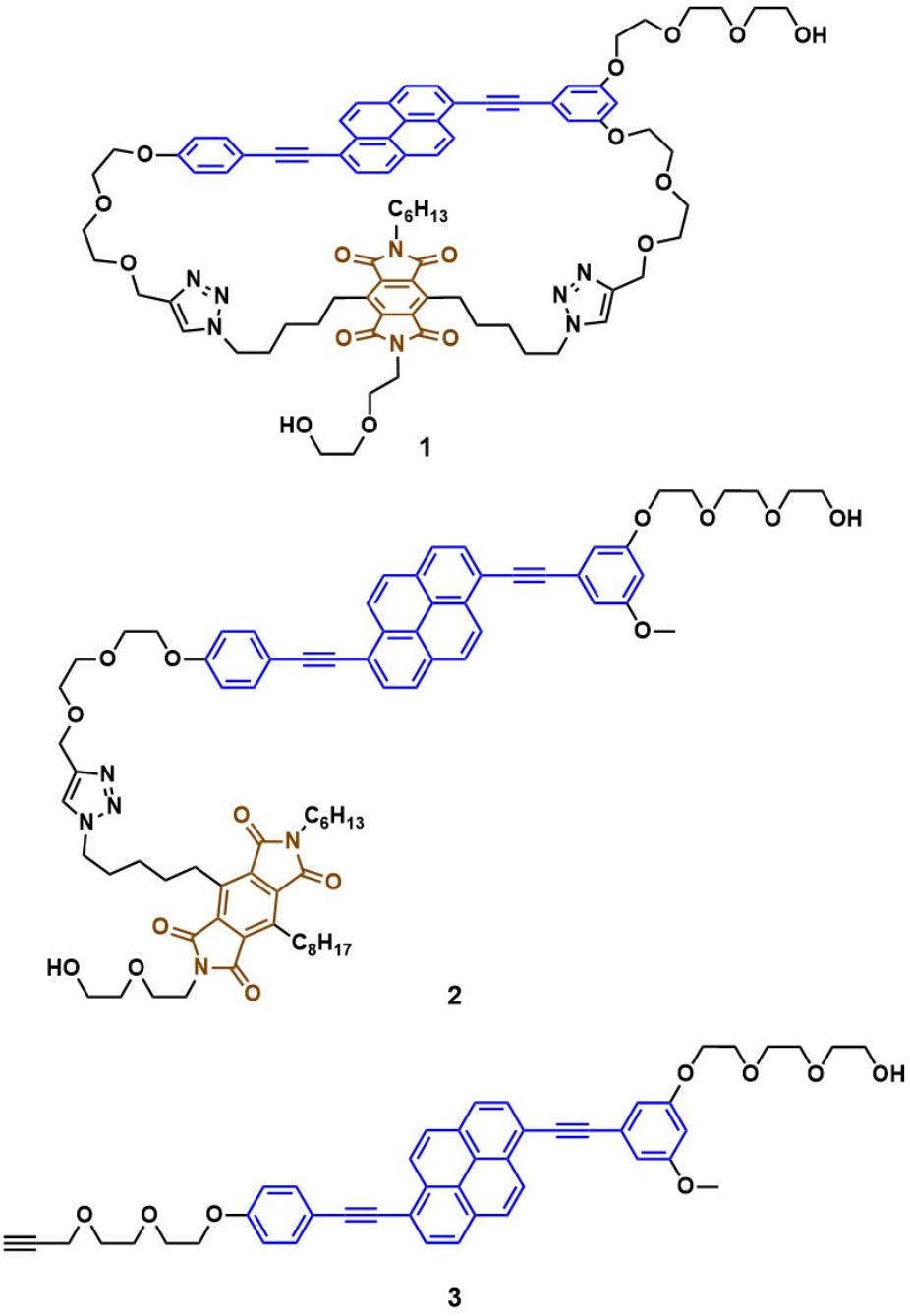

Figure 2-2. Molecular structures of cyclophane-based mechanophore **1**, acyclic reference compound **2**, and reference luminophore **3**.

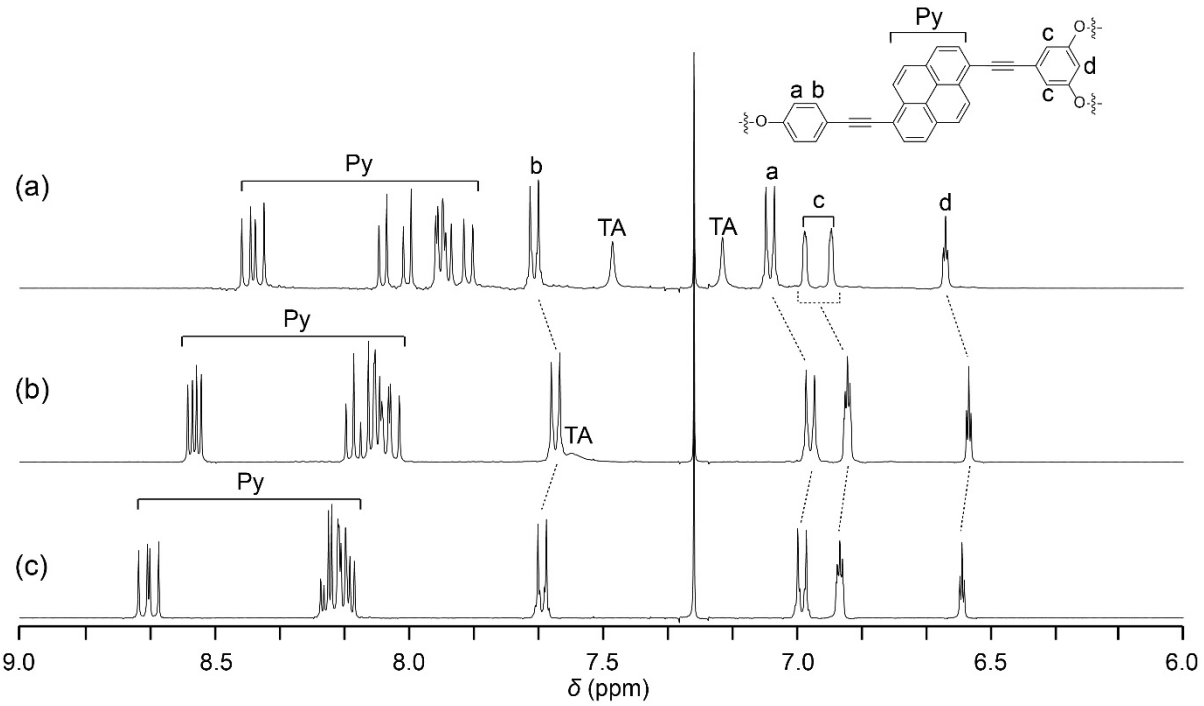

Figure 2-3. Partial ^{1}H NMR spectra of (a) **1**, (b) **2**, and (c) **3** in $CDCl_3$ at 293 K. The abbreviations TA and Py indicate the proton signals of triazole rings and the pyrene, respectively.

2.2.2 Photophysical Properties of Compounds 1–3

To probe how cyclophane-integration affects the 1,6-bis(phenylethynyl)pyrene-PMDI interactions, the photophysical properties of **1**–**3** were examined in toluene solutions (c = 1.0 × 10^{-5} M). The absorption spectrum of **3** displays a band with peaks at 406 and 412 nm (Figure 3a). Upon excitation, the solution fluoresces blue. The photoluminescence spectrum shows a vibronic structure with peaks at 438 and 466 nm (Figure 2-4b) and a high photoluminescence quantum yield (ϕ = 0.87) is observed. These characteristics match the ones of other 1,6-bis(phenylethynyl)pyrene derivatives.[56–58] The absorption spectrum of cyclophane **1** is slightly red-shifted *vis-à-vis* **3**, with maxima at 409 and 424 nm, and shows a characteristic tail into the red (Figure 2-4a). These features indicate ground-state CT interactions between luminophore and PMDI. The emission of the 1,6-bis(phenylethynyl)pyrene is strongly

quenched (ϕ = 0.01) (Figure 2-4b). Closer inspection reveals that the emission spectrum of **1** shows, besides weak signals at 440 and 466 nm, a broad, structureless band centered at 650 nm that is indicative of a CT-complex (Figure 2-4c).[62] This is supported by excitation spectra, which exclude exciplex formation. The excitation spectrum of cyclophane **1** in toluene monitored at emission wavelength of 650 nm (Figure 2-5a) has similar spectral features as the absorption spectrum of **1** (Figure 2-4a), suggesting that photons absorbed by the CT-complex contribute to the emission.

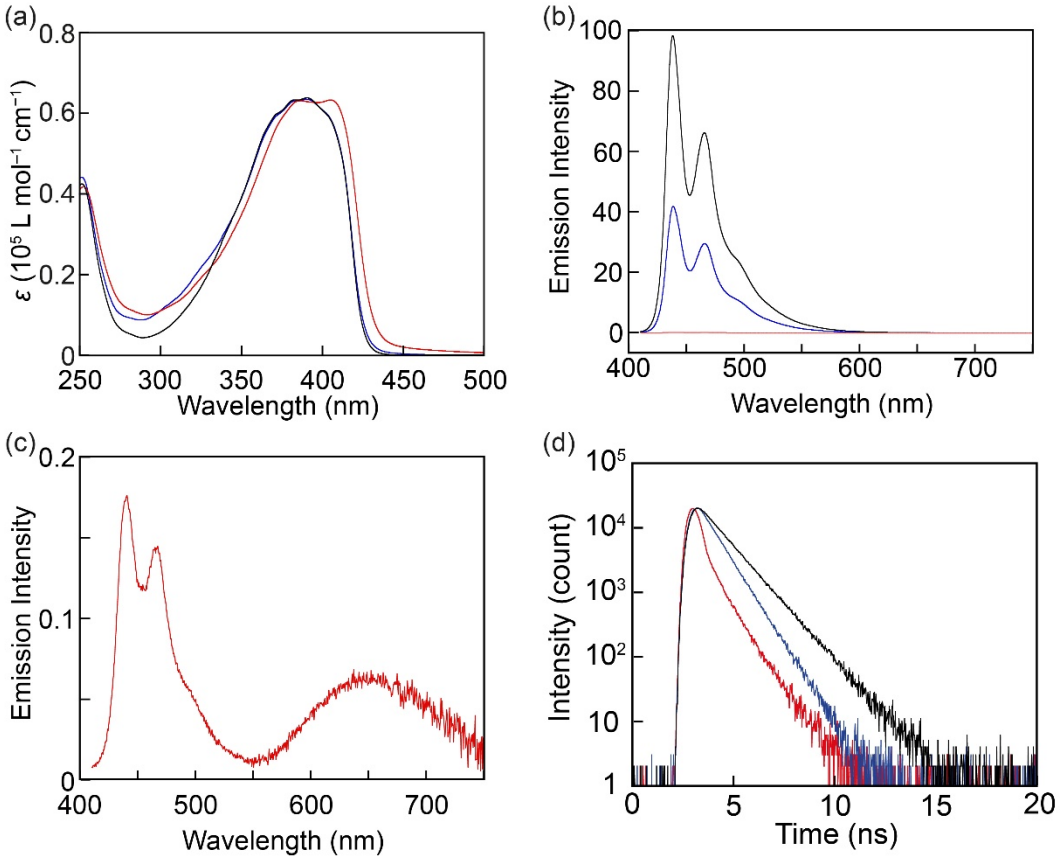

Figure 4. a) Absorption and b) photoluminescence spectra of **1** (red), **2** (blue), and **3** (black) in toluene. c) Magnified photoluminescence spectrum of **1** in toluene. d) Emission decay profiles of **1** (red), **2** (blue), and **3** (black) monitored at 440 nm in toluene. λ_{ex} = 400 nm for

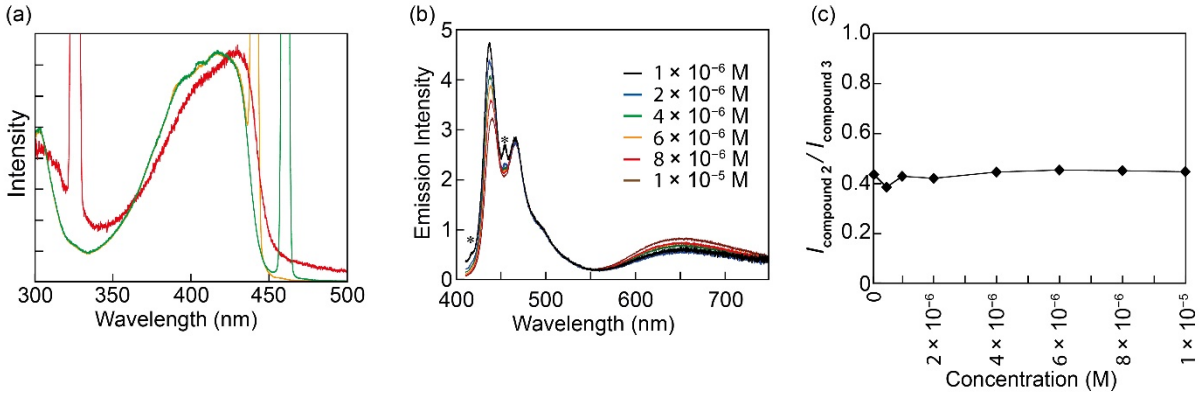

Figure 5. (a) Excitation spectra of cyclophane **1** in toluene recorded at emission wavelengths of 650 nm (red), 460 (green), and 440 nm (yellow) (c = 1.0 × 10^{-5} M). (b) Photoluminescence spectra of cyclophane **1** varying concentrations in toluene. The spectra were normalized at 466 nm. The emission peak labelled * originated from light-scattering in the instrument. The decrease in the monomer emission upon increasing the concentration of cyclophane **1** in toluene is due to the incremental effect of self-absorption. As the spectra were normalized to the emission intensity at 466 nm, the intensity of the CT emission band increased. (c) Emission intensity ratios of linear reference compound **2** and emitter **3** at 466 nm varying concentrations. All spectra were recorded with excitation wavelength of 400 nm at r.t.

The absorption spectral features of solutions of **1** are concentration-independent, which confirms that the CT-complexes form *intramolecularly* (Figure 2-5b). The absorption spectrum of **2** largely mirrors that of **3**, except below 370 nm, where the PMDI residue absorbs. CT-complex absorption and emission, as seen in cyclophane **1**, are negligible for compounds **2** and **3** (Figure 2-6a). The emission spectrum of **2** mirrors the one of **3**, albeit with a lower quantum efficiency (ϕ = 0.41), likely due to *dynamic* quenching. Also, in the case of **2**, a concentration series confirms that the effect is *intramolecular* (Figure 2-5c).

The steady-state emission measurements were complemented with time-resolved experiments. The emission decay profile of **3** in toluene, monitored at 440 nm, is well-fitted by a single-exponential decay with a lifetime (τ) of 1.2 ns (Figure 2-4d), similar to other 1,6-bis(phenylethynyl)pyrenes.[54,58] The emission decay of **2** is also exponential; the slightly lower lifetime (τ = 0.9 ns) reflects quenching through dynamic luminophore-PMDI encounters. A similar decay curve, indicating dynamic quenching, was also recorded for cyclophane **1** (τ = 0.8 ns) at 440 nm. Since the emission of most luminophores is quenched in **1**, due to static CT-complex formation, only a few luminophores undergo dynamic quenching. When the emission decay of **1** was monitored at 650 nm (Figure 2-6b), a biexponential decay with emission lifetimes of 1.0 and 1.6 ns was observed, confirming that the reddish-orange emission band is not due to phosphorescence.

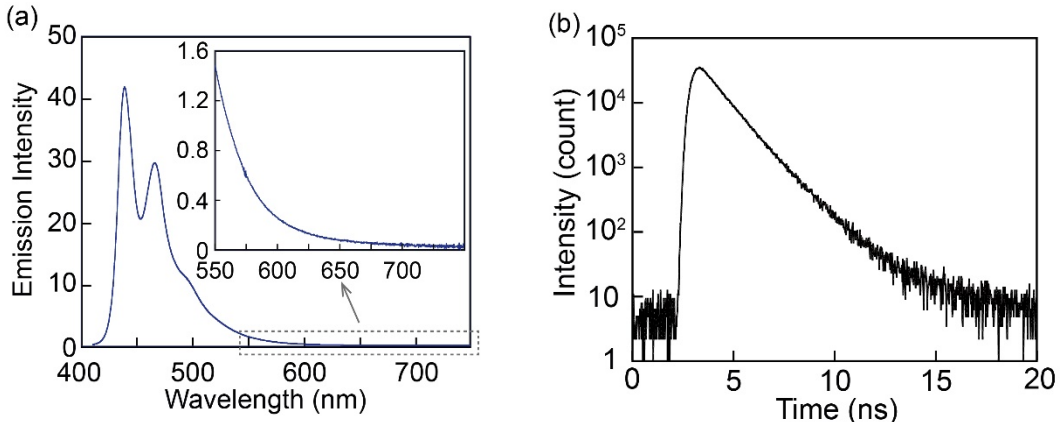

Figure 2-6. (a) Photoluminescence spectrum of linear reference compound **2** in toluene (c = 1.0 × 10^{-5} M) recorded with excitation wavelength of 400 nm at r.t. The inset is a magnified photoluminescence spectrum of **2**. (b) Emission decay profile of cyclophane **1** in toluene monitored at 650 nm with excitation at 405 nm.

2.2.3 Integration of Compounds 1 and 2 into Polyurethane

Cyclophane **1** was covalently embedded into a linear, segmented polyurethane elastomer that was previously functionalized with other mechanophores.[48–51,54] Thus, **1-PU**, containing cyclophane **1** mainly between soft segments, was prepared by the reaction of **1** (≈ 0.2 wt%) with telechelic poly(tetrahydrofuran)diol (M_n ≈ 2,000 g mol^{-1}), 1,4-butanediol, and 4,4′-methylenebis(phenylisocyanate). A reference polymer containing **2** in the same molar concentration (**2-PU**) and a reference **PU** without dyes were also synthesized. The ^{1}H NMR spectra display the characteristic peaks of the polyurethanes (Figure 2-7), whereas the concentration of **1** or **2** is too low to be discernible. However, the absorption and emission spectra of **1-PU** and **2-PU** in THF (Figure 2-8) unequivocally confirm the integration of **1** and **2** and reveal that their optical characteristics remain unchanged. Thermogravimetric analysis traces recorded for **1-PU**, **2-PU**, and **PU** are similar (Figure 2-9). Differential scanning calorimetry traces show weak endothermic peaks at 190 °C upon heating, and broad exothermic peaks around 100 °C upon cooling (Figure 2-10), which are associated with the melting and crystallization of hard block domains. Another endothermic peak on heating around 10 °C is associated with melting of the crystalized PTHF moieties.

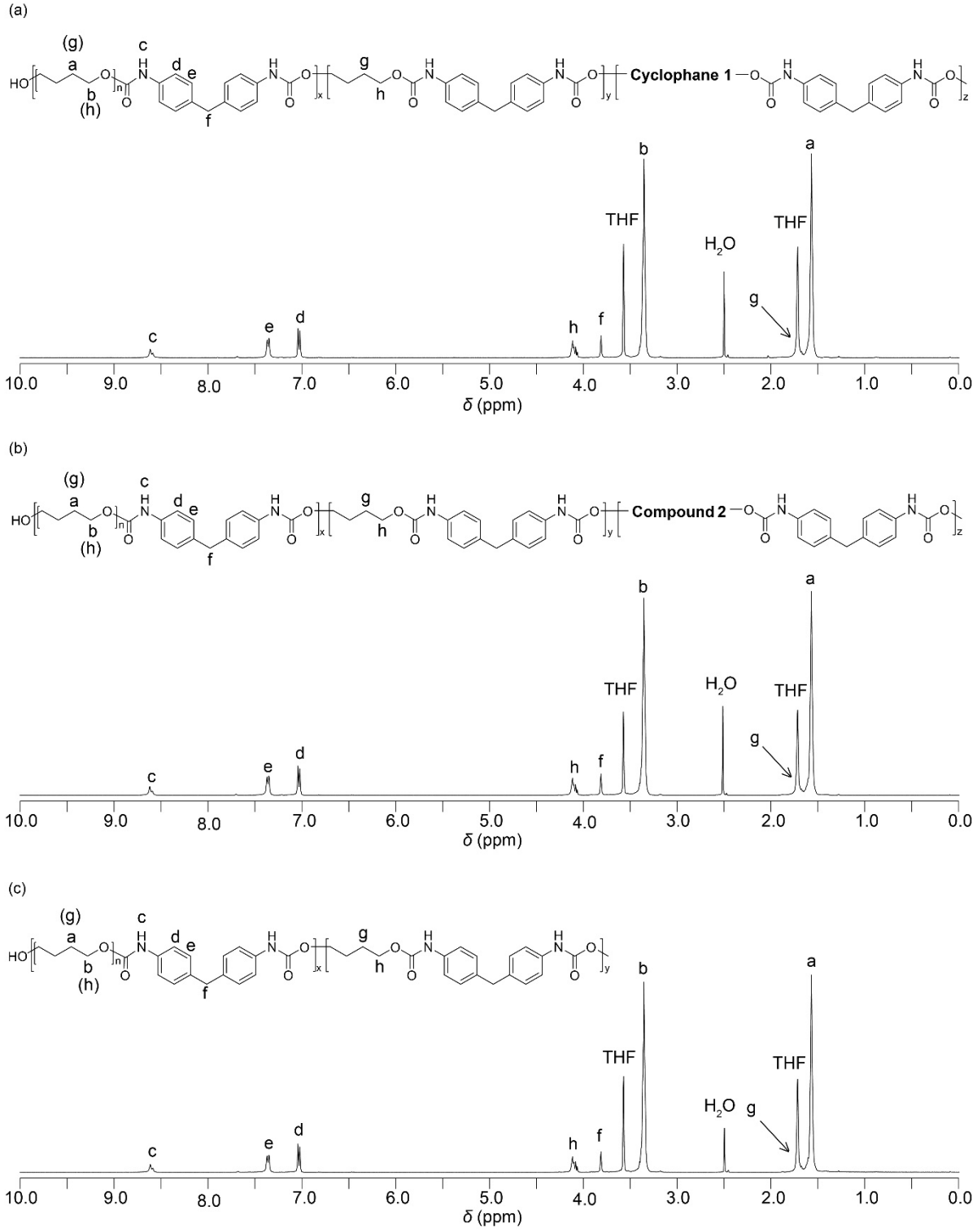

Figure 2-7. ^{1}H NMR spectra of (a) **1-PU**, (b) **2-PU**, and (c) **PU** in THF-d_8. Signals are characterized as protons of the polyurethane chains. No signals ascribed to the residues of compounds **1** and **2** are observed due to their low concentrations in **1-PU** and **2-PU**. All spectra were measured at 293 K.

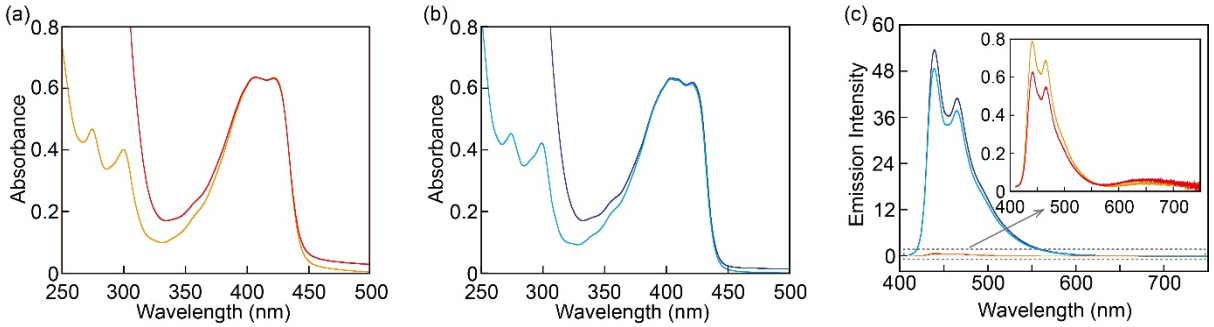

Figure 2-8. (a) Absorption spectra of cyclophane **1** (c = 1.0 × 10^{-5} M, yellow line) and **1-PU** (red line) in THF. (b) Absorption spectra of the linear reference compound **2** (c = 1.0 × 10^{-5} M, light blue line) and **2-PU** (blue line) in THF. (c) Photoluminescence spectra of cyclophane **1** (c = 1.0 × 10^{-5} M, yellow line), **1-PU** (red line), the linear reference compound **2** (c = 1.0 × 10^{-5} M, light blue line), and **2-PU** (blue line) in THF. The inset is magnified photoluminescence spectra of **1** and **1-PU**. The concentrations of the **1-PU** and **2-PU** solutions were adjusted so that the absorbances at 400 nm match those of the solutions of **1** and **2**, respectively. The photoluminescence spectra were recorded with excitation at 400 nm.

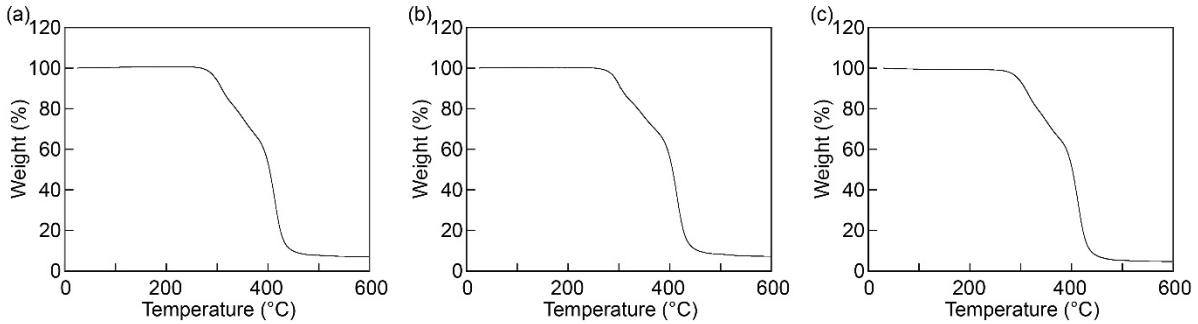

Figure 2-9. Thermogravimetric analysis traces of (a) **1-PU**, (b) **2-PU**, and (c) **PU**. The TGA experiments were conducted under N_2 at a heating rate of 10 ºC/min.

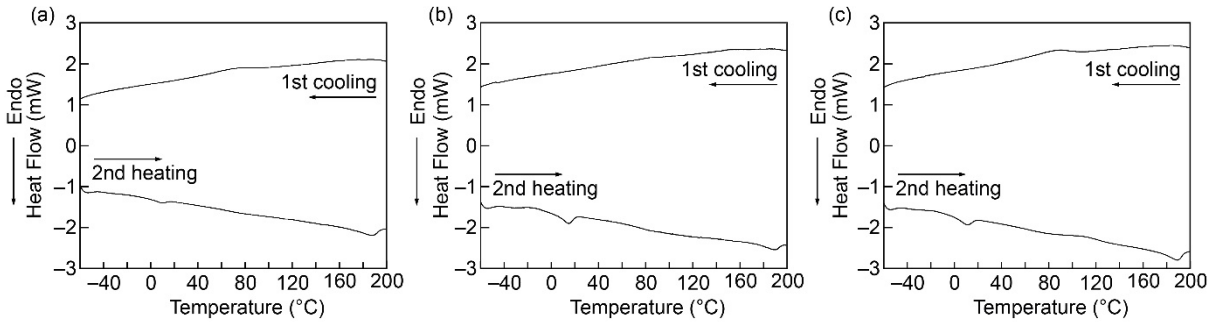

Figure 2-10. Differential scanning calorimetry traces of (a) **1-PU**, (b) **2-PU**, and (c) **PU**. The measurements were conducted under N_2. The heating and cooling rates were 10 ºC/min. Shown are the first cooling and the second heating traces.

Thin films of **1-PU**, **2-PU**, and **PU** were prepared by solution-casting from THF. For reference purposes, films of **PU** into which cyclophane **1** (**1inPU**) or luminophore **3** (**3inPU**) were physically doped were also prepared. Stress-strain curves acquired in uniaxial tensile tests (Figure 2-11) and dynamic mechanical analysis traces (Figure 2-12) reveal that **1-PU**, **2-PU**, and **PU** have similar (thermo)mechanical properties as similar polyurethanes,[48–51,54,63] with a rubbery regime from ≈ –40 to 160 °C, a strain at break of ≈ 700%, a tensile strength of ≈ 60 MPa, and a Young's modulus of ≈ 7 MPa. The introduction of **1** or **2** does not affect the mechanical properties of the polyurethanes.

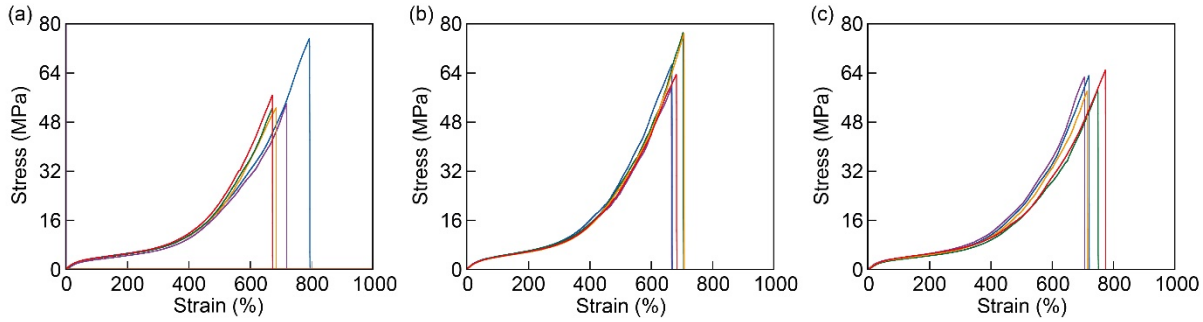

Figure 2-11. Stress-strain curves of (a) **1-PU**, (b) **2-PU**, and (c) **PU**. Each graph shows data obtained from five different specimen. The experiments were conducted with a strain rate of 2 mm/s at r.t.

Table 2-1. Overview of the mechanical properties of **1-PU**, **2-PU**, and **PU** films as determined from stress-strain curves recorded during uniaxial tensile deformation (see Figure 2-11).[a)]

	Elongation at break (%)	Stress at break (MPa)	Young's Modulus [b)] (MPa)
1-PU	710 ± 52	58 ± 10	6.2 ± 3.1
2-PU	686 ± 20	69 ± 8	8.0 ± 0.6
PU	734 ± 28	61 ± 3	7.4 ± 2.0

[a)]All data were extracted from the stress-strain curves shown in Figure 2-11 and represent averages of 5 measurements ± standard deviation. [b)]The Young's moduli were derived from the slopes of the stress-strain curves in the strain regime of 1.5–4.5%.

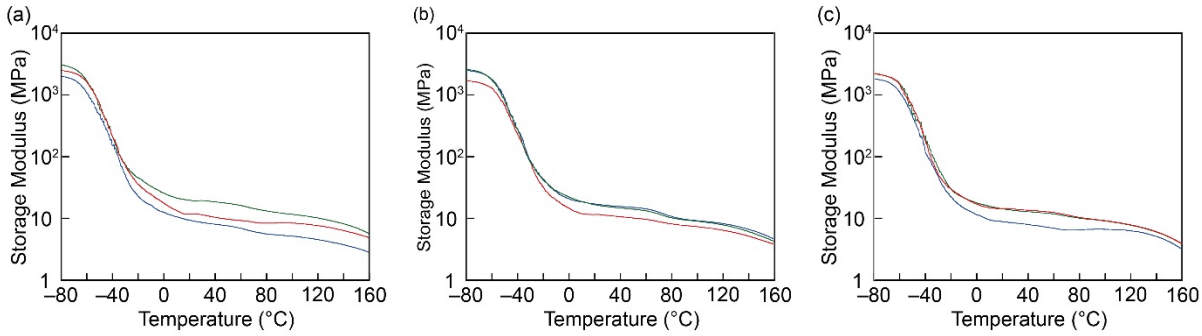

Figure 2-12. Dynamic mechanical analysis traces of (a) **1-PU**, (b) **2-PU**, and (c) **PU**. The DMA experiments were conducted under N_2 at a heating rate of 3 °C/min, a frequency of 1 Hz, and an amplitude of 15 µm.

2.2.4 Photophysical Properties of 1-PU, 2-PU, and 1inPU films

The **1-PU** films show orange fluorescence, however upon deformation, the color gradually changes to blue; the initial color is restored upon stress release (Figure 2-13a, 2-14a). This response is ascribed to the reversible separation of luminophore and quencher as depicted in Figure 1. Neither of the reference films shows a detectable emission color change upon deformation; regardless of the strain, **2-PU** and **1inPU** films show blue monomer emission and CT-complex dominated orange emission, respectively (Figure 2-13b,c, 2-14b,c).

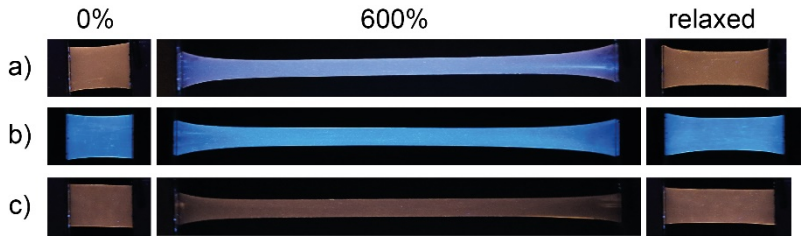

Figure 2-13. Pictures of a) **1-PU**, b) **2-PU**, and c) **1inPU** films before stretching (left), strained to 600% (center), and after stress release (right). All images were taken in the dark with excitation at 365 nm. The camera sensitivity was reduced for **2-PU** films because of their high fluorescence intensities.

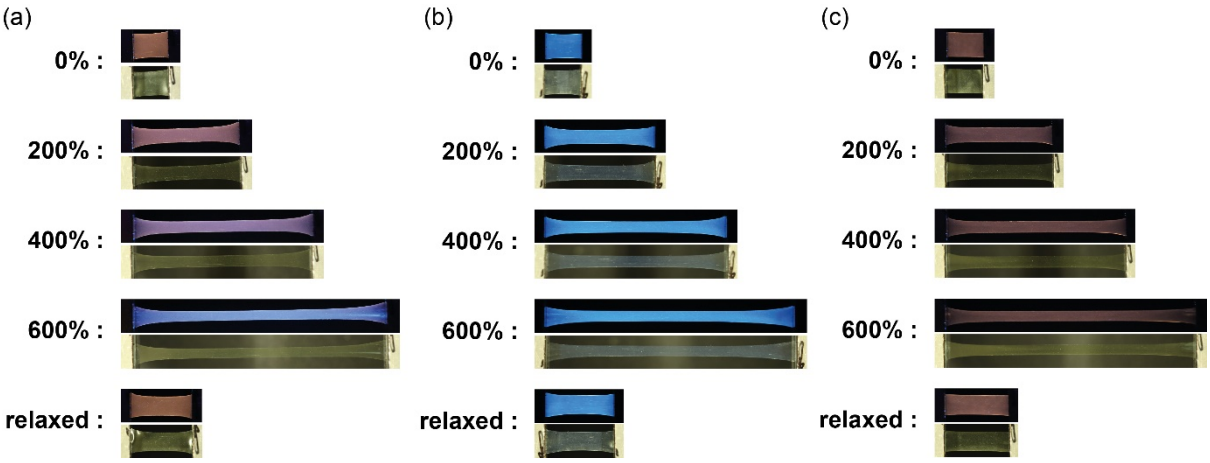

Figure 2-14. Photographs of **1-PU**, **2-PU**, and **1inPU** films in cyclic uniaxial deformation tests. In each set, the top image shows the photoluminescence of the film taken in the dark under 365 nm excitation light and the corresponding images shown below were taken under ambient illumination. All images were taken under ambient conditions at the stains indicated. The images in panel (b) were taken after reducing the sensitivity of the camera because the emission of **2-PU** films is much more intense than those of **1-PU** and **1inPU** films.

The mechanochromic response of **1-PU** was probed by *in situ* photoluminescence spectroscopy (Figure 2-15a,b). The emission spectrum of the unstretched **1-PU** film displays a broad structureless emission band with maximum at 580 nm and a slightly weaker, well-structured band with a peak at 464 nm associated with the emitter. The CT-complex emission is blue-shifted and more prominent in the solid **1-PU** film than in solutions of **1**, due to the limited mobility of the motif's components in the solid polymer. The conjugated moieties can relax in solution and assume low-energy configurations, while such rearrangements are suppressed in the solid polymer. This is supported by the fact that the CT-complex emission of **1** in toluene is blue-shifted in liquid nitrogen, whereas it is red-shifted upon heating **1-PU** films (Figures 2-16,2-17a). Furthermore, a red shift of the CT-complex emission was observed when the films were swelled with toluene or chlorobenzene (Figure 2-17b). The solid cyclophane **1** exhibits slightly blue shifted CT-complex emission with a maximum at 632 nm (Figure 2-16) compared to the CT-emission band of toluene solution, indicating that the blue-shift of CT-complex emission observed for **1-PU** films is not due to aggregation. The position of the CT-complex emission band is concentration-independent (Figure 2-18).

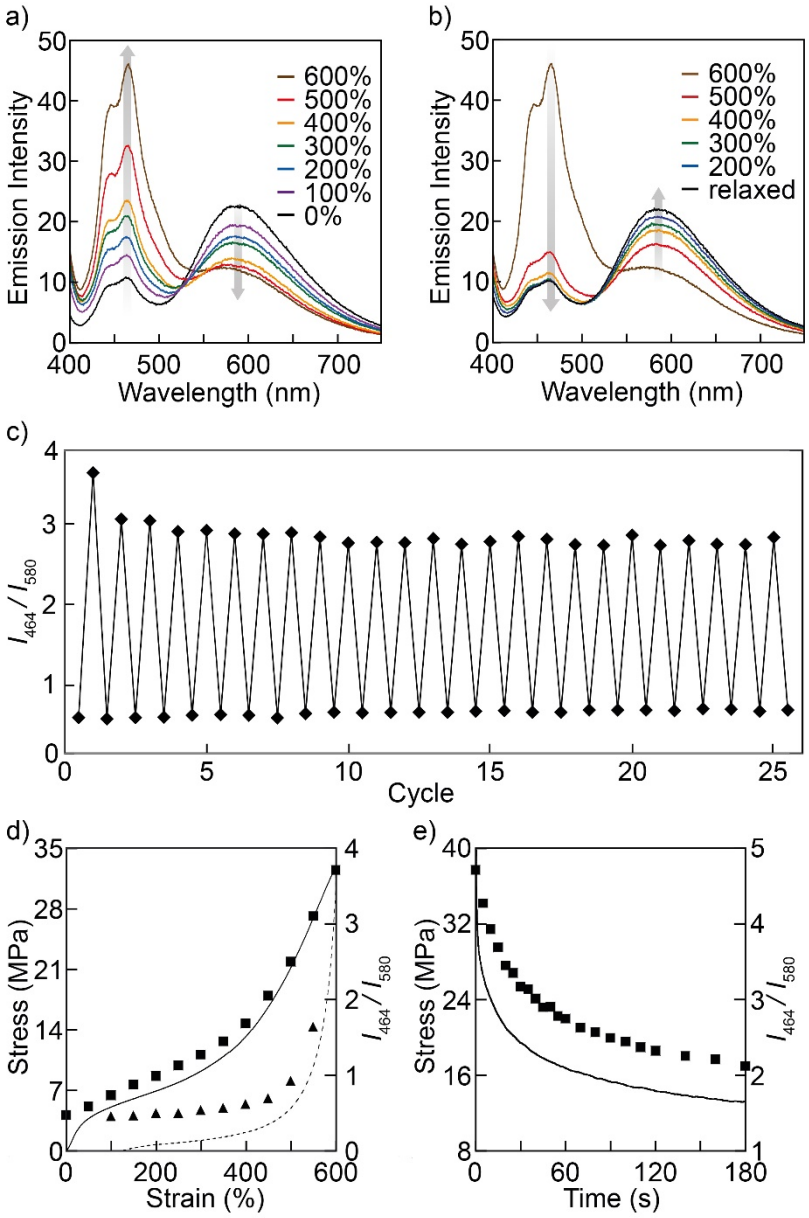

Figure 2-15. Photoluminescence spectra of a **1-PU** film recorded in the a) first stretching and b) release cycle at the indicated strains. The spectra were not normalized. c) Plots showing the I_{464}/I_{580} ratio in the stretched (600% strain) and relaxed state of a **1-PU** film over 25 cycles. d) Overlay of the stress-strain curves recorded in the first stretch (solid line) and release (dotted line) cycle of a **1-PU** film and the corresponding I_{464}/I_{580} values (stretching = squares, release = triangles). e) Overlay of the nominal stress (solid line) and I_{464}/I_{580} values (squares) as a function of time after straining a **1-PU** film to 600% and maintaining the strain.

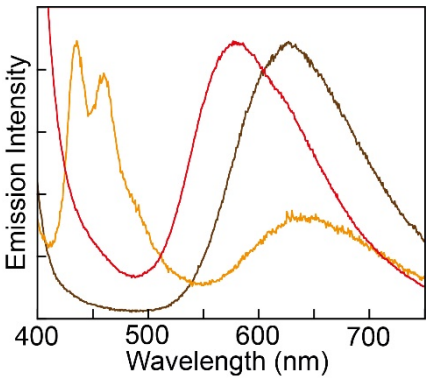

Figure 2-16. Photoluminescence spectra of cyclophane **1** in toluene at r.t. (c = 1.0 × 10^{-5} M, yellow line), in toluene at 77 K (c = 1.0 × 10^{-5} M, red line), and in the solid state at r.t. (brown line). The emission spectra were recorded with excitation at 365 nm.

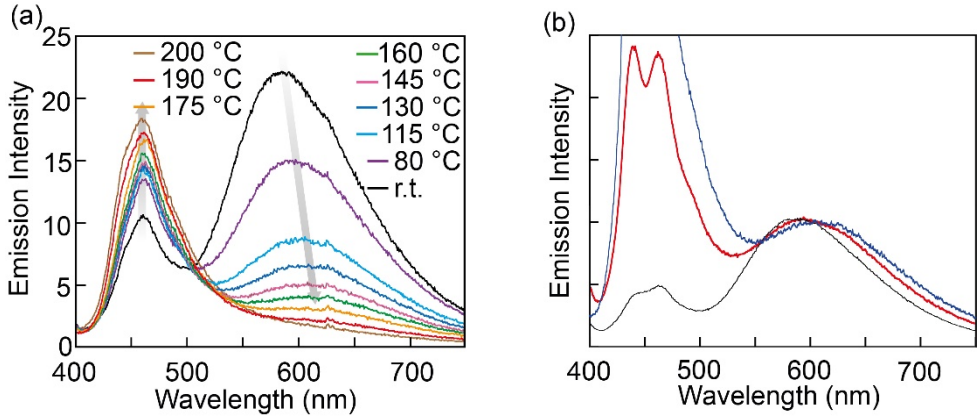

Figure 2-17. (a) Photoluminescence spectra of a **1-PU** film recorded upon heating from r.t. to 200 ºC. (b) Photoluminescence spectra of a pristine **1-PU** film (black line), a **1-PU** film swollen with chlorobenzene (blue line), and a **1-PU** film swollen with toluene (red line) recorded at r.t. The spectra were recorded with excitation at 365 nm.

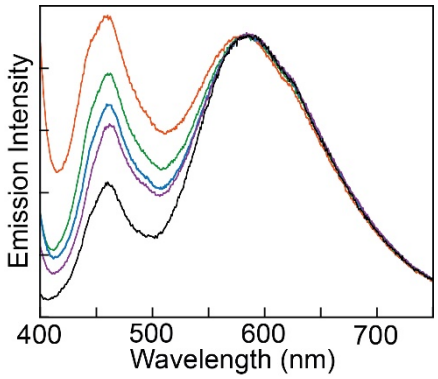

Figure 2-18. Photoluminescence spectra of blend films of **1-PU** and **PU** at r.t. **1-PU** : **PU** = 100 : 0 (black line), 80 : 20 (violet line), 60 : 40 (blue line), 40 : 60 (green line), and 20 : 80 (orange line). The spectra were recorded with excitation at 365 nm.

The relative emission intensity of the shorter-wavelength mode of the monomer band is reduced in the films relative to that of **1** and **3** in toluene (Figure 2-4b,c), because of self-absorption. Upon deformation of the **1-PU** film, the CT-complex emission intensity gradually decreases, while the monomer emission intensity increases (Figure 2-15a). Upon release of the stress, the changes are instantly reverted. However, the emission spectra acquired during the first stretch and release cycle at the same nominal strain differ (Figure 2-15b). The change observed upon decreasing the strain from 600% to 500% is much larger than the one observed when the sample is first stretched. This hysteresis is due to irreversible changes of the molecular arrangement upon stretching.[64,65] The differences diminish with the number of deformation cycles (Figure 2-19). The emission decay profiles of the **1-PU** films upon deformation show reversible changes when monitored at 580 nm (Figure 2-20). The relative ratios of monomer and CT-emission intensity (I_{464}/I_{580}) recorded for stretched and relaxed **1-PU** films remain constant over at least 24 cycles after the second cycle (Figure 2-15c). The response is instantly reversible, as demonstrated by manual cyclic tests with a frequency of up to 3 Hz.

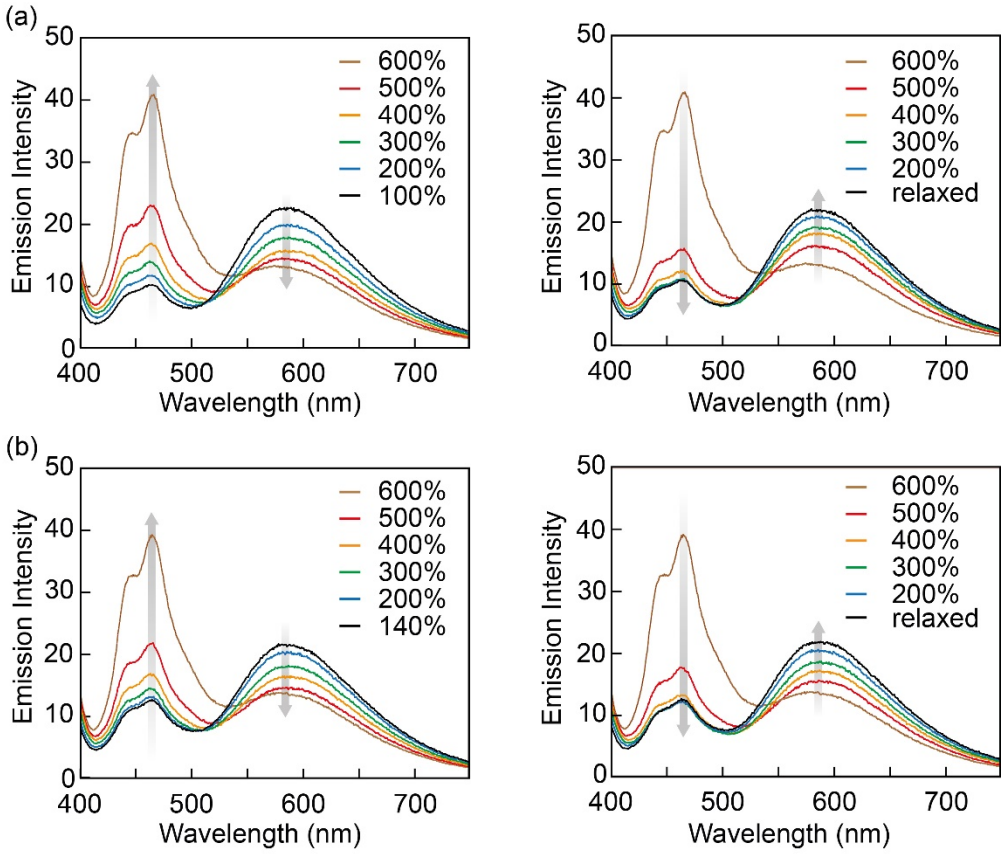

Figure 2-19. Photoluminescence spectra of a **1-PU** film recorded upon stretching (left) and releasing the stress (right) for (a) the second cycle and (b) the twenty-fifth cycle. All spectra were recorded with 365 nm excitation at r.t.

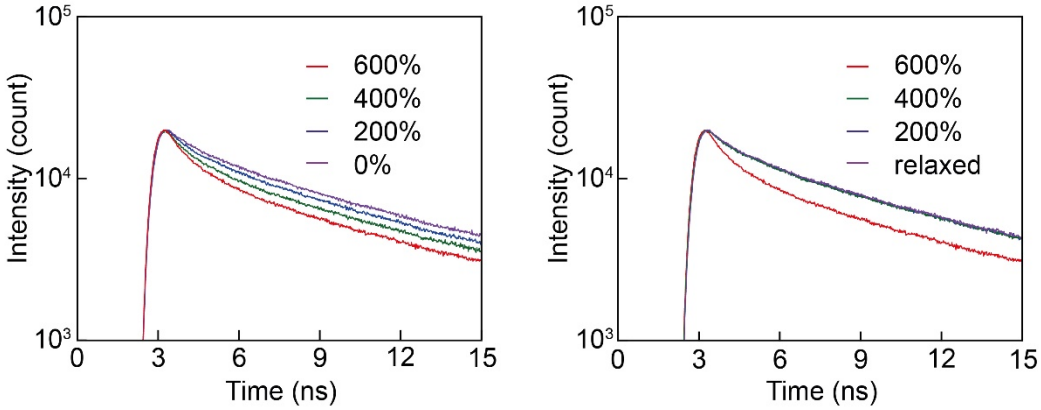

Figure 2-20. Emission decay profiles of the **1-PU** films upon stretching (left) and relaxing (right) at the indicated strains. All profiles were monitored at 580 nm with excitation at 365 nm light.

Overlays of the stress-strain curves and I_{464}/I_{580} of a **1-PU** film (Figure 2-15d) show that the optical signal correlates with the applied *stress*. While the stress required to deform the **1-PU** film is reduced after the first cycle (Figure 2-21a), due to permanent molecular rearrangements that are typical for thermoplastic polyurethanes,[64,65] the correlation between I_{464}/I_{580} and stress persists over at least 25 stretching and relaxation cycle (Figure 2-21b). Further, a stress-relaxation experiment was carried out by straining a **1-PU** film to 600% and maintaining the strain for 180 seconds (Figure 2-15e). Both the stress and I_{464}/I_{580} value gradually decrease over time with similar tendency. Interestingly, the optical property changes of a previously reported, otherwise identical polyurethane containing an excimer-forming cyclophane mechanophore correlate with the applied *strain*.[54] The differences would be related to the fact that the charge-transfer interactions between the luminophore and the quencher in the present cyclophane are stronger than the π-π interactions between the previously employed excimer-forming luminophores. However, further investigations in which the nature of polymer and the mechanophore are judiciously altered will be needed to unequivocally explain the differences in mechanochromic behavior that originate from such seemingly minor molecular modifications.

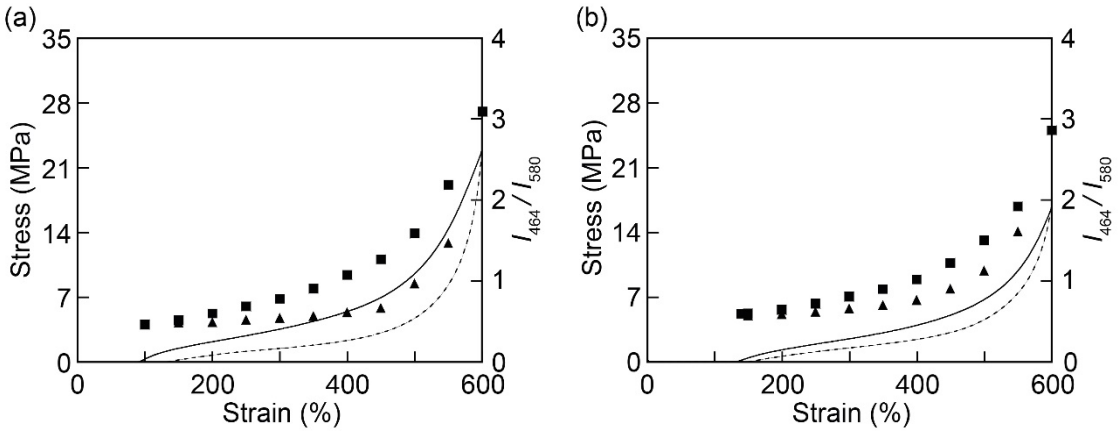

Figure 2-21. Overlays of the stress-strain curves recorded for (a) the second and (b) the twenty-fifth deformation (solid line) and relaxation (dotted line) cycles of a **1-PU** film and the ratios of monomer and CT complex emission intensities (I_{464}/I_{580}) recorded upon deformation (squares) and relaxation (triangles).

The **2-PU** reference films show an increase of the monomer emission intensity upon stretching, in spite of the fact that the film thickness and therewith absorbance decreases upon deformation. Thus, a part of this loop-forming motif functions as a turn-on mechanophore (Figure 2-23a) in which the fraction of quenched emitters decreases upon stretching, due to the spatial separation of luminophore and quencher. The response is reversible, but neither spectral shape nor color changes occur. Neither **3inPU** nor **1inPU** films show any significant changes upon deformation, beyond a reduction in emission intensity related to the reduced film thickness (Figure 2-23b,c). These observations clarify that the cyclic structure of **1** and its covalent integration into the polyurethane are prerequisites for the ratiometric mechanochromic luminescence observed for **1-PU**.

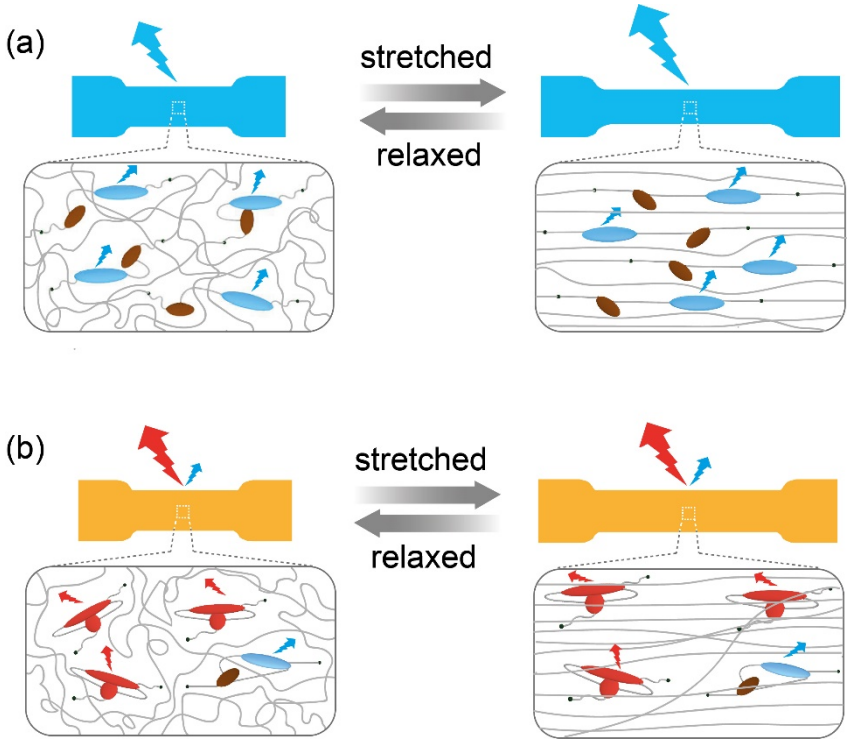

Figure 2-22. Schematic illustrations of deformation of (a) **2-PU** and (b) **1inPU** films.

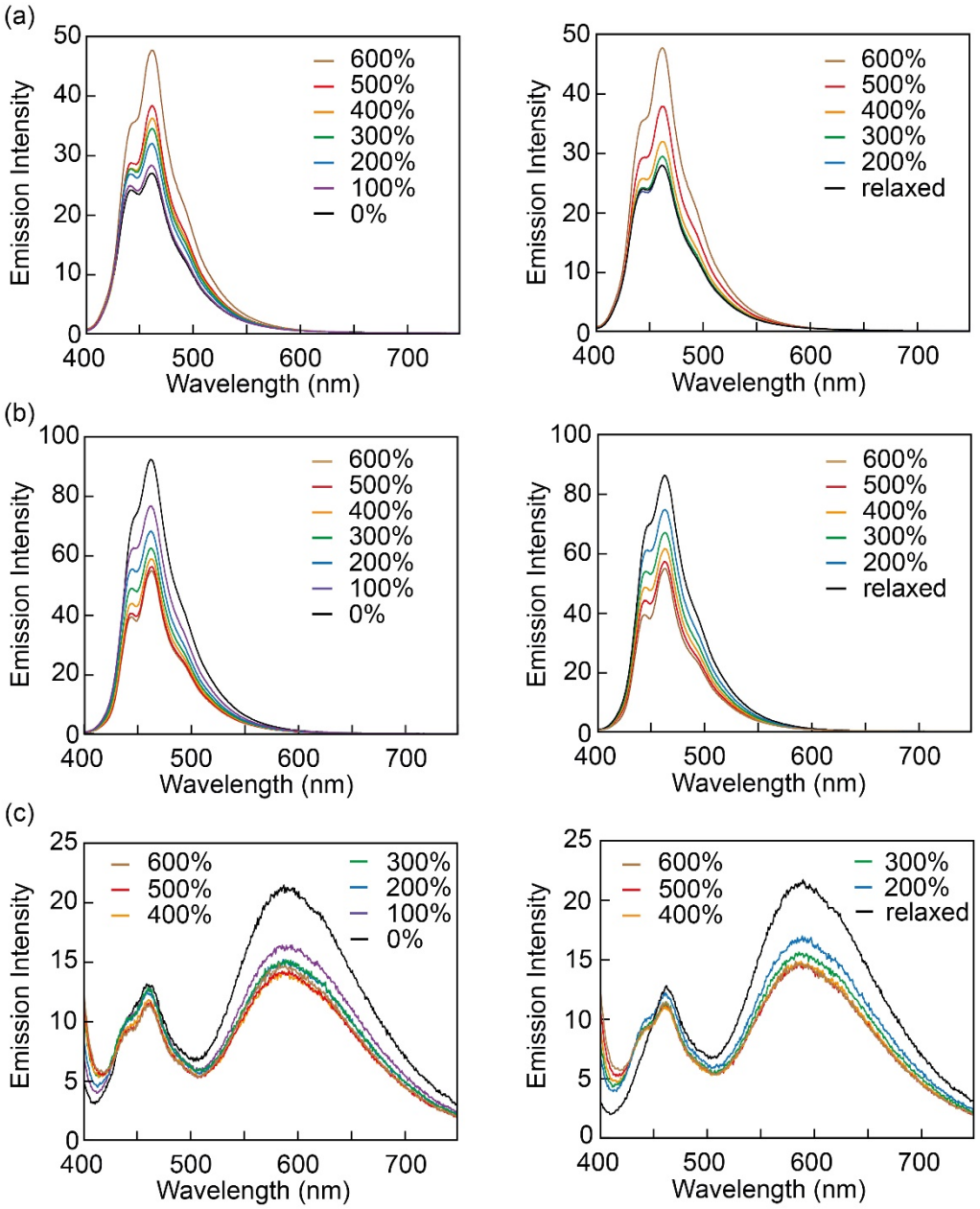

Figure 2-23. Photoluminescence spectra of (a) **2-PU**, (b) **3inPU**, and (c) **1inPU** films recorded upon stretching (left) and releasing the stress (right). All spectra were recorded with 365 nm excitation at r.t.

2.3 Conclusion

In summary, a new supramolecular cyclophane mechanophore was developed based on the change of emission species from CT-complex to monomer. This is the first supramolecular mechanophore in which CT-complex emission is strategically exploited. Mechanical activation causes the spatial separation of a 1,6-bis(phenylethynyl)pyrene luminophore and a pyromellitic diimide quencher and induces a pronounced change in the emission characteristics. Accordingly, the ratio of unperturbed luminophore to CT-complex emission intensity changes notably upon deforming films of a polyurethane elastomer containing the motif. The instantly reversible color change is clearly detectable by the unassisted eye. The optical changes can be expressed by a ratiometric signal that correlates with the applied stress.

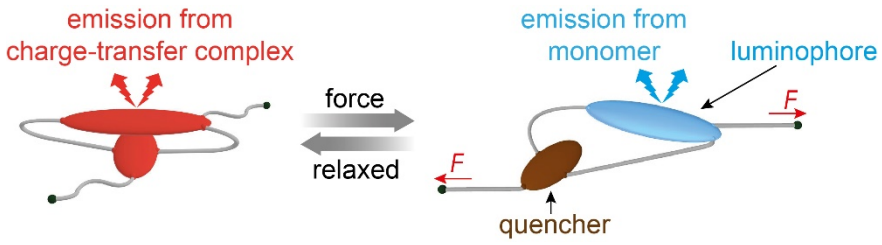

2.4 Experimental

General methods

All reagents and solvents were purchased from Kanto Chemical, Merck, Tokyo Kasei, or FUJIFILM Wako Pure Chemical Corporation and were used without further purification, unless otherwise noted. All reactions were carried out under nitrogen atmosphere unless specified otherwise. Flash silica gel column chromatography was conducted using a Biotage Isolera Flash system using SHOKO-scientific Purif-Pack-Ex cartridges. Silica gel from Kanto Chemicals (silica gel 60N, spherical, 40–50 μm) was used for conventional column chromatography. Recycling preparative gel permeation chromatography (GPC) was performed using a Japan Analytical Industry LaboACE. For polymer synthesis, inhibitor-free anhydrous tetrahydrofuran (FUJIFILM Wako Pure Chemical Corporation) was used as solvent. Hydroxyl-terminated poly(tetrahydrofuran) (M_n = 2,000 g/mol) was dried *in vacuo* at 100 °C for 2 h prior to polymer preparation. The remaining reagents for polymer synthesis, 1,4-butanediol, and 4,4'-bis(phenyl isocyanate) were distilled under vacuum and stored over molecular sieves at room temperature (r.t.) and 4 °C, respectively. Dibutyltin dilaurate was used as catalyst for the polymerizations without any purification. ^{1}H NMR spectra were obtained using a JEOL JNM-ECZ400S/L1 spectrometer. All chemical shifts are reported on the δ-scale in parts per million (ppm) relative to the signal of tetramethylsilane (TMS at 0.00 ppm) or residual solvent protons (THF at 1.72 ppm) as an internal standard. Coupling constants (J) are denoted in Hz and relative intensities are reported. Proton-decoupled ^{13}C NMR spectra were acquired on a JEOL JNM-ECZ400S/L1 spectrometer and all chemical shifts are expressed in ppm using solvents as the internal standards ($CDCl_3$ at 77.16 ppm; THF-d_8 at 67.21 ppm). Matrix-assisted laser desorption ionization time-of-flight (MALDI-TOF) mass spectroscopy was performed with a SHIMADZHU AXIMA-Performance. High-resolution electrospray ionization (ESI) mass

spectra were obtained on a high performance TOF-MS system Bruker Daltonics micrOTOF II. Absorption spectra were measured using a JASCO V-750 spectrophotometer. Steady-state fluorescence spectra of solutions were recorded with a JASCO FP-6500 and the spectra were corrected for the detector nonlinearity. Steady-state fluorescence spectra of polyurethane films during stretching were monitored with an Ocean Optics QEPro-FL equipped with an LLS-365 LED light source and a Reflection/Backscattering Probe R400-7-UV-VIS; these spectra were not corrected. Size-exclusion chromatography (SEC) experiments were performed on a SHIMADZU Nexera GPC system equipped with a GPC KF–805L column (ID = 8.0 mm, L = 300 mm, particle size = 10 μm). Samples were injected using THF as the eluent at 40 °C and a flow rate of 1.0 mL/min. For the data analysis, Labosolutions software (SHIMADZU) was used and molecular weights were calculated based on narrow-molecular-weight polystyrene calibration (1100–2,500,000 g/mol). Thermogravimetric analyses (TGA) were conducted under nitrogen with a Mettler-Toledo Star^e system at a heating rate of 10 °C/min. Differential scanning calorimetry (DSC) measurements were performed under N_2 on a Hitachi DSC7020 at heating and cooling rates of 10 °C/min. Dynamic mechanical analyses (DMA) were carried out under N_2 with a TA Instruments DMA Q800 at a heating rate of 3 °C/min, a frequency of 1 Hz, and an amplitude of 15 μm. Stress-strain measurements were conducted under ambient conditions with a SHIMADZU AGS-100NX equipped with a 100 N load cell at a strain rate of 2 mm/s. Time-resolved fluorescence decay measurements were carried out with a Hamamatsu Photonics Quantaurus-Tau. Quantum efficiencies were measured with a Hamamatsu Photonics Quantaurus-QY. Movies and photographs were captured with a Canon EOS 9000D camera stabilized with a tripod.

Synthesis of cyclophane 1, linear reference compound 2, and luminophore 3

The synthetic routes used to prepare compounds **1**, **2**, and **3** are shown in Schemes 2-1, 2-2, and 2-3. 2-(Pent-4-yn-1-yloxy)tetrahydro-*2H*-pyran, triethylene glycol *p*-toluenesulfonate, 1-bromo-6-{2-[4-(tetrahydro-2*H*-pyranyloxy)phenyl]ethynyl}pyrene, 2-[2-(prop-2-yn-1-yloxy)ethoxy]ethyl 4-methylbenzenesulfonate, and compound **25** were prepared according to reported procedures.[54,66–69]

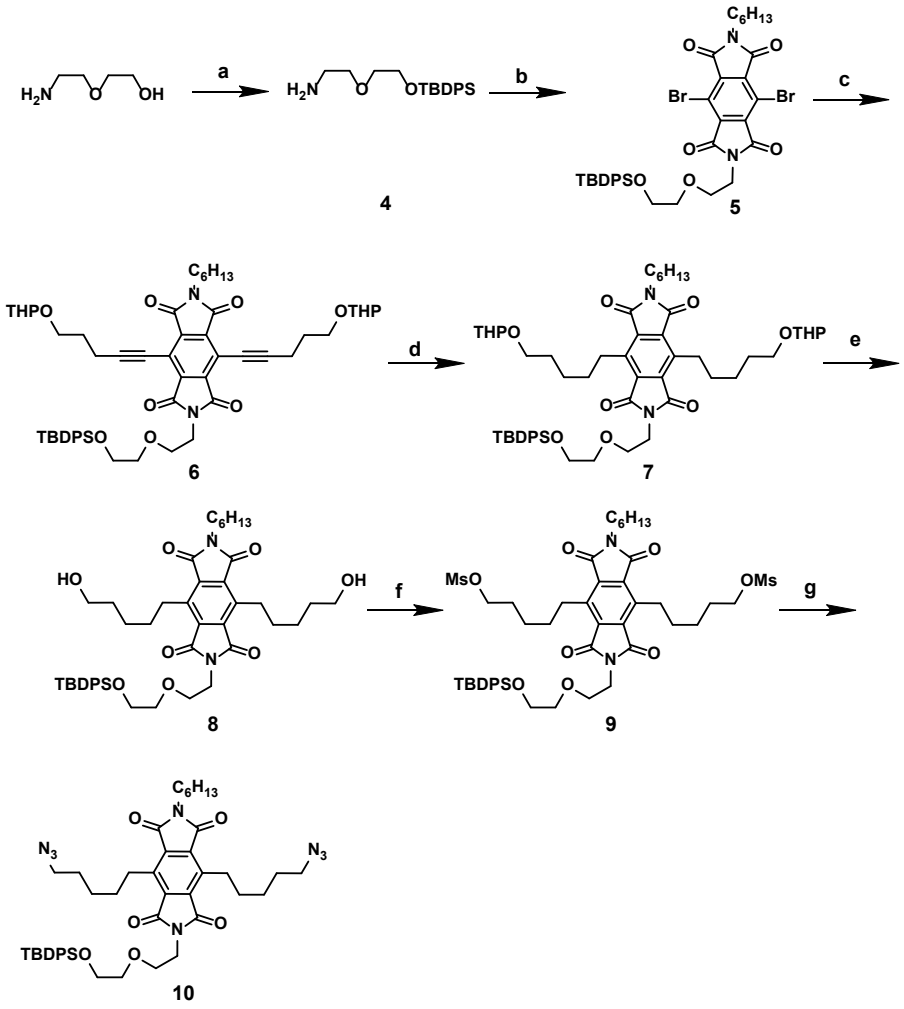

Scheme 2-1. Synthesis of quencher compound 10.

Conditions: (a) *tert*-butyldiphenylsilyl chloride, imidazole, CH_2Cl_2, r.t., 20 h; (b) dibromopyromellitic dianhydride, *n*-hexylamine, acetic acid, 120 °C, 20 h; (c) 2-(pent-4-yn-1-yloxy)tetrahydro-*2H*-pyran, $Pd(PPh_3)_2Cl_2$, CuI, $(i\text{-}Pr)_2NEt$, toluene, 100 °C, 24 h; (d) 10%

Pd/C, H_2, THF, ethyl acetate, r.t., 36 h; (e) pyridinium *p*-toluenesulfonate, THF/H_2O, ethanol, 60 °C, 4 h; (f) methanesulfonyl chloride, Et_3N, CH_2Cl_2, 0 °C, 3 h; (g) NaN_3, DMF, 80 °C, 4 h.

Compound 4. *tert*-Butyldiphenylsilyl chloride (5.82 g, 21.2 mmol) was added dropwise to a solution of 2-(2-aminoethoxy)ethanol (1.11 g, 10.6 mmol) and imidazole (2.16 g, 30.2 mmol) in CH_2Cl_2 (20 mL) and the mixture was stirred at r.t. for 20 h. The resulting reaction mixture was poured into ethyl acetate (100 mL) and washed with water (100 mL) and saturated aq. NaCl (2 × 50 mL). The organic layer was separated, dried over $MgSO_4$, filtered and the solvent was evaporated under reduced pressure. The crude product was purified by flash column chromatography on silica gel (eluent: gradient from CH_2Cl_2 to CH_2Cl_2/methanol/triethylamine = 87:10:3 v/v/v) to afford compound **4** (3.51 g, 10.2 mmol, 96%) as a colorless liquid.
^{1}H NMR (400 MHz, $CDCl_3$): δ = 1.05 (s, 9H), 2.93 (t, J = 5.2 Hz, 2H), 3.56–3.59 (m, 4H), 3.81 (t, J = 5.2 Hz, 2H), 7.36–7.45 (m, 6H), 7.67–7.69 (m, 4H). ^{13}C NMR (100 MHz, $CDCl_3$): δ = 19.25, 26.89, 41.02, 63.48, 70.85, 72.33, 127.75, 129.75, 133.61, 135.63. MS (MALDI-TOF): m/z: 343.21 (calcd. $[M]^+$ = 343.20).

Compound 5. A mixture of compound **4** (1.09 g, 3.19 mmol), *n*-hexylamine (532 mg, 5.32 mmol), and dibromopyromellitic dianhydride (1.00 g, 2.66 mmol) in acetic acid (50 mL) was stirred at 120 °C for 20 h. After cooling to r.t., water (100 mL) was slowly added to the reaction mixture. The resulting precipitate was filtered, dissolved in CH_2Cl_2 (100 mL), and washed with water (2 × 50 mL), and saturated aq. NaCl (100 mL). The organic layer was separated, dried over $MgSO_4$, filtered, and the solvent was evaporated under reduced pressure. The crude product was purified by flash column chromatography on silica gel (eluent: gradient from hexane/CH_2Cl_2 = 40:60 v/v to hexane/CH_2Cl_2 = 10:90 v/v) to afford compound **5** (906 mg, 1.15 mmol, 43%) as a pale yellow solid.

^{1}H NMR (400 MHz, $CDCl_3$): δ = 0.88 (t, J = 6.4 Hz, 3H), 0.98 (s, 9H), 1.27–1.39 (m, 6H), 1.66–1.73 (m, 2H), 3.59 (t, J = 4.8 Hz, 3H), 3.71–3.80 (m, 6H), 3.94 (t, J = 5.6 Hz, 2H), 7.34–7.41 (m, 6H), 7.63–7.66 (m, 4H). ^{13}C NMR (100 MHz, $CDCl_3$): δ = 14.15, 19.24, 22.57, 26.57, 26.84, 28.26, 31.37, 38.59, 39.22, 63.47, 67.40, 72.12, 114.21, 127.76, 129.70, 133.57, 133.66, 136.26, 163.41, 163.58. MS (MALDI-TOF): m/z: 805.58 (calcd. $[M+Na]^+$ = 805.09).

Compound 6. A mixture of compound **5** (1.57 g 2.00 mmol), 2-(pent-4-yn-1-yloxy)tetrahydro-*2H*-pyran, (1.36 g, 8.00 mmol), $Pd(PPh_3)_2Cl_2$ (140 mg, 0.200 mmol), CuI (38.1 mg, 0.200 mmol), $(i\text{-Pr})_2NEt$ (40 mL), and toluene (15 mL) was stirred under nitrogen atmosphere at 100 ^{o}C for 24 h. After cooling to r.t., the reaction mixture was poured into ethyl acetate (150 mL) and washed with 5% aq. HCl (2 × 100 mL), saturated aq. $NaHCO_3$ (100 mL), and saturated aq. NaCl (100 mL). The organic layer was separated, dried over $MgSO_4$, filtered, and the solvent was evaporated under reduced pressure. The crude product was purified by flash column chromatography on silica gel (eluent: gradient from CH_2Cl_2 to CH_2Cl_2/ethyl acetate = 85:15 v/v) to afford compound **6** (1.00 g, 1.04 mmol, 52%) as a brown solid.

^{1}H NMR (400 MHz, $CDCl_3$): δ = 0.88 (t, J = 6.8 Hz, 3H), 0.99 (s, 9H), 1.24–1.36 (m, 6H), 1.50–1.86 (m, 14H), 2.04 (quint, 4H), 2.73–2.83 (m, 4H), 3.48–3.53 (m, 2H), 3.58 (t, J = 5.2 Hz, 2H), 3.62–3.69 (m, 4H), 3.74–3.77 (m, 4H), 3.85–3.97 (m, 6H), 4.66 (t, J = 3.6 Hz 2H), 7.35–7.41 (m, 6H), 7.74–7.66 (m, 4H). ^{13}C NMR (100 MHz, $CDCl_3$): δ = 14.14, 17.53, 19.22, 19.60, 22.58, 25.59, 26.65, 26.83, 28.47, 28.54, 30.76, 31.45, 38.03, 38.63, 62.25, 63.47, 65.98, 67.73, 72.21, 72.70, 98.91, 107.69, 115. 78, 127.74, 129.67, 133.62, 135.67, 136.63, 136.66, 164.71, 164.90. MS (MALDI-TOF): m/z: 980.97 (calcd. $[M+Na]^+$ = 981.47).

Compound 7. 10% Pd/C (1.11 g) was added to a solution of compound **6** (1.00 g, 1.04 mmol) in a mixture of THF (20 mL) and ethyl acetate (200 mL), and the mixture was stirred under

hydrogen atmosphere at r.t. for 36 h. The Pd/C was filtered off and the solvent was evaporated under reduced pressure. The crude product was purified by flash column chromatography on silica gel (eluent: gradient from CH_2Cl_2 to CH_2Cl_2/ethyl acetate = 85:15 v/v) to afford compound **7** (604 mg, 0.624 mmol, 60%) as a colorless liquid.

^{1}H NMR (400 MHz, $CDCl_3$): δ = 0.88 (t, J = 7.2 Hz, 3H), 0.99 (s, 9H), 1.28–1.38 (m, 6H), 1.50–1.74 (m, 24H), 1.78–1.86 (m, 2H), 3.37–3.43 (m, 2H), 3.46–3.56 (m, 6H), 3.60 (t, J = 5.2 Hz, 2H), 3.66 (t, J = 7.2 Hz, 2H), 3.72–3.78 (m, 6H), 3.83–3.90 (m, 4H), 4.59 (t, J = 3.6 Hz, 2H), 7.32–7.42 (m, 6H), 7.64–7.67 (m, 4H). ^{13}C NMR (100 MHz, $CDCl_3$): δ = 14.09, 19.17, 19.64, 22.57, 25.58, 26.32, 26.28, 26.62, 26.79, 28.48, 29.47, 30.79, 31.08, 31.36, 37.64, 38.28, 62.20, 63.46, 67.48, 67.78, 72.04, 98.76, 127.70, 129.65, 133.57, 134.40, 135.61, 140.19, 166.89, 167.06. MS (MALDI-TOF): m/z: 989.94 (calcd. $[M+Na]^+$ = 989.53).

Compound 8. Pyridinium *p*-toluenesulfonate (1.15 g, 4.57 mmol) was added to a solution of compound **7** (443 mg, 0.458 mmol) in a mixture of THF (20 mL), ethanol (80 mL), and water (10 mL) and the mixture was stirred at 60 °C for 4 h. After cooling to r.t., the reaction mixture was poured into ethyl acetate (100 mL) and then washed with saturated aq. NaCl (2 × 100 mL). The organic layer was separated, dried over $MgSO_4$, filtered and the solvent was evaporated under reduced pressure. The crude product was purified by flash column chromatography on silica gel (eluent: gradient from CH_2Cl_2 to CH_2Cl_2/acetone = 85:15 v/v) to afford compound **8** (317 mg, 0.397 mmol, 87%) as a colorless solid.

^{1}H NMR (400 MHz, $CDCl_3$): δ = 0.89 (t, J = 7.2 Hz, 3H), 0.99 (s, 9H), 1.29–1.36 (m, 6H), 1.51–1.57 (m, 4H), 1.61–1.69 (m, 10H), 1.92 (s, 1H), 3.54 (t, J = 7.6 Hz, 4H), 3.59–3.68 (m, 8H), 3.75–3.79 (m, 4H), 3.89 (t, J = 5.6, Hz, 2H), 7.31–7.41 (m, 6H), 7.64–7.67 (m, 4H). ^{13}C NMR (100 MHz, $CDCl_3$): δ = 14.06, 19.14, 22.54, 25.96, 26.14, 26.59, 26.75, 28.43, 30.81,

31.32, 32.29, 37.63, 38.28, 62.74, 63.42, 67.73, 71.97, 127.67, 129.63, 133.52, 134.39, 135.57, 140.10, 166.92, 167.08. MS (MALDI-TOF): m/z: 821.06 (calcd. $[M+Na]^+$ = 821.42).

Compound 9. Methanesulfonyl chloride (113 mg, 0.986mmol) was added dropwise to a solution of compound **8** (315 mg, 0.394 mmol) and Et_3N (100 mg, 0.986 mmol) in CH_2Cl_2 (10 mL) at 0 °C, and the reaction mixture was stirred for 3 h. The resulting reaction mixture was poured into ethyl acetate (100 mL) and washed with 5% aq. HCl (50 mL), saturated aq. $NaHCO_3$ (100 mL), and saturated aq. NaCl (100 mL). The organic layer was separated, dried over $MgSO_4$, filtered and the solvent was evaporated under reduced pressure. The crude product was purified by flash column chromatography on silica gel (eluent: gradient from CH_2Cl_2 to CH_2Cl_2/ethyl acetate = 90:10 v/v) to afford compound **9** (330 mg, 0.345 mmol, 88%) as a colorless liquid.

^1H NMR (400 MHz, $CDCl_3$): δ = 0.89 (t, J = 6.8 Hz, 3H), 0.98 (s, 9H), 1.29–1.33 (m, 6H), 1.57–1.70 (m, 10H), 1.84 (quint, 4H), 3.00 (s, 6H), 3.54 (t, J = 7.6 Hz, 4H), 3.61 (t, J = 5.2 Hz, 2H), 3.67 (t, J = 7.2 Hz, 2H), 3.76–3.79 (m, 4H), 3.89 (t, J = 5.6 Hz, 2H), 4.25 (t, J = 6.4 Hz, 4H) 7.33–7.4 (m, 6H), 7.64–7.66 (m, 4H). ^{13}C NMR (100 MHz, $CDCl_3$): δ = 14.00, 19.07, 22.46, 25.38, 25.77, 26.52, 26.9, 28.35, 28.41, 30.05, 31.24, 37.19, 37.65, 38.24, 63.36, 67.63, 69.94, 71.95, 127.62, 129.57, 133.45, 134.35, 135.49, 139.59, 166.80, 166.95. MS (MALDI-TOF): m/z: 977.40 (calcd. $[M+Na]^+$ = 977.37).

Compound 10. NaN_3 (55.2 mg, 0.850 mmol) was added to a solution of compound **9** (325 mg, 0.340 mmol) in DMF (30 mL) and the mixture was stirred at 80 °C for 4 h. After cooling to r.t., the reaction mixture was poured into ethyl acetate (100 mL) and then washed with saturated aq. NH_4Cl (4 × 50 mL) and saturated aq. NaCl (100 mL). The organic layer was separated, dried over $MgSO_4$, filtered and the solvent was evaporated under reduced pressure. The crude

product was purified by flash column chromatography on silica gel (eluent: gradient from CH_2Cl_2 to CH_2Cl_2/ethyl acetate = 95:5 v/v) to afford compound **10** (236 mg, 0.278 mmol, 82%) as a colorless liquid.

^{1}H NMR (400 MHz, $CDCl_3$): δ = 0.89 (t, J = 6.8 Hz, 3H), 0.98 (s, 9H), 1.30–1.36 (m, 6H), 1.50–1.58 (m, 4H), 1.61–171 (m, 10H), 3.28 (t, J = 6.8 Hz, 4H), 3.53 (t, J = 7.6 Hz, 4H), 3.60 (t, J = 5.2 Hz, 2H), 3.67 (t, J = 7.6 Hz, 2 H), 3.75–3.78 (m, 4H), 3.89 (t, J = 5.6 Hz, 2H), 7.33–7.42 (m, 6H), 7.63–7.66 (m, 4H). ^{13}C NMR (100 MHz, $CDCl_3$): δ = 14.14, 19.24, 22.64, 26.06, 26.69, 26.84, 26.92, 28.54, 30.52, 31.42, 37.77, 38.41, 51.46, 63.52, 67.82, 72.10, 127.76, 129.71, 133.63, 134.50, 135.67, 139.94, 166.96, 167.12. MS (MALDI-TOF): m/z: 871.04 (calcd. $[M+Na]^+$ = 871.43).

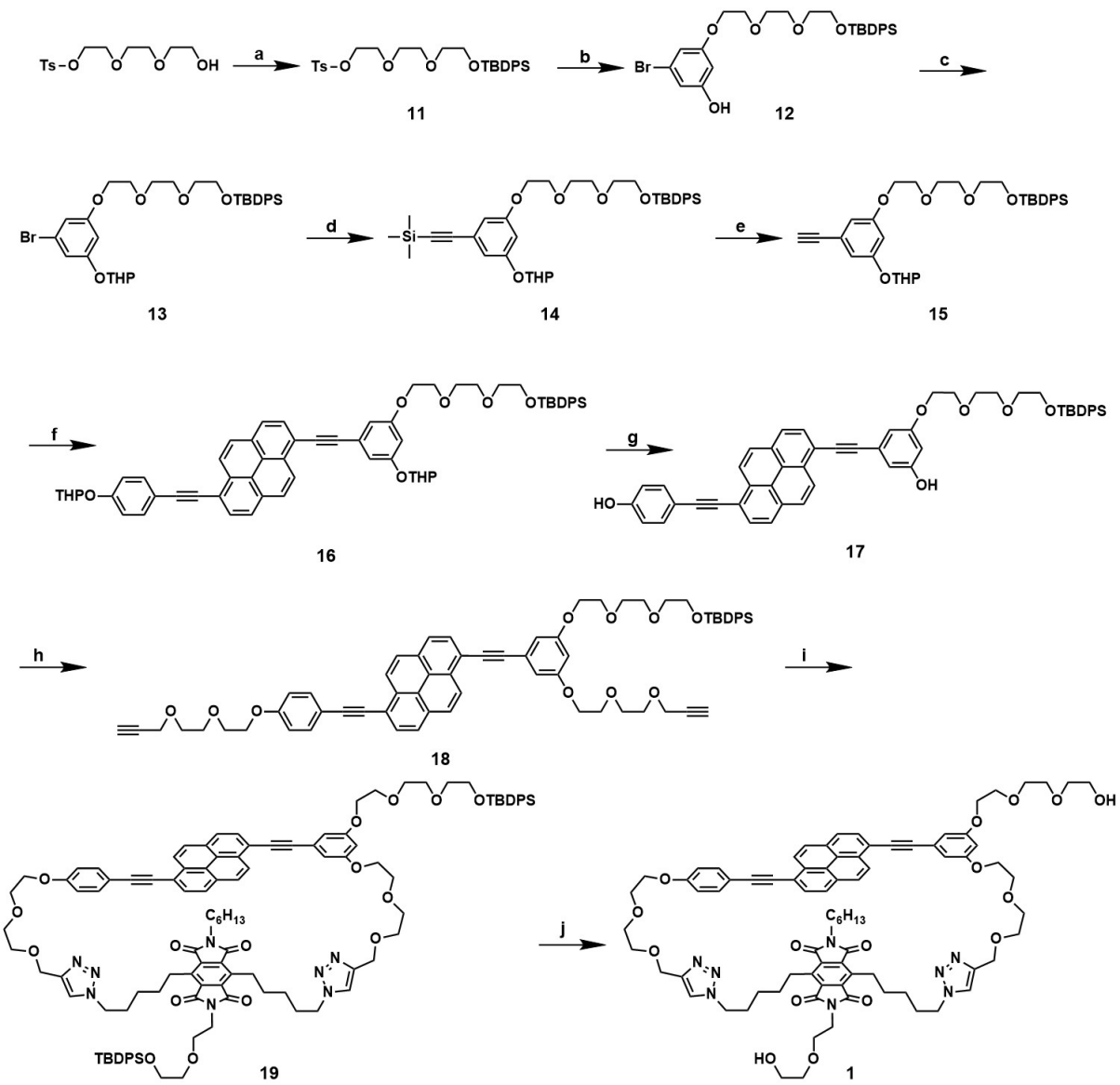

Scheme 2-2. Synthesis of Cyclophane 1.

Conditions: (a) *tert*-butyldiphenylsilyl chloride, imidazole, CH_2Cl_2, r.t., 20 h; (b) 5-bromoresorcinol, K_2CO_3, DMF, 80 °C, 7 h; (c) pyridinium *p*-toluenesulfonate, 3,4-dihydro-2*H*-pyran, CH_2Cl_2, r.t., 12 h; (d) trimethylsilylacetylene, $Pd(PPh_3)_4$, CuI, $(i\text{-Pr})_2NH$, THF, 80 °C, 20 h; (e) K_2CO_3, THF, MeOH, r.t., 4 h; (f) 1-bromo-6-{2-[4-(tetrahydro-2*H*-pyranyl-oxy)phenyl]ethynyl}pyrene, $Pd(PPh_3)_4$, CuI, $(i\text{-Pr})_2NH$, THF, 80 °C, 22 h; (g) pyridinium *p*-toluenesulfonate, THF, ethanol, 80 °C, 2 h; (h) 2-[2-(prop-2-yn-1-yloxy)ethoxy]ethyl 4-

methylbenzenesulfonate, K_2CO_3, DMF, 80 °C, 18 h; (i) compound **10**, CuI, $(i\text{-Pr})_2NEt$, $CHCl_3$, 55 °C, 24 h; (j) $Et_3N{\cdot}3HF$, Et_3N, THF, 70 °C, 24 h.

Compound 11. A mixture of triethylene glycol *p*-toluenesulfonate (12.2 g, 39.9 mmol), *tert*-butyldiphenylsilyl chloride (13.2 g, 47.9 mmol), imidazole (8.16 g, 120 mmol) in CH_2Cl_2 (200 mL) was stirred at r.t. for 20 h. The resulting reaction mixture was poured into CH_2Cl_2 (100 mL) and then washed with water (2 × 50 mL), and saturated aq. NaCl (100 mL). The organic layer was separated, dried over $MgSO_4$, filtered and the solvent was evaporated under reduced pressure. The crude product was purified by flash column chromatography on silica gel (eluent: gradient from hexane/ethyl acetate = 90:10 v/v to hexane/ethyl acetate = 70:30 v/v) to afford compound **11** (18.7 g, 34.4 mmol, 86%) as a colorless liquid.

^{1}H NMR (400 MHz, $CDCl_3$): δ = 1.04 (s, 9H), 2.41 (s, 3H), 3.53–3.59 (m, 6H), 3.67 (t, J = 5.2 Hz, 2H), 3.79 (t, J = 5.2 Hz, 2H), 4.13 (t, J = 5.2 Hz, 2 H), 7.28 (d, J = 8.0 Hz, 2 H), 7.35–7.44 (m, 6 H), 7.66–7.69 (m, 4 H), 7.77–7.79 (m, 2 H). ^{13}C NMR (100 MHz, $CDCl_3$): δ = 19.26, 21.72, 26.88, 63.47, 68.78, 69.35, 70.77, 70.88, 72.54, 127.37, 128.06, 129.73, 129.89, 133.01, 133.70, 135.67, 144.85. MS (MALDI-TOF): m/z: 565.24 (calcd. $[M+Na]^+$ = 565.21).

Compound 12. A mixture of compound **11** (18.7 g, 34.4 mmol), 5-bromoresorcinol (7.15 g, 37.8 mmol), and K_2CO_3 (14.3 g, 103 mmol) in DMF (200 mL) was stirred at 80 °C for 7 h. After cooling to the r.t., most of the DMF was evaporated under reduced pressure. The reaction mixture was then poured into ethyl acetate (200 mL) and washed with saturated NH_4Cl (4 × 200 mL) and saturated aq. NaCl (200 mL). The organic layer was separated, dried over $MgSO_4$, filtered and the solvent was evaporated under reduced pressure. The crude product was purified by flash column chromatography on silica gel (eluent: gradient from

hexane/ethyl acetate = 95:5 v/v to hexane/ethyl acetate = 60:40 v/v) to afford compound **12** (7.50 g, 13.4 mmol, 35%) as a colorless liquid.

^{1}H NMR (400 MHz, $CDCl_3$): δ = 1.04 (s, 9H), 3.61 (t, J = 5.2 Hz, 2H), 3.69 (s, 4H), 3.78–3.82 (m, 4 H), 3.97–3.99 (m, 2H), 6.30 (t, J = 2.0 Hz, 1H), 6.43 (s, 1H), 6.54 (t, J = 2.0 Hz, 1H), 6.58 (t, J = 2.0 Hz, 1H), 7.34–7.43 (m, 6H), 7.66–7.68 (m, 4H). ^{13}C NMR (100 MHz, $CDCl_3$): δ = 19.24, 26.88, 63.41, 67.40, 69.73, 70.75, 70.79, 72.59, 101.65, 109.77, 111.97, 122.70, 127.75, 129.75, 133.57, 135.65, 157.97, 160.25. MS (MALDI-TOF): m/z: 581.19 (calcd. $[M+Na]^+$ = 581.13).

Compound 13. A mixture of compound **12** (1.65 g, 2.95 mmol), pyridinium *p*-toluenesulfonate (156 mg, 0.621 mmol), and 3,4-dihydro-2*H*-pyran (322 g, 3.83 mmol), in CH_2Cl_2 (20 mL), was stirred at r.t. for 12 h. The resulting reaction mixture was poured into ethyl acetate (100 mL) and washed with water (2 × 50 mL) and saturated aq. NaCl (100 mL). The organic layer was separated, dried over $MgSO_4$, filtered and the solvent was evaporated under reduced pressure. The crude product was purified by flash column chromatography on silica gel (eluent: gradient from hexane/ethyl acetate = 95:5 v/v to hexane/ethyl acetate = 80:20 v/v) to afford compound **13** (1.50 g, 2.33 mmol, 79 %) as a colorless liquid.

^{1}H NMR (400 MHz, $CDCl_3$): δ = 1.05 (s, 9H), 1.54–1.72 (m, 3H), 1.80–1.84 (m, 2H), 1.91–1.99 (m, 1H), 3.57–3.63 (m, 3H), 3.65–3.70 (m, 4H), 4.04–4.06 (m, 2H), 5.35 (t, J = 3.2 Hz, 1H), 6.56 (t, J = 2.0 Hz, 1H), 6.70 (t, J = 2.0 Hz, 1H), 6.83 (t, J = 2.0 Hz, 1H), 7.35–7.44 (m, 6H), 7.67–7.70 (m, 4H). ^{13}C NMR (100 MHz, $CDCl_3$): δ = 18.65, 19.28, 25.16, 26.90, 30.25, 62.05, 63.52, 67.79, 69.64, 70.99, 72.57, 76.84, 77.16, 77.48, 96.50, 102.58, 111.36, 112.60, 122.71, 127.72, 129.71, 133.73, 135.69, 158.66, 160.33. MS (MALDI-TOF): m/z: 665.45 (calcd. $[M+Na]^+$ = 665.19).

Compound 14. A mixture of compound **13** (2.63 g, 4.09 mmol), trimethylsilylacetylene (2.01 g, 20.5 mmol), $Pd(PPh_3)_4$ (236 mg, 0.204 mmol), CuI (38.9 mg, 0.204 mmol), and $(i\text{-Pr})_2NH$ (10 mL) in THF (30 mL) was stirred under nitrogen atmosphere at 80 °C for 20 h. After cooling to r.t., the reaction mixture was poured into ethyl acetate (200 mL) and washed with 5% aq. HCl (2 × 100 mL), saturated aq. $NaHCO_3$ (100 mL), and saturated aq. NaCl (100 mL). The organic layer was separated, dried over $MgSO_4$, filtered, and the solvent was evaporated under reduced pressure. The crude product was purified by flash column chromatography on silica gel (eluent: gradient from hexane/ethyl acetate = 95:5 v/v to hexane/ethyl acetate = 80:20 v/v) to afford compound **14** (2.64 g, 3.99 mmol, 98%) as a brown liquid.

^{1}H NMR (400 MHz, $CDCl_3$): δ = 0.23 (s, 9H), 1.05 (s, 9H), 1.54–1.73 (m, 3H), 1.80–1.84 (m, 2H), 1.92–2.00 (m, 1H), 3.57–3.64 (m, 3H), 3.65–3.70 (m, 4H), 3.80–3.89 (m, 5H), 4.06–4.08 (m, 2H), 5.37 (t, J = 3.2 Hz, 1H), 6.61 (t, J = 2.0 Hz, 1H), 6.63–6.64 (m, 1H), 6.78–6.79 (m, 1H), 7.33–7.44 (m, 6H), 7.67–7.70 (m, 4H). ^{13}C NMR (100 MHz, $CDCl_3$): δ = 0.10 18.75, 19.33, 25.27, 26.94, 30.37, 62.08, 63.56, 67.69, 69.77, 70.95, 71.02, 72.61, 93.74, 96.40, 105.14, 111.03, 112.87, 124.32, 127.77, 129.75, 133.79, 135.75, 157.89, 159.55. MS (MALDI-TOF): m/z: 660.65 (calcd. $[M]^+$ = 660.33).

Compound 15. A mixture of compound **14** (2.39 g, 3.62 mmol) and K_2CO_3 (2.50 g, 18.1 mmol) was stirred in a THF/MeOH (1:4 v/v) mixture (25 mL) at r.t. for 4 h. The reaction mixture was then poured into ethyl acetate (200 mL) and washed with saturated aq. NaCl (2 × 100 mL). The organic layer was separated, dried over $MgSO_4$, filtered, and the solvent was evaporated under reduced pressure. The crude product was purified by flash column chromatography on silica gel (eluent: gradient from hexane/ethyl acetate = 95:5 v/v to hexane/ethyl acetate = 80:20 v/v) to afford compound **15** (1.30 g, 2.60 mmol, 72 %) as a brown liquid.

^{1}H NMR (400 MHz, $CDCl_3$): δ = 1.05 (s, 9H), 1.55–1.72 (m, 3H), 1.80–1.87 (m, 2H), 1.92–2.00 (m, 1 H), 3.56–3.64 (m, 3H), 3.65–3.71 (m, 4H), 3.80–3.89 (m, 5H), 4.05–4.08 (m, 2H), 5.36 (t, J = 3.2 Hz, 1H), 6.65 (t, J = 2.0 Hz, 1H), 6.66–6.68 (m, 1H), 6.80–6.82 (m, 1H), 7.35–7.43 (m, 6H), 7.67–7.69 (m, 4H). ^{13}C NMR (100 MHz, $CDCl_3$): δ = 18.64, 19.17, 25.09, 26.82, 30.21, 61.92, 63.44, 67.57, 69.58, 70.77, 70.85, 72.47, 76.88, 83.57, 105.01, 111.28, 112.93, 123.25, 127.63, 129.61, 133.64, 135.58, 157.88, 159.52. MS (MALDI-TOF): m/z: 611.25 (calcd. $[M+Na]^+$ = 611.28).

Compound 16. A mixture of compound **15** (940 mg, 1.88 mmol), 1-bromo-6-{2-[4-(tetrahydo-2*H*-pyranyloxy)phenyl]ethynyl}pyrene (904 mg, 1.88 mmol), $Pd(PPh_3)_4$ (108 mg, 9.35×10^{-2} mmol), CuI (17.8 mg, 9.35×10^{-2} mmol), and $(i\text{-Pr})_2NH$ (10 mL) in THF (30 mL) was stirred under nitrogen atmosphere at 80 °C for 20 h. After cooling to r.t., the reaction mixture was poured into ethyl acetate (200 mL) and washed with 5% aq. HCl (2 × 100 mL), saturated aq. $NaHCO_3$ (100 mL), and saturated aq. NaCl (100 mL). The organic layer was separated, dried over $MgSO_4$, filtered, and the solvent was evaporated under reduced pressure. The crude product was purified by flash column chromatography on silica gel (eluent: gradient from hexane/ethyl acetate = 80:20 v/v to hexane/ethyl acetate = 50:50 v/v) to afford compound **16** (812 mg, 0.821 mmol, 44%) as a yellow solid.

^{1}H NMR (400 MHz, $CDCl_3$): δ = 1.06 (s, 9H), 1.57–1.72 (m, 3H), 1.85–1.89 (m, 2H), 1.98–2.02 (m, 1H), 3.59–3.72 (m, 8H), 3.82–3.96 (m, 6H), 4.13–4.16 (m, 2H), 5.44–5.47 (m, 2H), 6.71 (t, J = 2.4 Hz, 1H), 6.90–6.91 (m, 1H), 7.04–7.05 (m, 1H), 7.07–7.10 (m, 1H), 7.34–7.40 (m, 6H), 7.62–7.64 (m, 2H), 7.68–7.71(m, 4H), 8.02–8.14 (m, 6H), 8.56 (d, J = 6.0 Hz, 1H), 8.58 (d, J = 6.4 Hz, 1H). ^{13}C NMR (100 MHz, $CDCl_3$): δ = 18.75, 18.78, 19.28, 25.22, 25.26, 26.92, 30.32, 30.40, 62.12, 63.55, 67.73, 69.77, 70.90, 70.99, 72.59, 87.47, 88.25, 95.56, 95.73, 96.31, 96.51, 104.77, 111.00, 112.56, 116.44, 116.61, 118.21, 118.88, 124.17, 124.69, 125.05,

125.19, 126.08, 126.35, 127.73, 127.97, 128.17, 129.71, 129.79, 129.95, 130.89, 131.20, 131.81, 132.07, 133.14, 133.76, 135.69, 157.37, 158.14, 159.78. MS (MALDI-TOF): m/z: 1011.91 (calcd. $[M+Na]^+$ = 1011.43).

Compound 17. Pyridinium *p*-toluenesulfonate (2.06 g, 8.21 mmol) was added to a solution of compound **16** (812 mg, 0.821 mmol) in a mixture of THF (20 mL) and water (10 mL) and the reaction mixture was stirred at 80 °C for 2 h. After cooling to r.t., the reaction mixture was poured into ethyl acetate (100 mL) and then washed with saturated aq. NaCl (2 × 100 mL). The organic layer was separated, dried over $MgSO_4$, filtered and the solvent was evaporated under reduced pressure. The crude product was purified by flash column chromatography on silica gel (eluent: gradient from CH_2Cl_2 to CH_2Cl_2/acetone = 95:5 v/v) to afford compound **17** (600 mg, 0.731 mmol, 89 %) as a yellow solid.

^{1}H NMR (400 MHz, $CDCl_3$): δ = 1.05 (s, 9H), 3.67 (t, J = 5.2 Hz, 2H), 3.79 (s, 4H), 3.85 (t, J = 5.2 Hz, 2H), 3.88–3.91 (m, 2H), 4.07–4.09 (m, 2H), 6.44 (t, J = 2.4 Hz, 1H), 6.63 (s, 1H), 6.79 (s, 1H), 6.85 (d, J = 7.6 Hz, 2H), 7.33–7.43 (m, 6H), 7.51–7.56 (m, 3H), 7.62–7.76 (m, 7H), 7.84 (d, J = 8.0 Hz, 1H), 7.89 (d, J = 8.0 Hz, 1H), 8.15 (d, J = 9.2 Hz, 1H), 8.33 (d, J = 8.8 Hz, 1H). ^{13}C NMR (100 MHz, $CDCl_3$): δ = 19.31, 26.94, 63.47, 67.31, 70.04, 70.90, 72.69, 87.32, 88.50, 95.32, 95.61, 103.42, 109.86, 111.74, 115.60, 115.95, 117.86, 118.53, 123.50, 124.57, 124.70, 125.03, 125.72, 125.76, 127.26, 127.75, 127.83, 129.26, 129.57, 129.83, 130.39, 130.63, 131.29, 131.71, 133.47, 133.59, 135.72, 156.38, 159.63. MS (MALDI-TOF): m/z: 820.46 (calcd. $[M+Na]^+$ = 820.32).

Compound 18. A mixture of compound **17** (200 mg, 0.244 mmol), 2-[2-(prop-2-yn-1-yloxy)ethoxy]ethyl 4-methylbenzenesulfonate (182 mg, 0.609 mmol), and K_2CO_3 (101 mg, 0.731 mmol) in DMF (200 mL) was stirred at 80 °C for 18 h. After cooling to r.t., most of the

DMF was evaporated under reduced pressure. The reaction mixture was then poured into ethyl acetate (200 mL) and washed with saturated NH_4Cl (4 × 200 mL) and saturated aq. NaCl (200 mL). The organic layer was separated, dried over $MgSO_4$, filtered and the solvent was evaporated under reduced pressure. The crude product was purified by flash column chromatography on silica gel (eluent: gradient from hexane/ethyl acetate = 50:50 v/v to hexane/ethyl acetate = 20:80 v/v) to afford compound **18** (203 mg, 0.189 mmol, 78 %) as a yellow solid.

^{1}H NMR (400 MHz, $CDCl_3$): δ = 1.05 (s, 9H), 2.44–2.46 (m, 2H), 3.63 (t, J = 5.2 Hz, 2H), 3.68–3.79 (m, 12H), 3.83 (t, J = 5.2 Hz, 2H), 3.87–3.90 (m, 4H), 4.14–4.20 (m, 6H), 4.23 (s, 2H), 4.23 (s, 2H), 6.56 (t, J = 2.4 Hz, 1H), 6.87–6.88 (m, 2H), 6.95–6.98 (m, 2H), 7.35–7.43 (m, 6H), 7.62–7.66 (m, 2H), 7.68–7.71 (m, 4H), 8.10–8.19 (m, 6H), 8.61 (d, J = 9.2 Hz, 1H), 8.64 (d, J = 9.2 Hz, 1H). ^{13}C NMR (100 MHz, $CDCl_3$): δ = 19.31, 26.94, 58.59, 63.57, 67.59, 67.75, 69.26, 69.79, 70.95, 71.03, 72.62, 74.78, 79.70,79.73, 87.43, 88.26, 95.53, 95.75, 103.15, 110.49, 114.90, 115.78, 118.22, 119.00, 124.30, 124.70, 125.14, 125.31, 126.16, 126.51, 127.75, 128.08, 128.32, 129.74, 129.89, 130.04, 130.97, 131.33, 131.90, 132.20, 133.27, 133.78, 135.72, 159.14, 159.84, 159.89. MS (MALDI-TOF): m/z: 1072.90 (calcd. $[M+Na]^+$ = 1072.46).

Compound 19. A mixture of compound **18** (126 mg, 0.118 mmol), compound **10** (100 mg, 0.118 mmol), CuI (56.1 mg, 0.294 mmol), and (i-Pr)$_2$NEt (50 mL) in $CHCl_3$ (250 mL) was stirred at 55 °C for 24 h. After cooling to r.t., the reaction mixture was washed with 5% aq. HCl (3 × 100 mL), saturated aq. $NaHCO_3$ (100 mL), and saturated aq. NaCl (100 mL). The organic layer was separated, dried over $MgSO_4$, filtered, and the solvent was evaporated under reduced pressure. The crude product was purified by flash column chromatography on silica

gel (eluent: gradient from CH_2Cl_2 to CH_2Cl_2/acetone = 70:30 v/v) to afford compound **19** (162 mg, 8.41×10^{-2} mmol, 71%) as a reddish-orange solid.

^{1}H NMR (400 MHz, $CDCl_3$): δ = 0.90 (t, J = 6.8 Hz, 3H), 0.99 (s, 9H), 1.06 (s, 9H), 1.22–1.38 (m, 14H), 1.60–1.63 (m, 2H), 1.77–1.82 (m, 4H), 2.58–2.63 (m, 2H), 2.81–2.85 (m, 2H), 3.47 (t, J = 7.6 Hz, 2H), 3.63–3.66 (m, 4H), 3.71– 3.85 (m, 22H), 3.88–3.92 (m, 6H), 4.06–4.12 (m, 4H), 4.18 (t, J = 5.2 Hz, 2H), 4.23 (t, J = 4.4 Hz, 2H), 4.28–4.30 (m, 2H), 4.72 (s, 1H), 4.76 (s, 1H), 6.61 (t, J = 2.4 Hz, 1H), 6.91–6.91 (m, 1H), 6.70–7.00 (m, 1H), 7.07 (d, J = 8.8 Hz, 2H), 7.20 (s, 1H), 7.31–7.44 (m, 12H), 7.50 (s, 1H), 7.64–7.66 (m, 4H), 7.69–7.71 (m, 6H), 7.86 (d, J = 9.2 Hz, 1H), 7.91–7.96 (m, 4H), 8.00 (d, J = 8.0 Hz, 1H), 8.08 (d, J = 7.6 Hz, 1H), 8.39 (d, J = 9.2 Hz, 1H), 8.46 (d, J = 8.8 Hz, 1H). ^{13}C NMR (100 MHz, $CDCl_3$): δ = 14.18, 19.26, 19.32, 22.71, 25.50, 25.91, 26.83, 26.89, 26.94, 27.21, 28.67, 28.90, 29.11, 29.29, 29.38, 31.49, 37.44, 38.10, 50.37, 50.53, 63.58, 64.93, 65.16, 67.86, 67.93, 67.97, 68.16, 69.62, 69.72, 69.80, 69.83, 69.96, 70.96, 71.06, 71.13, 71.32, 72.10, 72.64, 87.57, 88.18, 96.02, 96.44, 102.86, 110.13, 111.10, 115.37, 115.75, 118.48, 119.15, 122.97, 123.56, 123.59, 124.71, 124.93, 125.07, 126.19, 126.37, 127.77, 127.78, 128.07, 129.75, 130.30, 132.74, 132.84, 133.42, 133.61, 133.78, 135.66, 135.73, 138.48, 138.53, 159.62, 160.11, 160.16, 166.06, 166.19, 166.20. MS (MALDI-TOF): m/z: 1921.37 (calcd. $[M]^+$ = 1920.90).

Compound 1. $Et_3N{\cdot}3HF$ (161 mg, 0.999 mmol) was added to a solution of compound **19** (120 mg, 6.24×10^{-2} mmol) and Et_3N (101 mg, 0.999 mmol) in THF (15 mL) and the mixture was stirred at 70 °C for 24 h. After cooling to r.t., the reaction mixture was washed with saturated aq. $NaHCO_3$ (100 mL) and saturated aq. NaCl (100 mL). The organic layer was separated, dried over $MgSO_4$, filtered, and the solvent was evaporated under reduced pressure. The crude product was purified by flash column chromatography on silica gel (eluent: gradient from

CH_2Cl_2/acetone = 70:30 v/v to acetone) to afford compound **1** (72.1 mg, 4.95×10^{-2} mmol, 79%) as a reddish-orange solid.

^{1}H NMR (400 MHz, $CDCl_3$): δ = 0.87–0.91 (m, 3H), 1.24–1.33 (m, 14H), 1.56–1.61 (m, 2H), 1.79 (quint, 4H), 2.60–2.64 (m, 2H), 2.67–2.71 (m, 2H), 2.74–2.78 (m, 2H), 3.45 (t, J = 7.6 Hz, 2H), 3.62–3.65 (m, 4H), 3.70–3.79 (m, 20H), 3.87–3.92 (m, 6H), 4.06–4.13 (m, 4H), 4.19–4.24 (m, 4H), 4.27–4.29 (m, 2H), 4.69 (s, 2H), 4.74 (s, 2H), 6.61 (t, J = 2.4 Hz, 1H), 6.91–6.91 (m, 1H), 6.97–6.98 (m, 1H), 7.06 (d, J = 8.8 Hz, 2H), 7.19 (s, 1H), 7.47 (s, 1H), 7.66 (d, J = 8.8 Hz, 2H), 7.83 (d, J = 9.2 Hz, 1H), 7.89–7.93 (m, 3H), 7.99 (d, J = 8.0 Hz, 1H), 8.05 (d, J = 8.4 Hz, 1H), 8.37 (d, J = 9.2 Hz, 1H), 8.40 (d, J = 9.2 Hz, 1H). ^{13}C NMR (100 MHz, $CDCl_3$): δ = 14.16, 22.68, 25.47, 25.79, 26.74, 26.80, 27.03, 28.63, 28.78, 29.01, 29.25, 29.80, 31.45, 37.40, 38.09, 50.26, 50.39, 61.81, 61.84, 64.92, 65.12, 67.78, 67.95, 68.16, 68.33, 69.59, 69.73, 69.82, 69.95, 70.48, 70.97, 71.08, 71.27, 72.28, 72.65, 87.51, 96.02, 96.49, 102.88,110.14, 111.06, 115.38, 115.66, 118.41, 119.16, 122.74, 123.49, 124.69, 124.85, 125.02, 126.10, 126.35, 127.71, 128.02, 129.81, 130.22, 130.33, 130.71, 131.28, 131.70, 132.57, 132.63, 132.79, 132.86, 133.37, 138.52, 138.54, 145.25, 145.53, 159.61, 160.03, 160.10, 166.03, 166.10, 166.23, 166.32. HRMS (ESI-TOF): m/z: 1467.6544 (calcd. $[M+Na]^+$ = 1467.6529.

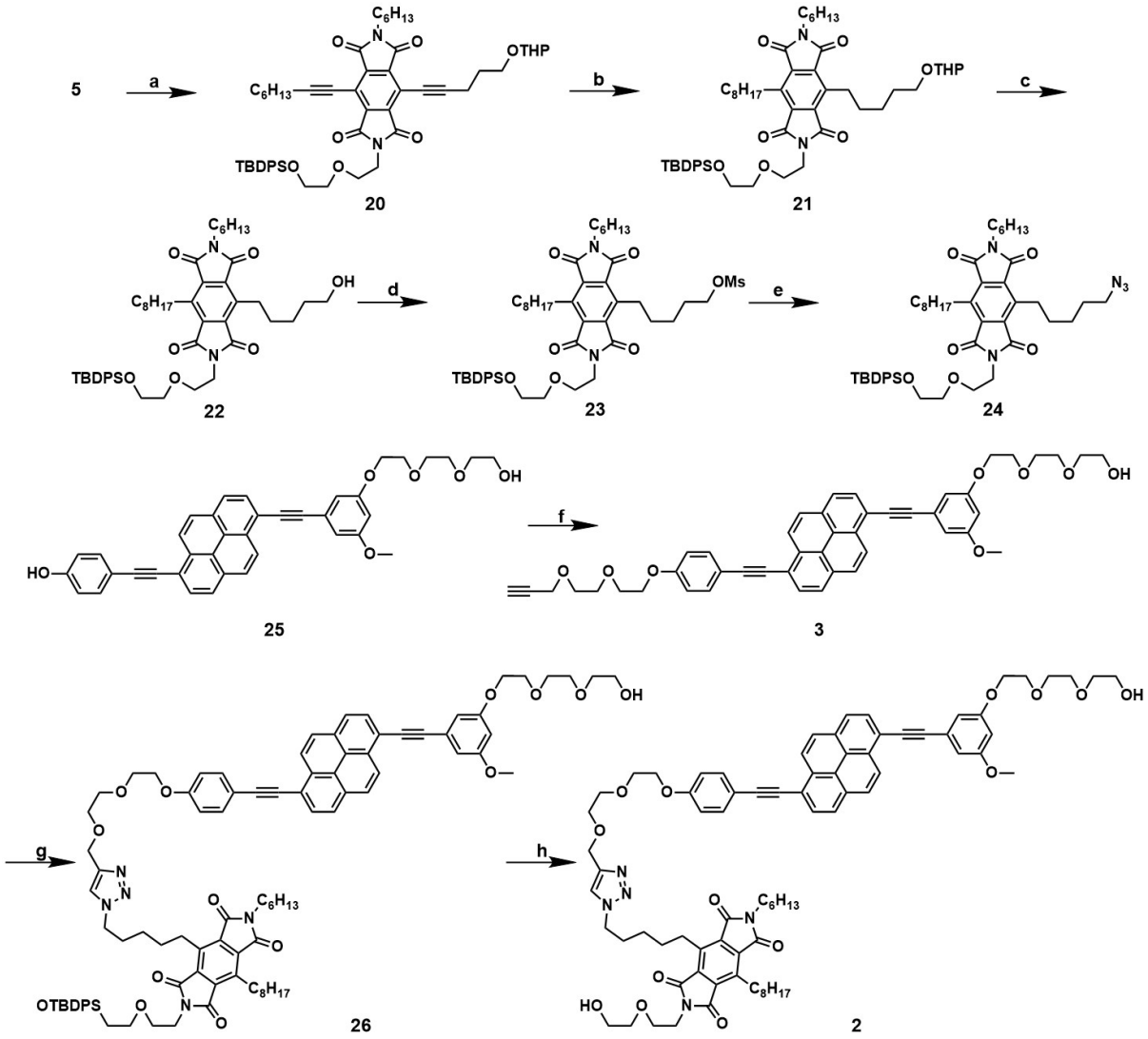

Scheme 2-3. Synthesis of compound 2 and 3.

Conditions: (a) 2-(pent-4-yn-1-yloxy)tetrahydro-*2H*-pyran, 1-octyne, $Pd(PPh_3)_2Cl_2$, CuI, $(i\text{-}Pr)_2NEt$, toluene, 100 °C, 24 h; (b) Pd/C, H_2, THF, ethyl acetate, r.t., 36 h; (c) pyridinium *p*-toluenesulfonate, THF, H_2O, ethanol, 60 °C, 2 h; (d) methanesulfonyl chloride, Et_3N, CH_2Cl_2, 0 °C, 1.5 h; (e) NaN_3, DMF, 80 °C, 2 h; (f) 2-[2-(prop-2-yn-1-yloxy)ethoxy]ethyl 4-methylbenzenesulfonate, K_2CO_3, DMF, 80 °C, 18 h; (g) compound **24**, CuI, $(i\text{-}Pr)_2NEt$, $CHCl_3$, 55 °C, 24 h; (h) $Et_3N{\cdot}3HF$, Et_3N, THF, 70 °C, 24 h.

Compound 20. A mixture of compound **5** (1.72 g 2.19 mmol), 2-(pent-4-yn-1-yloxy)tetrahydro-*2H*-pyran, (730 mg, 4.39 mmol), 1-octyne (484 mg, 4.39 mmol), $Pd(PPh_3)_2Cl_2$ (154 mg, 0.220 mmol), CuI (41.9 mg, 0.220 mmol), $(i\text{-Pr})_2NEt$ (40 mL), and toluene (10 mL) was stirred under nitrogen atmosphere at 100 °C for 24 h. After cooling to r.t., the reaction mixture was poured into ethyl acetate (150 mL) and washed with 5% aq. HCl (2 × 100 mL), saturated aq. $NaHCO_3$ (100 mL), and saturated aq. NaCl (100 mL). The organic layer was separated, dried over $MgSO_4$, filtered, and the solvent was evaporated under reduced pressure. The crude product was purified by flash column chromatography on silica gel (eluent: gradient from CH_2Cl_2 to CH_2Cl_2/ethyl acetate = 90:10 v/v) to afford compound **20** (888 mg, 0.985 mmol, 45%) as a brown solid.

^{1}H NMR (400 MHz, $CDCl_3$): δ = 0.87–0.92 (m, 6H), 1.00 (s, 9H), 1.32–1.36 (m, 10H), 1.50–1.86 (m, 12H), 2.05 (quint, 2H), 2.46 (t, J = 7.2 Hz, 2H), 2.73–2.83 (m, 2H), 3.47–3.53 (m, 4H), 3.56 (t, J = 5.2 Hz, 2H), 3.62– 3.71 (m, 3H), 3.85–3.98 (m, 4H), 4.67 (t, J = 3.6 Hz, 1H), 7.35–7.41 (m, 6H), 7.64–7.66 (m, 4H). ^{13}C NMR (100 MHz, $CDCl_3$): δ = 14.04, 14.10, 17.42, 19.12, 19.51, 20.47, 22.48, 22.56, 25.52, 26.55, 26.75, 28.14, 28.36, 28.45, 28.65, 30.67, 31.35, 37.93, 38.51, 62.11, 63.38, 65.88, 67.64, 72.13, 72.43, 72.63, 98.79, 107.50, 108.47, 115.53, 115.83, 127.65, 129.57, 133.54, 135.57, 136.52, 164.59, 164.78. MS (MALDI-TOF): m/z: 923.84 (calcd. $[M+Na]^+$ = 923.46).

Compound 21. 10% Pd/C (500 mg) was added to a solution of compound **20** (390 mg, 0.433 mmol) in a mixture of THF (20 mL) and ethyl acetate (200 mL), and the mixture was stirred under hydrogen atmosphere at r.t. for 36 h. The Pd/C was filtered off and the solvent was evaporated under reduced pressure. The crude product was purified by flash column

chromatography on silica gel (eluent: gradient from CH_2Cl_2 to CH_2Cl_2/ethyl acetate = 90:10 v/v) to afford compound **21** (259 mg, 0.285 mmol, 66%) as a colorless liquid.

^{1}H NMR (400 MHz, $CDCl_3$): δ = 0.86–0.91 (m, 6H), 0.98 (s, 9H), 1.26–1.32 (m, 14H), 1.42–1.85 (m, 18H), 3.37–3.42 (m, 1H), 3.46–3.55 (m, 5H), 3.60 (t, J = 5.2 Hz, 2H), 3.66 (t, J = 7.6 Hz, 2H), 3.72– 3.77 (m, 5H), 3.83–3.90 (m, 3H), 4.58 (t, J = 3.6 Hz, 1H), 7.31–7.42 (m, 6H), 7.64–7.67 (m, 4H). ^{13}C NMR (100 MHz, $CDCl_3$): δ = 14.13, 14.25, 19.22, 19.69, 22.62, 22.79, 25.63, 26.33, 26.45, 26.67, 26.83, 28.53, 29.38, 29.42, 29.53, 29.82, 30.10, 30.83, 31.12, 31.42, 31.98, 37.67, 38.32, 62.25, 63.51, 67.54, 67.83, 72.90, 98.82, 127.74, 129.69, 133.62, 134.44, 135.66, 140.15, 140.56, 166.97, 167.14. MS (MALDI-TOF): m/z: 931.53 (calcd. $[M+Na]^+$ = 931.72).

Compound 22. Pyridinium *p*-toluenesulfonate (387 mg, 1.54 mmol) was added to a solution of compound **21** (140 mg, 0.154 mmol) in a mixture of THF (20 mL), ethanol (80 mL), and water (10 mL) and the mixture was stirred at 60 ºC for 2 h. After cooling to r.t., the reaction mixture was poured into ethyl acetate (100 mL) and then washed with saturated aq. NaCl (2 × 100 mL). The organic layer was separated, dried over $MgSO_4$, filtered and the solvent was evaporated under reduced pressure. The crude product was purified by flash column chromatography on silica gel (eluent: gradient from CH_2Cl_2 to CH_2Cl_2/acetone = 85:15 v/v) to afford compound **22** (114 mg, 0.139 mmol, 90%) as a colorless liquid.

^{1}H NMR (400 MHz, $CDCl_3$): δ = 0.86–0.91 (m, 6H), 0.98 (s, 9H), 1.26–1.36 (m, 14H), 1.41–1.69 (m, 12H), 3.50–3.55 (m, 4H), 3.59 (t, J = 5.2 Hz, 2H), 3.64–3.68 (m, 4H), 3.75–3.78 (m, 4H), 3.88 (t, J = 5.6 Hz, 2H), 7.32–7.42 (m, 6H), 7.64–7.67 (m, 4H). ^{13}C NMR (100 MHz, $CDCl_3$): δ = 14.14, 14.26, 19.23, 22.63, 22.81, 26.05, 26.21, 26.47, 26.69, 26.84, 28.54, 29.40, 29.42, 30.11, 30.89, 31.43, 31.99, 32.39, 37.70, 38.35, 63.00, 63.51, 67.85, 72.08, 127.76,

129.71, 133.63, 134.47, 135.67, 140.02, 140.65, 166.97, 167.07, 167.13, 167.22. MS (MALDI-TOF): m/z: 847.47 (calcd. $[M+Na]^+$ = 847.50).

Compound 23. Methanesulfonyl chloride (32 mg, 0.276 mmol) was added dropwise to a solution of compound **22** (91.0 mg, 0.110 mmol) and Et_3N (28 mg, 0.276 mmol) in CH_2Cl_2 (10 mL) at 0 °C, and the reaction mixture was stirred for 1.5 h. The resulting reaction mixture was poured into ethyl acetate (100 mL) and washed with 5% aq. HCl (50 mL), saturated aq. $NaHCO_3$ (100 mL), and saturated aq. NaCl (100 mL). The organic layer was separated, dried over $MgSO_4$, filtered and the solvent was evaporated under reduced pressure. The crude product was purified by flash column chromatography on silica gel (eluent: gradient from CH_2Cl_2 to CH_2Cl_2/ethyl acetate = 95:5 v/v) to afford compound **23** (82.1 mg, 9.09×10^{-2} mmol, 83%) as a colorless liquid. ^{1}H NMR (400 MHz, $CDCl_3$): δ = 0.86–0.90 (m, 6H), 0.98 (s, 9H), 1.26–1.32 (m, 14H), 1.42–1.49 (m, 2H), 1.56–1.69 (m, 10H), 1.84 (quint, 2H), 3.01 (s, 3H), 3.50–3.54 (m, 4H), 3.56 (t, J = 5.2 Hz, 2H), 3.66 (t, J = 7.6 Hz, 2H), 3.75– 3.77 (m, 4H), 3.88 (t, J = 5.6 Hz, 2H), 4.25 (t, J = 6.4 Hz, 2H), 7.32–7.42 (m, 6H), 7.63–7.66 (m, 4H). ^{13}C NMR (100 MHz, $CDCl_3$): δ = 14.14, 14.26, 19.24, 22.63, 22.81, 25.60, 25.94, 26.49, 26.69, 26.84, 28.53, 28.59, 29.40, 29.42, 30.11, 30.26, 31.42, 31.99, 37.43, 37.74, 38.38, 63.52, 67.83, 70.03, 72.10, 127.76, 129.72, 133.63, 134.46, 134.49, 135.67, 139.46, 140.83, 166.92, 167.06, 167.08, 167.22. MS (MALDI-TOF): m/z: 925.45 (calcd. $[M+Na]^+$ = 925.25).

Compound 24. NaN_3 (23.8 mg, 0.365 mmol) was added to a solution of compound **23** (165 mg, 0.183 mmol) in DMF (20 mL) and the mixture was stirred at 80 °C for 2 h. After cooling to r.t., the reaction mixture was poured into ethyl acetate (100 mL) and washed with saturated aq. NH_4Cl (4 × 50 mL) and saturated aq. NaCl (100 mL). The organic layer was separated, dried over $MgSO_4$, filtered and the solvent was evaporated under reduced pressure. The crude

product was purified by flash column chromatography on silica gel (eluent: gradient from hexane/CH_2Cl_2 = 15:85 v/v to CH_2Cl_2) to afford compound **24** (129 mg, 0.152 mmol, 83%) as a colorless liquid. ^{1}H NMR (400 MHz, $CDCl_3$): δ = 0.86–0.90 (m, 6H), 0.98 (s, 9H), 1.26–1.36 (m, 14H), 1.42–1.49 (m, 2H), 1.50–1.71 (m, 12H), 3.28 (t, J = 6.8 Hz, 2H), 3.50–3.54 (m, 4H), 3.59 (t, J = 5.2 Hz, 2H), 3.67 (t, J = 7.6 Hz, 2H), 3.75–3.78 (m, 4H), 3.88 (t, J = 5.6 Hz, 2H), 7.32–7.42 (m, 6H), 7.63–7.66 (m, 4H). ^{13}C NMR (100 MHz, $CDCl_3$): δ = 14.14, 14.27, 19.25, 22.65, 22.82, 26.06, 26.49, 26.70, 26.85, 26.94, 28.56, 29.41, 29.43, 29.84, 30.12, 30.53, 31.44, 32.00, 37.73, 38.38, 51.47, 63.53, 67.85, 72.11, 127.76, 129.71, 133.65, 134.48, 135.68, 139.69, 140.75, 166.95, 167.05, 167.12, 167.21. MS (MALDI-TOF): m/z: 872.48 (calcd. $[M+Na]^+$ = 872.77).

Compound 3. A mixture of compound **25** (100 mg, 0.167 mmol), 2-[2-(prop-2-yn-1-yloxy)ethoxy]ethyl 4-methylbenzenesulfonate (60.0 mg, 0.201 mmol), and K_2CO_3 (69.2 mg, 0.503 mmol) in DMF (30 mL) was stirred at 80 °C for 18 h. After cooling to the r.t., most of the DMF was evaporated under reduced pressure. The reaction mixture was then poured into ethyl acetate (100 mL) and washed with saturated NH_4Cl (4 × 50 mL) and saturated aq. NaCl (100 mL). The organic layer was separated, dried over $MgSO_4$, filtered and the solvent was evaporated under reduced pressure. The crude product was purified by flash column chromatography on silica gel (eluent: gradient from CH_2Cl_2 to CH_2Cl_2/acetone = 80:20 v/v) to afford compound **3** (81.7 mg, 0.113 mmol, 68 %) as a yellow solid.

^{1}H NMR (400 MHz, $CDCl_3$): δ = 2.37 (t, J = 6.4 Hz, 1H), 2.46 (t, J = 2.4 Hz, 1H), 3.62–3.66 (m, 2H), 3.72–3.81 (m, 10H), 3.87 (s, 3H), 3.90–4.93 (m, 4H), 4.20–4.22 (m, 4H), 4.24 (d, J = 2.4 Hz, 2H), 6.57 (t, J = 2.4 Hz, 1H), 6.88–6.90 (m, 2H), 6.97–6.99 (m, 2H), 7.64–7.67 (m, 2H), 8.14–8.22 (m, 6H), 8.64–8.69 (m, 2H). ^{13}C NMR (100 MHz, $CDCl_3$): δ = 55.63, 58.58, 61.88, 67.57, 67.66, 69.23, 69.76, 69.78, 70.47, 70.78, 70.94, 72.63, 74.79, 79.69, 87.42, 88.30,

95.46, 95.73, 102.60, 109.92, 110.11, 114.88, 115.77, 118.13, 118.97, 124.24, 124.78, 125.11, 125.28, 126.09, 126.46, 128.02, 128.27, 129.85, 130.02, 130.92, 131.30, 131.84, 132.14, 131.26, 159.10, 159.82, 160.71. HRMS (ESI-TOF): m/z: 745.2764 (calcd. $[M+Na]^+$ = 745.2777).

Compound 26. A mixture of compound **3** (80.2 mg, 0.111 mmol), compound **24** (94.4 mg, 0.111 mmol), CuI (106 mg, 0.555 mmol), and $(i\text{-Pr})_2$NEt (20 mL) in $CHCl_3$ (100 mL) was stirred at 60 °C for 24 h. After cooling to r.t., the reaction mixture was washed with 5% aq. HCl (2 × 100 mL), saturated aq. $NaHCO_3$ (100 mL), and saturated aq. NaCl (100 mL). The organic layer was separated, dried over $MgSO_4$, filtered, and the solvent was evaporated under reduced pressure. The crude product was purified by flash column chromatography on silica gel (eluent: gradient from CH_2Cl_2 to CH_2Cl_2/acetone = 80:20 v/v) to afford compound **26** (110 mg, 6.99×10^{-2} mmol, 63%) as a reddish-orange solid.

^{1}H NMR (400 MHz, $CDCl_3$): δ = 0.84–0.90 (m, 6H), 0.98 (s, 9H), 1.26–1.34 (m, 14H), 1.37–1.66 (m, 12H), 1.92–1.99 (quint, 2H), 2.46 (s, 1H), 3.34–3.41 (m, 4H), 3.57–3.66 (m, 6H), 3.72– 3.78 (m, 14H), 3.83 (t, J = 5.2 Hz, 2H), 3.86 (s, 3H), 3.88–3.92 (m, 4H), 4.19–4.22 (m, 4H), 4.32 (t, J = 7.2 Hz, 2H), 4.72 (s, 2H), 6.57 (t, J = 2.0 Hz, 1H), 6.88–6.89 (m, 2H), 6.94–6.96 (m, 2H), 7.32–7.40 (m, 6H), 7.55 (s, 1H), 7.62–7.65 (m, 6H), 8.06–8.19 (m, 6H), 8.59 (d, J = 4.0 Hz, 1H), 8.61 (d, J = 4.0 Hz, 1H). ^{13}C NMR (100 MHz, $CDCl_3$): δ = 14.12, 14.24, 19.24, 22.63, 22.80, 25.85, 26.39, 26.70, 26.85, 28.53, 29.38, 29.62, 29.83, 29.97, 30.08, 31.33, 31.41, 31.97, 37.67, 38.31, 50.20, 55.66, 61.93, 63.52, 64.89, 67.72, 63.52, 64.89, 67.72, 67.74, 67.83, 69.81, 70.54, 71.00, 72.09, 72.65, 87.44, 88.21, 95.61, 95.83, 102.71, 109.99, 110.19, 114.97, 115.80, 118.31, 119.00, 122.65, 124.22, 124.79, 125.14, 125.29, 126.20, 126.46, 127.76, 128.06, 128.28, 129.71, 129.88, 130.12, 130.92, 131.26, 131.81, 132.15, 133.30,

133.64, 134.17, 134.21, 135.66, 139.17, 140.56, 145.12, 159.22, 159.88, 160. 77, 166.73, 166.88, 166.91, 167.04. MS (MALDI-TOF): m/z: 1571.75 (calcd. $[M+Na]^+$ = 1571.77).

Compound 2. $Et_3N{\cdot}3HF$ (81.9 mg, 0.509 mmol) was added to a solution of compound **26** (80.0 mg, 5.09×10^{-2} mmol) and Et_3N (52.1 mg, 0.509 mmol) in THF (10 mL) and it was stirred at 70 °C for 24 h. After cooling to r.t., the reaction mixture was washed with saturated aq. $NaHCO_3$ (100 mL) and saturated aq. NaCl (2 × 100 mL). The organic layer was separated, dried over $MgSO_4$, filtered, and the solvent was evaporated under reduced pressure. The crude product was purified by flash column chromatography on silica gel (eluent: gradient from CH_2Cl_2/acetone = 80:20 v/v to CH_2Cl_2/acetone = 30:70 v/v) to afford compound **2** (62.1 mg, 4.65×10^{-2} mmol, 91%) as a reddish-orange solid.

^{1}H NMR (400 MHz, $CDCl_3$): δ = 0.83–0.88 (m, 6H), 1.24–1.29 (m, 14H), 1.35–1.63 (m, 10H), 1.92–1.98 (m, 2H), 2.49 (t, J = 6.0 Hz, 1H), 2.59 (t, J = 6.0 Hz, 1H), 3.28–3.34 (m, 4H), 3.54–3.59 (m, 4H), 3.62–3.77 (m, 16H), 3.81 (t, J = 5.2 Hz, 2H), 3.85 (s, 3H), 3.87–3.91 (m, 4H), 4.18–4.21 (m, 4H), 4.31 (t, J = 7.2 Hz, 2H), 4.71 (s, 2H), 6.55 (t, J = 2.0 Hz, 1H), 6.86–6.88 (m, 2H), 6.95 (d, J = 8.8 Hz, 2H), 7.58 (s, 1H), 7.61 (d, J = 8.4 Hz, 2H), 8.02–8.16 (m, 6H), 8.53–8.57 (m, 2H). ^{13}C NMR (100 MHz, $CDCl_3$): δ = 14.13, 14.24, 22.64, 22.80, 25.85, 26.42, 26.57, 27.71, 28.54, 29.39, 29.57, 29.94, 30.06, 31.35, 31.42, 31.87, 31.97, 37.73, 38.35, 50.14, 53.90, 55.68, 61.85, 61.94, 64.88, 67.76, 68.27, 69.83, 70.54, 71.01, 72.27, 72.67, 87.45, 88.21, 95.64, 95.85, 102.74, 110.01, 110.22, 115.01, 115.81, 118.34, 119.02, 122.70, 124.24, 125.16, 125.31, 126.23, 126.49, 128.09, 128.30, 129.90, 130.14, 130.95, 131.84, 132.17, 133.32, 134.09, 134.32, 134.36, 139.29, 140.70, 145.15, 159.25, 159.89, 160.79, 166.83, 166.83, 166.96, 167.00, 167.17. HRMS (ESI-TOF): m/z: 1356.6473 (calcd. $[M+Na]^+$ = 1356.6460).

Polymer synthesis

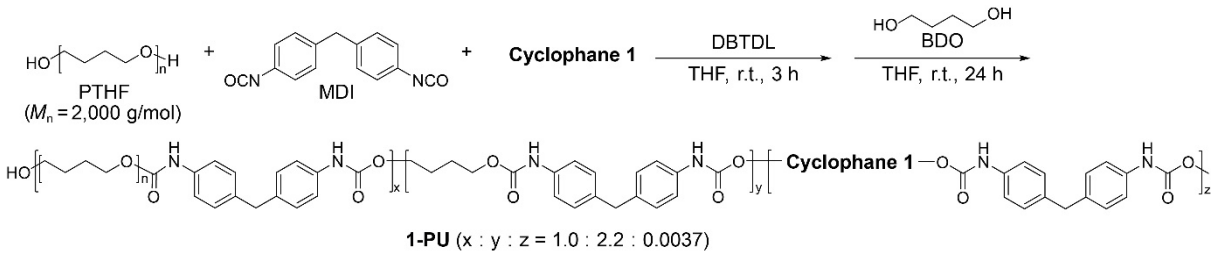

1-PU (x : y : z = 1.0 : 2.2 : 0.0037)

Synthesis of polyurethane 1-PU. To a stirred mixture of hydroxyl-terminated poly(tetrahydrofuran) (M_n = 2,000 g/mol, 3.00 g, 1.50 mmol), cyclophane **1** (8.73 mg, 6.00 × 10^{-3} mmol), and 4,4′-methylenebis(phenylisocyanate) (1.26 g, 5.04 mmol) in THF (30 mL), dibutyltin dilaurate (2 drops) was added and the reaction mixture was stirred at r.t. under nitrogen gas atmosphere for 3 h with a magnetic stir bar. A solution of 1,4-butanediol (297 mg, 3.26 mmol) in THF (10 mL) was added and the reaction mixture was stirred for another 24 h at r.t. under nitrogen gas atmosphere. Methanol (5 mL) was added and the reaction mixture was stirred for 30 min. The reaction mixture was then poured into methanol (1000 mL) and the mixture was stirred for 2 min. The pale yellow precipitate was filtered off and dissolved in THF (200 mL). The resulting solution was directly added to hexane (900 mL) through a cotton filter. The precipitate was filtered off and dried *in vacuo* for 24 h at r.t. to afford **1-PU** as a yellow rubbery solid (4.41 g, 98%, M_n = 121 kDa).

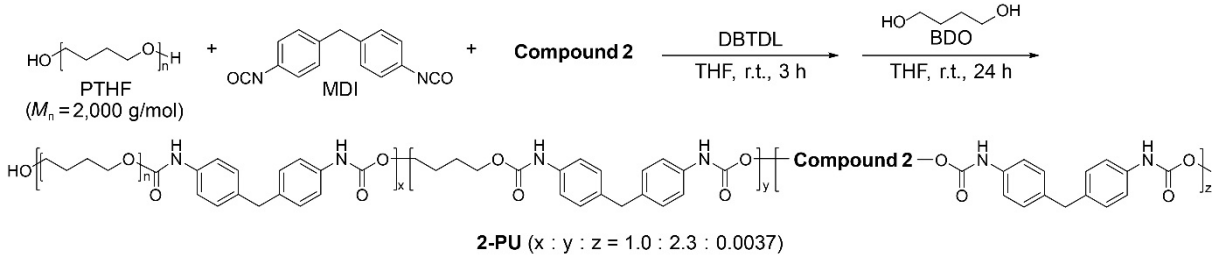

2-PU (x : y : z = 1.0 : 2.3 : 0.0037)

Synthesis of polyurethane 2-PU. To a stirred mixture of hydroxyl-terminated poly(tetrahydrofuran) (M_n = 2,000 g/mol, 3.00 g, 1.50 mmol), linear reference compound **2** (8.00 mg, 6.00 × 10^{-3} mmol), and 4,4′-methylenebis(phenylisocyanate) (1.26 g, 5.04 mmol) in THF (30 mL), dibutyltin dilaurate (2 drops) was added and the reaction mixture was stirred at

r.t. under nitrogen atmosphere for 3 h with a magnetic stir bar. A solution of 1,4-butanediol (297 mg, 3.26 mmol) in THF (10 mL) was added and the reaction mixture was stirred for another 24 h at r.t. under nitrogen gas atmosphere. Methanol (5 mL) was added and the reaction mixture was stirred for 30 min. The reaction mixture was then poured into methanol (1000 mL) and the reaction mixture was stirred for 2 min. The pale yellow precipitate was filtered and dissolved in THF (200 mL). The resulting solution was directly added to hexane (900 mL) through a cotton filter. The precipitate was filtered off and dried *in vacuo* for 24 h at r.t. to afford **2-PU** as a pale yellow rubbery solid (4.40 g, 98%, M_n = 134 kDa).

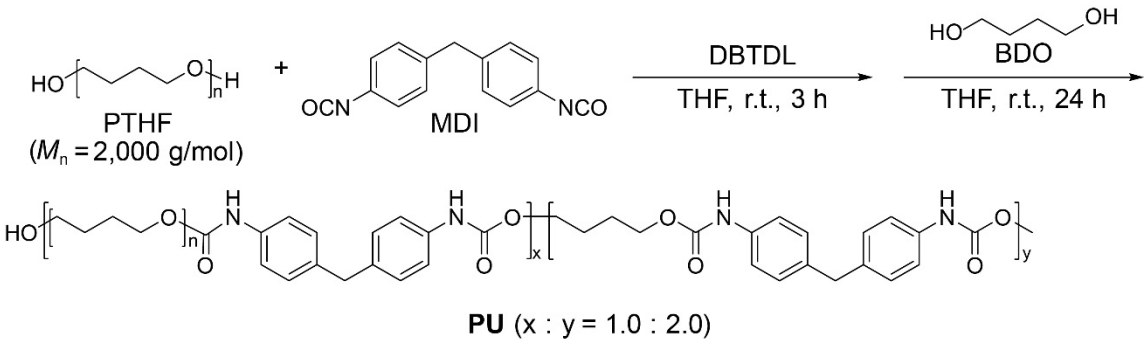

PU (x : y = 1.0 : 2.0)

Synthesis of polyurethane PU. To a stirred mixture of hydroxyl-terminated poly(tetrahydrofuran) (M_n = 2,000 g/mol, 3.00 g, 1.50 mmol), and 4,4′-methylenebis(phenylisocyanate) (1.26 g, 5.04 mmol) in THF (30 mL), dibutyltin dilaurate (2 drops) was added and the reaction mixture was stirred at r.t. under nitrogen atmosphere for 3 h with a magnetic stir bar. A solution of 1,4-butanediol (297 mg, 3.26 mmol) in THF (10 mL) was added and the reaction mixture was stirred for another 24 h at r.t. under nitrogen gas atmosphere. Methanol (5 mL) was added and the reaction mixture was stirred for 30 min. The reaction mixture was then poured into methanol (1000 mL) and the reaction mixture was stirred for 2 min. The pale yellow precipitate was filtered and dissolved in THF (200 mL). The resulting solution was directly added to hexane (900 mL) through a cotton filter. The precipitate

was filtered off and dried *in vacuo* for 24 h at r.t. to afford **PU** as a white rubbery solid (4.24 g, 94%, M_n = 110 kDa).

Preparation of polyurethane films

Preparation of 1-PU, 2-PU, and PU films. The polyurethanes (**1-PU**, **2-PU**, and **PU**, 300 mg) were dissolved in THF (7–8 mL) and the solutions were divided between two square-shaped poly(tetrafluoroethylene) molds (51 × 51 × 5.0 mm). The molds were placed under an inverted funnel to reduce the evaporation rate. The solvent was slowly evaporated overnight under ambient conditions and the resulting films were further dried *in vacuo* at r.t. overnight. The slightly opaque **1-PU**, **2-PU**, and **PU** films were smooth and had a thickness of 60–100 μm. The **1-PU** and **2-PU** films are yellow, while the **PU** films were white.

Preparation of 1inPU films. The polyurethane **PU** (300 mg) and compound **1** (0.660 mg, 4.54 × 10^{-4} mmol) were dissolved in THF (7–8 mL) and the solution was divided between two square-shaped poly(tetrafluoroethylene) molds (51 × 51 × 5.0 mm). The molds were placed under an inverted funnel to reduce the evaporation rate. The solvent was slowly evaporated overnight under ambient conditions and the resulting films were further dried *in vacuo* at r.t. overnight. The slightly opaque yellow films were smooth and had a thickness of 60–100 μm.

Preparation of 3inPU films. The polyurethane **PU** (300 mg) and compound **3** (0.321 mg, 4.54 × 10^{-4} mmol) were dissolved in THF (7–8 mL) and the solution was divided between two square-shaped poly(tetrafluoroethylene) molds (51 × 51 × 5.0 mm). The molds were placed under an inverted funnel to reduce the evaporation rate. The solvent was slowly evaporated overnight under ambient conditions and the resulting films were further dried *in vacuo* at r.t. overnight. The slightly opaque yellow films were smooth and had a thickness of 60–100 μm.

1-PU, **2-PU**, **PU**, **1inPU** or **3inPU** films were cut into dog-bone-shaped specimens that were used in the various measurements. Typical dimensions: 8 mm × 26 mm.

Preparation of 1-PU and PU blend films. A series of blend films was prepared to study the concentration dependency of **1** in polyurethane films. Varying amounts of **1-PU** and **PU** (**1-PU** (120 mg) and **PU** (30 mg), **1-PU** (90 mg) and **PU** (60 mg), **1-PU** (60 mg) and **PU** (90 mg), or **1-PU** (30 mg) and **PU** (120 mg)) were dissolved in THF (3.5–4 mL) and the solutions were transferred to square-shaped poly(tetrafluoroethylene) molds (51 × 51 × 5.0 mm). The molds were placed under an inverted funnel to reduce the evaporation rate. The solvent was slowly evaporated overnight under ambient conditions and the resulting films were further dried *in vacuo* at r.t. overnight. The slightly opaque yellow to pale yellow films were smooth and had a thickness of 60–100 μm.

2.5 References

[1] M. M. Caruso, D. A. Davis, Q. Shen, S. A. Odom, N. R. Sottos, S. R. White, J. S. Moore, *Chem. Rev.* **2009**, *109*, 5755–5798.

[2] J. Li, C. Nagamani, J. S. Moore, *Acc. Chem. Res.* **2015**, *48*, 2181–2190.

[3] G. De Bo, *Macromolecules* **2020**, *53*, 7615–7617.

[4] H. Traeger, D. J. Kiebala, C. Weder, S. Schrettl, *Macromol. Rapid Commun.* **2021**, *42*, 2000573.

[5] Y. Chen, G. Mellot, D. van Luijk, C. Creton, R. P. Sijbesma, *Chem. Soc. Rev*. **2021**, *50*, 4100–4140.

[6] S. He, M. Stratigaki, S. P. Centeno, A. Dreuw, R. Göstl, *Chem. - Eur. J.* **2021**, *27*, 15889−15897.

[7] D. A. Davis, A. Hamilton, J. Yang, L. D. Cremar, D. Van Gough, S. L. Potisek, M. T. Ong, P. V. Braun, T. J. Martinez, S. R. White, J. S. Moore, N. R. Sottos, *Nature* **2009**, *459*, 68−72.

[8] C. K. Lee, D. A. Davis, S. R. White, J. S. Moore, N. R. Sottos, P. V. Braun, *J. Am. Chem. Soc.* **2010**, *132*, 16107−16111.

[9] T. A. Kim, M. J. Robb, J. S. Moore, S. R. White, N. R. Sottos, *Macromolecules* **2018**, *51*, 9177−9183.

[10] Y. Lin, M. H. Barbee, C.-C. Chang, S. L. Craig, *J. Am. Chem. Soc.* **2018**, *140*, 15969−15975.

[11] M. J. Robb, T. A. Kim, A. J. Halmes, S. R. White, N. R. Sottos, J. S. Moore, *J. Am. Chem. Soc.* **2016**, *138*, 12328−12331.

[12] M. E. McFadden, M. J. Robb, *J. Am. Chem. Soc.* **2019**, *141*, 11388−11392.

[13] M. E. McFadden, M. J. Robb, *J. Am. Chem. Soc*. **2021**, *143*, 7925−7929.

[14] R. Göstl, R. P. Sijbesma, *Chem. Sci.* **2016**, *7*, 370−375.

[15] A. R. Sulkanen, J. Sung, M. J. Robb, J. S. Moore, *J. Am. Chem. Soc.* **2019**, *141*, 4080−4085.

[16] C. Baumann, M. Stratigaki, S. P. Centeno, R. Göstl, *Angew. Chem. Int. Ed.* **2021**, *60*, 13287−13293; *Angew. Chem.* **2021**, *133*, 13398−13404.

[17] Y. Chen, A. J. H. Spiering, S. Karthikeyan, G. W. M. Peters, E. W. Meijer, R. P. Sijbesma, *Nat. Chem.* **2012**, *4*, 559−562.

[18] E. Ducrot, Y. Chen, M. Bulters, R. P. Sijbesma, C. Creton, *Science* **2014**, *344*, 186−189.

[19] Z. Chen, J. A. M. Mercer, X. Zhu, J. A. H. Romaniuk, R. Pfattner, L. Cegelski, T. J. Martinez, N. Z. Burns, Y. Xia, *Science* **2017**, *357*, 475−479.

[20] M. Horst, J. Yang, J. Meisner, T. B. Kouznetsova, T. J. Martínez, S. L. Craig, Y. Xia, *J. Am. Chem. Soc.* **2021**, *143*, 12328−12334.

[21] K. Imato, A. Irie, T. Kosuge, T. Ohishi, M. Nishihara, A. Takahara, H. Otsuka, *Angew. Chem. Int. Ed.* **2015**, *54*, 6168−6172; *Angew. Chem.* **2015**, *127*, 6266−6270.

[22] T. Kosuge, X. Zhu, V. M. Lau, D. Aoki, T. J. Martinez, J. S. Moore, H. Otsuka, *J. Am. Chem. Soc.* **2019**, *141*, 1898−1902.

[23] S. Kato, S. Furukawa, D. Aoki, R. Goseki, K. Oikawa, K. Tsuchiya, N. Shimada, A. Maruyama, K. Numata, H. Otsuka, *Nat. Commun.* **2021**, *12*, 126.

[24] K. Seshimo, S. Hio, W. Takuma, A. Daisuke, S. Hajime, M. Koichiro, M. Yuchen, I. Akira, N. Shotaro, K. Takashi, I. Hiroshi, O. Hideyuki, *Angew. Chem. Int. Ed.* **2021**, *60*, 8406−8409; *Angew. Chem.* **2021**, *133*, 8487−8490.

[25] Y. Lu, H. Sugita, K. Mikami, D. Aoki, H. Otsuka, *J. Am. Chem. Soc.* **2021**, *143*, 17744−17750.

[26] H. Qian, N. S. Purwanto, D. G. Ivanoff, A. J. Halmes, N. R. Sottos, J. S. Moore, *Chem.* **2021**, *7*, 1080−1091.

[27] J. R. Hemmer, C. Rader, B. D. Wilts, C. Weder, J. A. Berrocal, *J. Am. Chem. Soc.* **2021**, *143*, 18859−18863.

[28] Y.-K. Song, K.-H. Lee, W.-S. Hong, S.-Y. Cho, H.-C. Yu, C.-M. Chung, *J. Mater. Chem.* **2012**, *22*, 1380−1386.

[29] Z. S. Kean, G. R. Gossweiler, T. B. Kouznetsova, G. B. Hewage, S. L. Craig, *Chem. Commun.* **2015**, *51*, 9157−9160.

[30] Z. Wang, Z. Ma, Y. Wang, Z. Xu, Y. Luo, Y. Wei, X. A. Jia, *Adv. Mater.* **2015**, *27*, 6469−6474.

[31] M. Karman, E. Verde-Sesto, C. Weder, Y. C. Simon, *ACS Macro Lett.* **2018**, *7*, 1099−1104.

[32] A. O. Razgoniaev, L. M. Glasstetter, T. B. Kouznetsova, K. C. Hall, M. Horst, S. L. Craig, K. L. Franz, *J. Am. Chem. Soc.* **2021**, *143*, 1784−1789.

[33] G. A. Filonenko, J. R. Khusnutdinova, *Adv. Mater.* **2017**, *22*, 1700563.

[34] G. A. Filonenko, D. Sun, M. Weber, C. Müller, E. A. Pidko, *J. Am. Chem. Soc.* **2019**, *141*, 9687−9692.

[35] Q. Verolet, A. Rosspeintner, S. Soleimanpour, N. Sakai, E. Vauthey, S. Matile, *J. Am. Chem. Soc.* **2015**, *137*, 15644−15647.

[36] A. Colom, E. Derivery, S. Soleimanpour, C. Tomba, M. Dal Molin, N. Sakai, M. González-Gaitán, S. Matile, A. Roux, *Nat. Chem.* **2018**, *10*, 1118−1125.

[37] J. Garcia-Calvo, J. Maillard, I. Fureraj, K. Strakova, A. Colom, V. Mercier, A. Roux, E. Vauthey, N. Sakai, *J. Am. Chem. Soc.*, **2020**, *142*, 12034–12038.

[38] T. Yamakado, K. Otsubo, A. Osuka, S. Saito, *J. Am. Chem. Soc.* **2018**, *140*, 6245–6248.

[39] R. Kotani, S. Yokoyama, S. Nobusue, S. Yamaguchi, A. Osuka, H. Yabu, S. Saito, *Nat. Commun.* **2022**, *13*, 303.

[40] T. Yamakado, S. Saito, *J. Am. Chem. Soc.* **2022**, *144*, 2804−2815.

[41] M. Raisch, W. Maftuhin, M. Walter, M. A. Sommer, *Nat. Commun.* **2021**, *12*, 4243.

[42] N. Bruns, K. Pustelny, L. M. Bergeron, T. A. Whitehead, D. S. Clark, *Angew. Chem. Int. Ed.* **2009**, *48*, 5666−5669; *Angew. Chem.* **2009**, *121*, 5776−5779.

[43] M. Taki, T. Yamashita, K. Yatabe, V. Vogel, *Soft Matter* **2019**, *15*, 9388−9393.

[44] R. Merindol, G. Delechiave, L. Heinen, L. H. Catalani, A. Walther, *Nat. Commun.* **2019**, *10*, 528.

[45] R. Glazier, J. M. Brockman, E. Bartle, A. L. Mattheyses, O. Destaing, K. Salaita, *Nat. Commun.* **2019**, *10*, 4507.

[46] S. Ogi, K. Sugiyasu, M. Takeuchi, *Bull. Chem. Soc. Jpn.* **2011**, *84*, 40−48.

[47] H. Hu, X. Cheng, Z. Ma, R. P. Sijbesma, Z. Ma, *J. Am. Chem. Soc.* **2022**, *144*, 9971−9979

[48] Y. Sagara, M. Karman, E. Verde-Sesto, K. Matsuo, Y. Kim, N. Tamaoki, C. Weder, *J. Am. Chem. Soc.* **2018**, *140*, 1584−1587.

[49] Y. Sagara, M. Karman, A. Seki, M. Pannipara, N. Tamaoki, C. Weder, *ACS Cent. Sci.* **2019**, *5*, 874−881.

[50] T. Muramatsu, Y. Sagara, H. Traeger, N. Tamaoki, C. Weder, *ACS Appl. Mater. Interfaces* **2019**, *11*, 24571−24576.

[51] T. Muramatsu, Y. Okado, H. Traeger, S. Schrettl, N. Tamaoki, W. Weder, Y. Sagara, *J. Am. Chem. Soc.* **2021**, *143*, 9884−9892.

[52] H. Traeger, Y. Sagara, D. J. Kiebala, S. Schrettl, C. Weder, *Angew. Chem. Int. Ed.* **2021**, *60*, 16191−16199; *Angew. Chem.* **2021**, *133*, 16327−16335.

[53] H. Traeger, Y. Sagara, J. A. Berrocal, S. Schrettl, C. Weder, ***Polym. Chem.*** **2022**, ***13***, 2860−2869.

[54] Y. Sagara, H. Traeger, J. Li, Y. Okado, S. Schrettl, N. Tamaoki, C. Weder, *J. Am. Chem. Soc.* **2021**, *143*, 5519−5525.

[55] K. Imato, R. Yamanaka, H. Nakajima, N. Takeda, *Chem. Commun.* **2020**, *56*, 7937−7940.

[56] C. V. Suneesh, K. R. Gopidas, *J. Phys. Chem. C* **2010**, *114*, 18725−18734.

[57] Y. Sagara, C. Weder, N. Tamaoki, *Chem. Mater.* **2017**, *29*, 6145−6152.

[58] S. Shimizu, S. Thazhathethil, K. Takahashi, T. Nakamura, Y. Sagara, *Mol. Syst. Des. Eng.* **2021**, *6*, 1039–1046.

[59] S. Amemori, K. Kokado, K. Sada, *Angew. Chem. Int. Ed.* **2013**, *52*, 4174−4178; *Angew. Chem.* **2013**, *125*, 4268−4272.

[60] S. B. Krishnan, R. Krishnan, K. R. Gopidas, *Chem. - Eur. J.* **2018**, *24*, 11451.

[61] V. V. Rostovtsev, L. G. Green, V. V. Fokin, K. B. Sharpless*Angew. Chem. Int. Ed.* **2002**, *41*, 2596–2599; *Angew. Chem.* **2002**, *114*, 2708–2711.

[62] S. K. Park, I. Cho, J. Gierschner, J. H. Kim, J. H. Kim, J. E. Kwon, O. K. Kwon, D. R. Whang, J.-H Park, B.-K An, S. Y. Park, *Angew. Chem. Int. Ed.* **2016**, *55*, 203−207; *Angew. Chem.* **2016**, *128*, 203−215.

[63] M. A. Ayer, Y. C. Simon, C. Weder, *Macromolecules* **2016**, *49*, 2917−2927.

[64] H. J. Qi, M. C. Boyce, *Mech. Mater.* **2005**, *37*, 817−839.

[65] J. Yi, M. C. Boyce, G. F. Lee, E. Balizer, *Polymer* **2006**, *47*, 319−329.

[66] E. Piers, J. M. Chong, H. E. Morton, *Tetrahedron* **1989**, *45*, 363–380.

[67] P. S. Shirude,V. A. Kumar, K. N. Ganesh, *Eur. J. Org. Chem.* **2005**, 5207–5215.

[68] C. V. Yelamaggad, G. Shanker, *Tetrahedron* **2008**, *64*, 3760–3771.

[69] J. Cao, Y. Liu, L. Zhang, F. Du, Y. Ci, Y. Zhang, J. Qiao, *J. Radioanal. Nucl. Chem.* **2017**, *312*, 263–276.

Chapter 3

Conclusion and Perspective

In this thesis, the author developed a cyclophane-based supramolecular mechanophore utilizing charge-transfer interactions.

The mechanochromic mechanophores are reliable molecular probes for the easy and discernible detection of polymer failures owing to the changes in the absorption or photoluminescence properties. Supramolecular mechanophores do not require covalent bond scission for their activation, the activation is based on altering π- π interactions or charge-transfer (CT) interactions in the molecules. As described in the first chapter of thesis, the supramolecular mechanophores possess several advantages over covalent mechanophores, including instant reversibility and low activation energy. However, the number of supramolecular mechanophores is still limited.

Considering the advantages of supramolecular mechanophores, as discussed in chapter 2, the author developed a cyclophane-based supramolecular mechanophore that contains a 1,6-bis(phenylethynyl)pyrene luminophore and a pyromellitic diimide quencher. When the mechanophore was dissolved in toluene, the blue monomer emission of the luminophore is effectively quenched and a faint reddish-orange emission that originates from a CT-complex was observed. A polyurethane elastomer containing the mechanophore displays orange emission in the absence of force, which is dominated by the CT-emission. Uniaxial tensile stretching causes ratiometric changes in emission color, due to the spatial separation between the luminophore and quencher. The ratiometric emission color change in response to mechanical force was instantly reversible. The ratio of the two emission intensities correlates with the applied stress. Stretching of polyurethane film that contains physically doped cyclophane did not exhibit emission color changes. The different mechanoresponsive behavior of the films confirms that the covalent integration of cyclophane plays a pivotal role to achieve the ratiometric emission color change.

Cyclophane-based supramolecular mechanophores utilizing charge-transfer interactions are suitable candidates to study the deformation events in polymers. There are several conventional methods to calculate the forces in large objects. However, methods to study the force generates in the tiny objects and methods for single molecular level detection of force are still under development. Supramolecular mechanophores are appropriate to study the forces in the range of nN to pN. Different cyclophane-based supramolecular mechanophores showing on-off switching of emission or ratiometric change of emission could be developed by changing the luminophore or quencher. By replacing the luminophores, we could achieve cyclophanes with different emission colors after activation. Moreover, we could study the significance of ring size to enable unambiguous and effective mechanochromic luminescent behavior by varying the ring size. To extent the repertoire of the supramolecular mechanophores we could easily develop various mechanophores by changing the molecular design to catenanes, knots, and other interlocked molecules. The supramolecular mechanophores including the cyclophane described in this thesis after appropriate modification on the molecular structure would be suitable to detect weak forces working in the living tissues.

List of Publications

Original Papers

(1) Shakkeeb Thazhathethil, Tatsuya Muramatsu, Nobuyuki Tamaoki, Christoph Weder, Yoshimitsu Sagara, "Excited state charge-transfer complexes enable fluorescence color changes in a supramolecular cyclophane mechanophore", *Angew. Chem. Int. Ed.* **2022**, *61*, e202209225, *Angew. Chem.* **2022**, *134*, e202209225. **(Selected as back cover)**

(2) Shohei Shimizu, Shakkeeb Thazhathethil, Kiyonori Takahashi, Takayoshi Nakamura, Yoshimitsu Sagara, "Crystal structure of a 1,6-bis(phenylethynyl)pyrene-based cyclophane that exhibits mechanochromic luminescence", *Mol. Syst. Des. Eng.* **2021**, *6*, 1039–1046.

A Journal of the German Chemical Society

Angewandte International Edition Chemie

GDCh

www.angewandte.org

2022–61/42

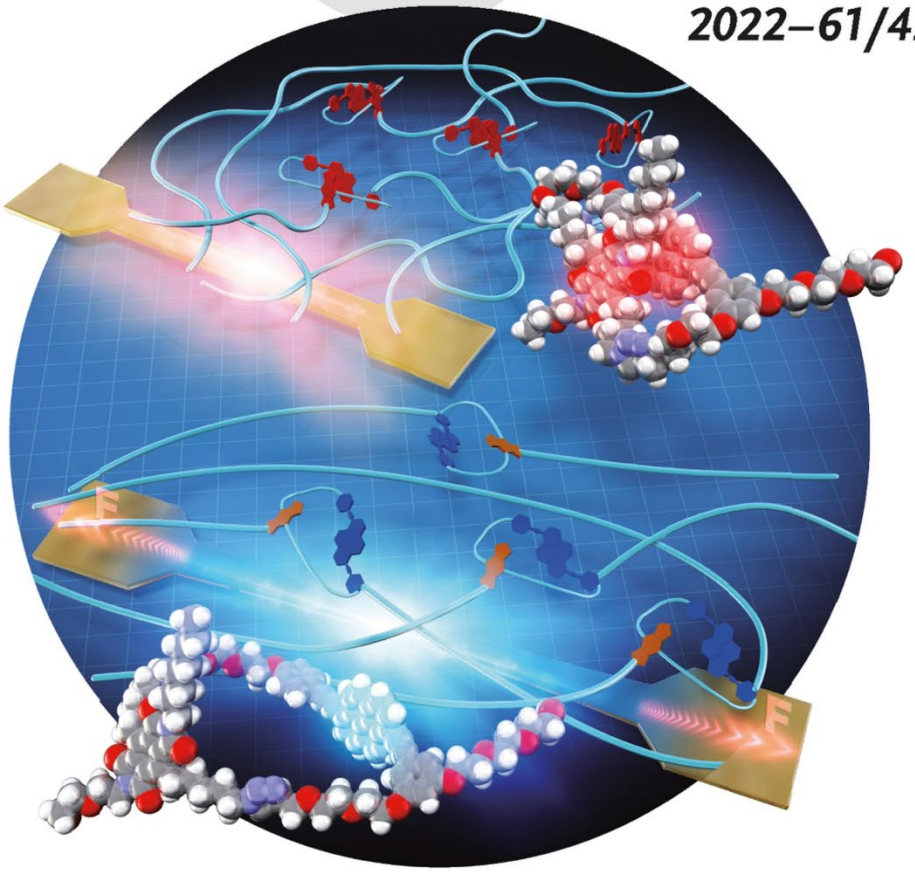

Mechanochromic mechanophores ...

... visualize stress applied to polymers. In their Communication (e202209225), Christoph Weder, Yoshimitsu Sagara et al. demonstrate the first cyclophane mechanophore utilizing charge–transfer complex emission. Polyurethane elastomer films in which the mechanophore is covalently embedded exhibit instantly reversible emission color change between orange and blue upon deformation. The spatial separation of the luminophore and quencher leads to vivid mechanochromic luminescence.

WILEY-VCH

Acknowledgement

The research works presented in this thesis were carried out under the supervision of Prof. Nobuyuki Tamaoki and Assoc. Prof. Yoshimitsu Sagara from Hokkaido University (October 2019 to March 2020) and Tokyo Institute of Technology (July 2020 to August 2022).

First of all, the author is deeply grateful to Prof. Nobuyuki Tamaoki and Yoshimitsu Sagara for their constant encouragement and generous guidance. The kind instructions and constructive criticism by Assoc. Prof. Yoshimitsu Sagara helped the author to learn the qualities of a researcher including paper writing and conference presentation.

The author is grateful to Prof. Christoph Weder, University of Fribourg for his valuable comments and enormous support, which helped the author to complete the work comprised in this thesis. Moreover, the thermogravimetric analysis and dynamic mechanical analysis were conducted at Prof. Weder's laboratory.

The author expresses his gratitude to all the members of laboratory of smart molecules at Hokkaido University including Dr. Sampreeth Thayyil, Dr. Hashim P.K., Dr. Yuna Kim, Dr. Kazuya Matsuo, Dr. Amrutha A. S., Dr. Md. Jahirul Islam, Dr. Shariful Haque, Mr. Kaito Ueda, Mr. Jiajun Qi, Mr. Runze Lin, Mr. Shinya Yutani, Mr. Yuji Okada, and former secretory of laboratory, Ms. Emi Kobayashi for their cooperation and support during his stay in Hokkaido. The author expresses his gratitude to the members of Sagara group including Mr. Tatsuya Muramatsu, Mr. Shohei Shimizu, Ms. Keiko Hiratsuka, Mr. Takumi Kuroda, Mr. Liu Qiming, Mr. Fazil T.S., Mr. Liu Silu, Mr. Keigo Nonaka, Mr. Ryusei Mori, and Ms. Tianyue Zhang for creating an enjoyable research life in Tokyo.

The author greatly thanks Dr. Mohammed Mustafa T.N. (University of Calicut), Dr. Anil Kumar G. M. (Tokyo Institute of Technology), and all other friends for hearty support

and constant encouragement. The author has always been refreshed by various types of discussions with them during the course period.

The author was financially supported by a Japanese government MEXT (Ministry of Education, Culture, Sports, Science and Technology) fellowship through Hokkaido University International Graduate Program during the doctoral course.

Finally, the author expresses his sincere gratitude towards his parents Mr. Muhammadali, Mrs. Mariya, grandfather Mr. Moiduppa, grandmother Mrs. Asiya, brothers, Mr. Ashique, Mr. Abdul Vahid, sister Ms. Shifana, and all other family members for their prayers, love, and motivation during the entire duration of the course. Without their constant encouragement, the author could not have completed this thesis.